Moscow State University
Quantum Technology Centre seminars
March 9, 2021

Tissue Optics and Tissue Optical Clearing for in-depth Imaging

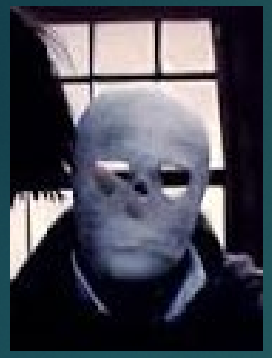

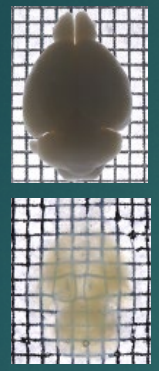

The Invisible Man
Herbert G. Wells
1897

Valery V. Tuchin

Saratov State University (National Research University)
Tomsk State University (National Research University)
ITMO University (National Research University)
Institute of Precision Mechanics and Control of the RAS
Bach Institute of Biochemistry, Research Center of Biotechnology of the RAS
Russia
tuchinvv@mail.ru

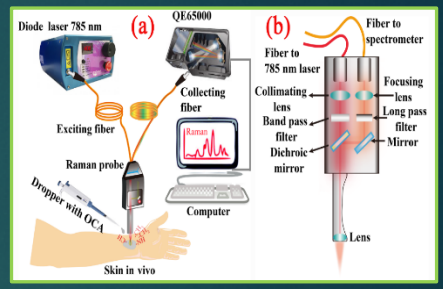

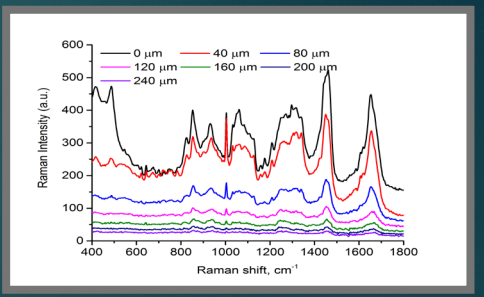

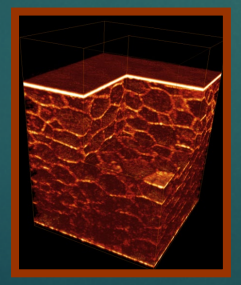

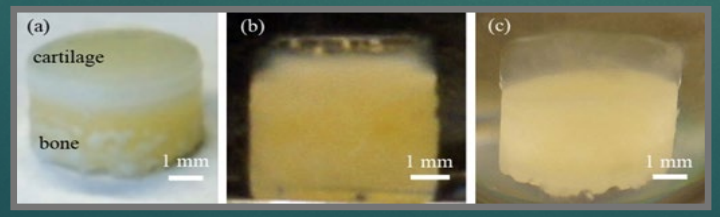

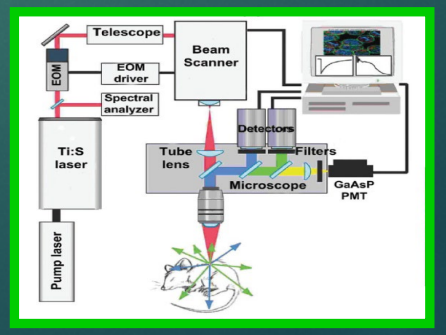

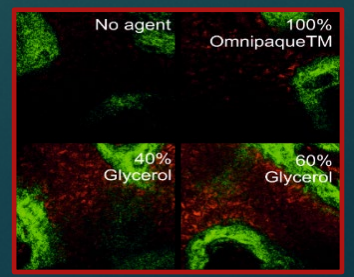

Outline

- Motivation
- Tissue ‘optical windows’
- Fundamentals of tissue optical clearing (OC) and optical clearing agents (OCAs)
- Quantification of optical properties
- Collimated transmittance, free and bound water
- OC of pathological tissues
- Creation of UV window
- Confocal Raman spectroscopy of skin
- Nonlinear optical imaging
- Optical coherence tomography (OCT)
- Photoacoustic microscopy and flow cytometry
- Speckle dynamic microscopy
- MRI agents
- Enhanced FLIM
- Luminescence: upconversion nanoparticles
- Tissue phantoms for OC
- OCAs for THz waves
- Summary
- OC multimodality concept
- Conclusion

Motivation: Challenges of Optical Imaging

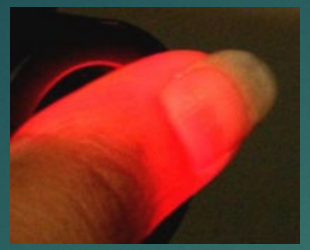

Soft limit ~ δ

1 – 2 mm

$$\delta = 1/\sqrt{3\mu_a\left(\mu_a + \mu_s'\right)}$$

Hard limit ~10 δ

$$\mathrm{MFP} = l_{ph} = 1/(\mu_a + \mu_s)^{-1}$$

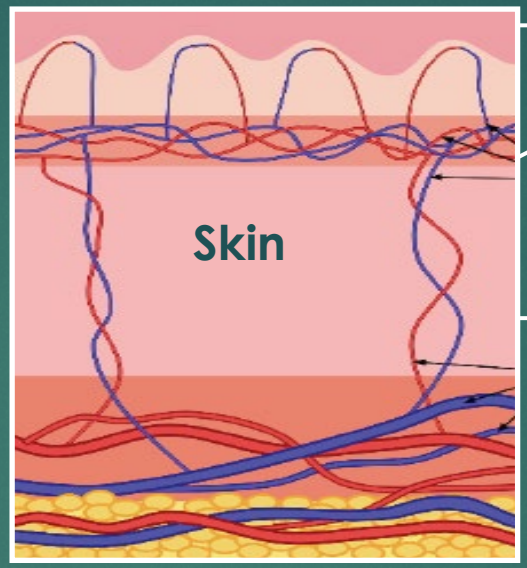

OM, SNOM

CFM, 2PM, SHM, etc.

OCT

DOT,
UOT, PAT

OM: Optical microscopy
SNOM: Scanning near-field optical microscopy
CFM: Confocal microscopy
2PM: Two-photon microscopy
SHM: Second harmonic microscopy
OCT: Optical coherence tomography
DOT: Diffuse optical tomography
UOT: Ultrasound-modulated optical tomography
PAT: Photoacoustic tomography

Laser Treatment

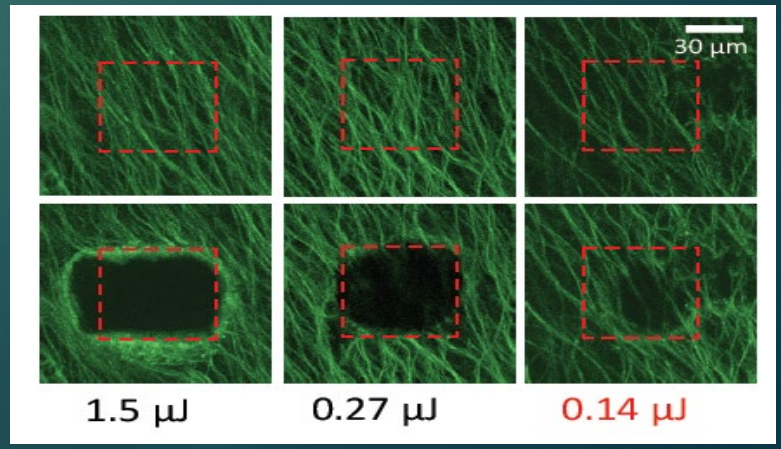

Tissue ‘optical windows’

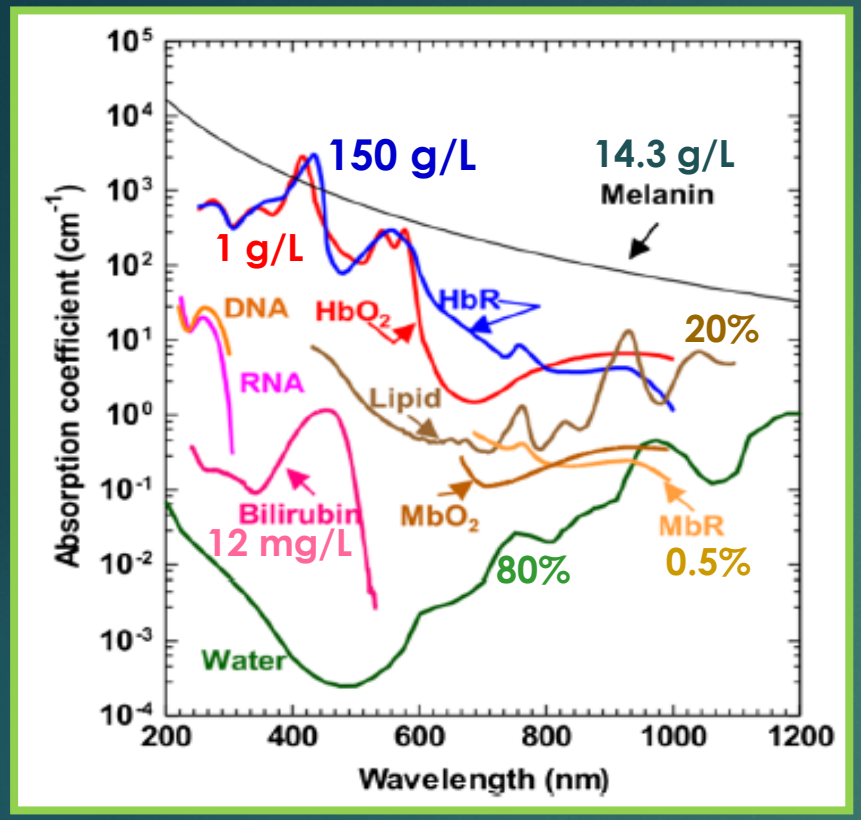

Y. Zhou, et al. J. Biomed. Opt. 21(6), 061007 (2016)

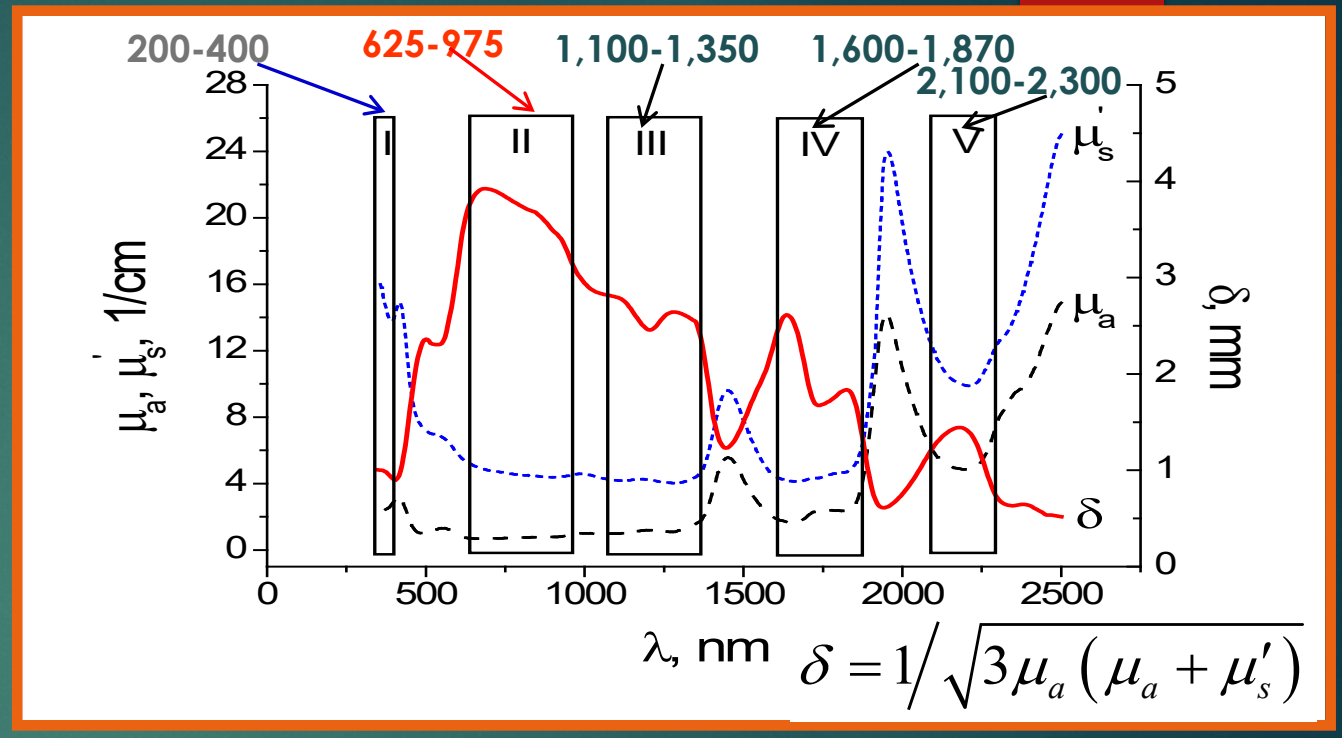

Absorption (μ_a) and reduced scattering (μ_s') coefficients, and light penetration depth (δ) of peritoneum within tissue ‘optical windows’
Bashkatov A. N. *et al* . *Opt. Spectrosc.* **120 (1)**, 1-8, 2016

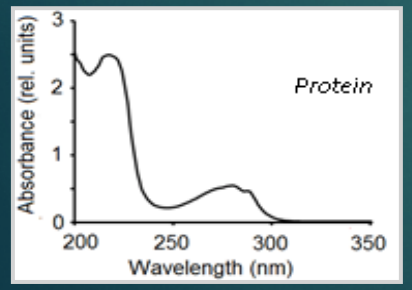

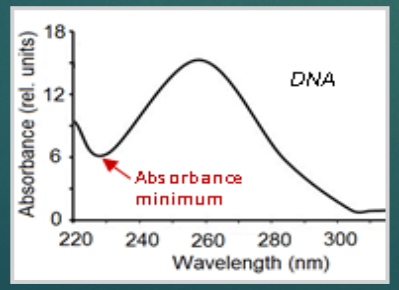

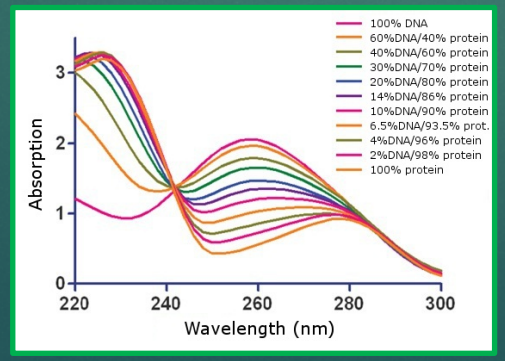

Rat muscle treatment with 20% glucose solution

P. Peixoto, et al., *J. Biomed. Photon.Eng* **1**(4) 255, 2016

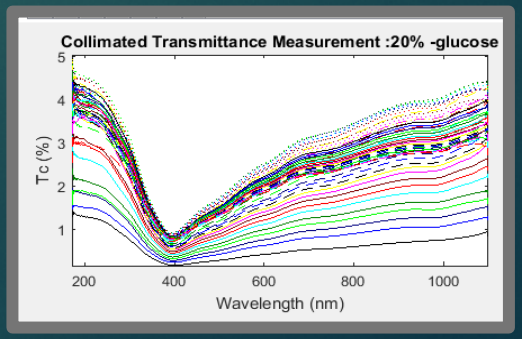

http://elte.prompt.hu/sites/default/files/tananyagok/IntroductionToPracticalBiochemistry/ch04s06.html

Brief history of tissue optical clearing (OC)

https://www.flickr.com/photos/baggis/3084210290

https://fr.wikipedia.org/wiki/Tipi#/media/File:Fredenbaum-100719-15599-.jpg

The optical clearing (OC) technique has been intuitively used by mankind since ancient times

Northern ancient European inhabitants used dried animal skin to construct the walls of their dwellings or dehydrated seal intestines for windows, so that light could enter inside

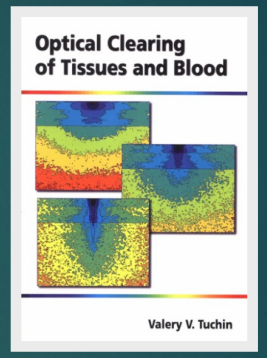

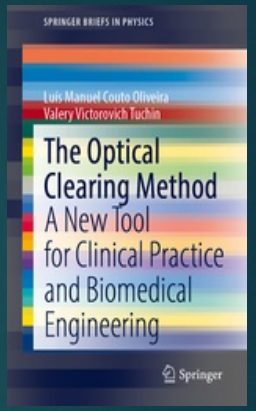

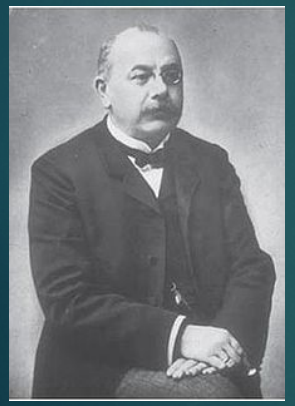

https://en.wikipedia.org/wiki/Werner_Spalteholz

Early OC offers for medical purposes are also known, but the major evidence of this technique has been discovered more than 100 years by the German anatomist Werner Spalteholz (*Spalteholz*, 1911, 1914)

He realized that muscle tissue becomes transparent when dehydrated with the use of alcohol followed by clove oil or xylene and then stored in Canadian balsam (*Richardson et al.*, 2015; *Azwendt et al.*, 2016; *Azaripour et al.*, 2016)

He immediately comprehended the occurrence of the RI matching mechanism, and the evidence of tissue shrinkage due to initial dehydration mechanism has been reported in 1939 (*Cumley et al.*, 1939)

However, only in the late 80's and early 90's of the last century, this technology was started to be purposefully developed to solve the problems of rapidly developing optical methods of medical diagnostics and therapy (*Tuchin*, 2006; *Zhu et al.*, 2013; *Richardson et al.*, 2015; *Azaripour et al.*, 2016)

In the meantime, the OC technique has proved itself powerful in the UV, visible to NIR/FIR ranges (*Zhu et al.*, 2013, 2018; *Genina et al.*, 2015; *Richardson et al.*, 2015; *Azwendt et al.*, 2016; *Azaripour et al.*, 2016; *Oliveira et al.*, 2018; *Tainaka et al.* 2018; *Oliveira & Tuchin* 2019 ……..)

Immersion Optical Clearing Method

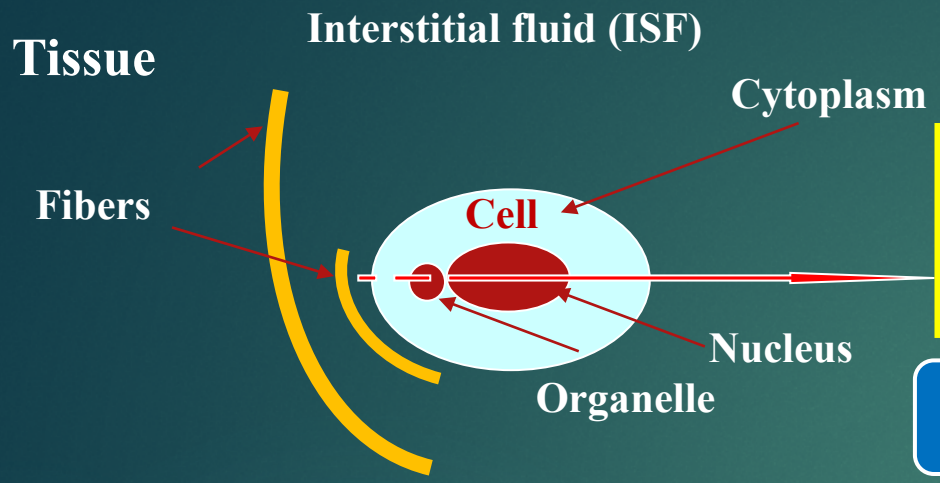

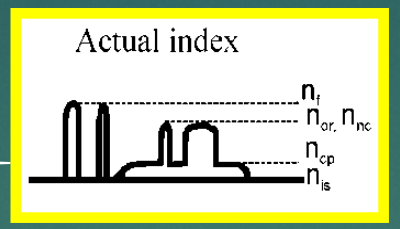

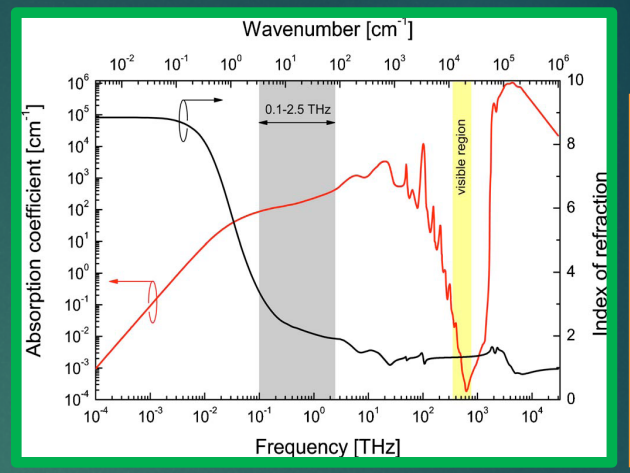

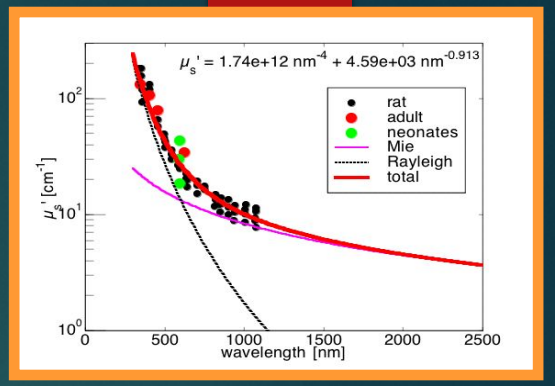

$$\mu_s' = \mu_s(1-g) \sim d^2\rho(d/\lambda)^{0.37}(m-1)^2$$

$$m \equiv n_s/n_0$$

(1) Tissue/cell dehydration caused by osmotic action of an OCA
(2) OCA diffusion into the tissue/cell, replacement water by an OCA
Both mechanisms are important for THz spectroscopy/imaging
(1) and (2) are followed by:

- Tissue shrinkage: less thickness and better ordering of collagen fibers with volume fraction $f_c(t)$ caused by temporal/reversible dehydration

$$\mu_s' = \mu_s(1-g) \sim [1-f_c(t)]^3/[1+f_c(t)]$$

- Refractive index matching of tissue/cell components and ISF/cytoplasm
- Disruption of the collagen molecules hydration shell (alteration of the hydrodynamic radius) and its reversible dissociation

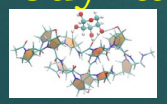

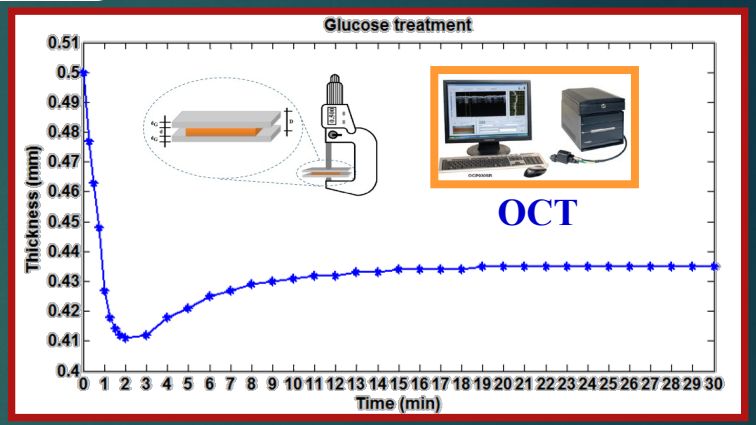

Human eye ball

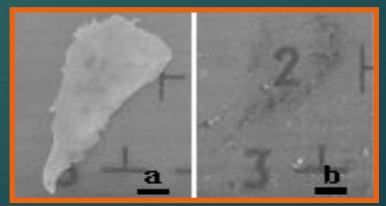

Rabbit *dura mater*, 1-min in glycerol

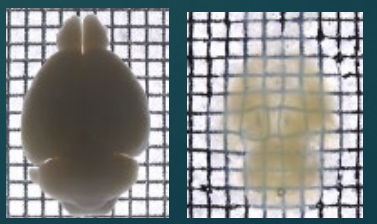

Mouse whole brain

V.V. Tuchin, *Tissue Optics*, 3rd edition, SPIE Press, **PM 254**, 2015

Ordering of collagen fibers

EMI :

Cornea

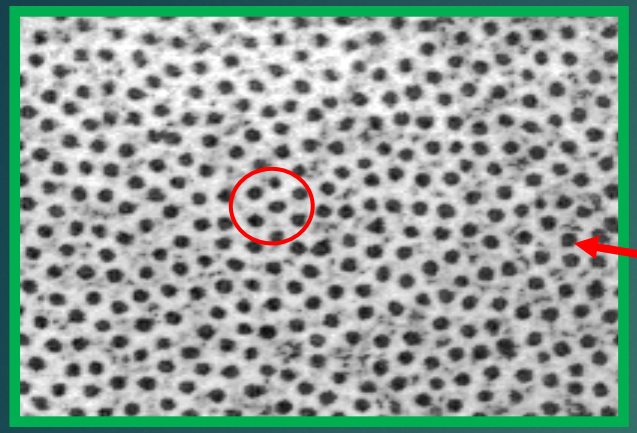

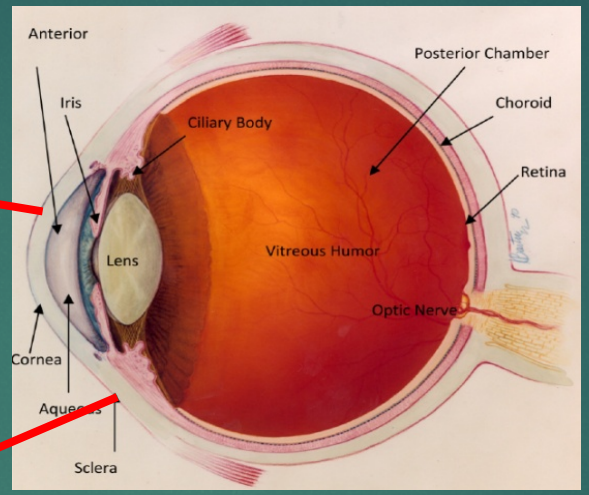

Sclera

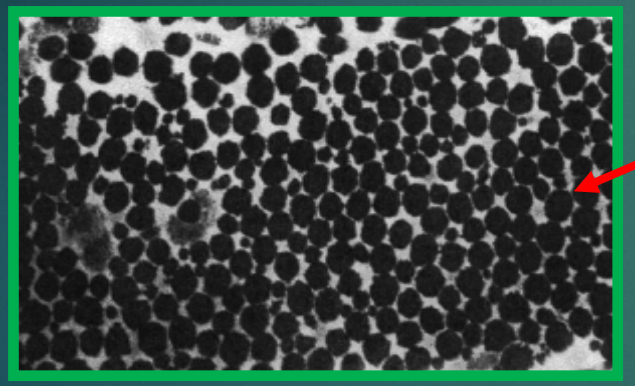

From *Oliveira et al.*, SFM, 2020

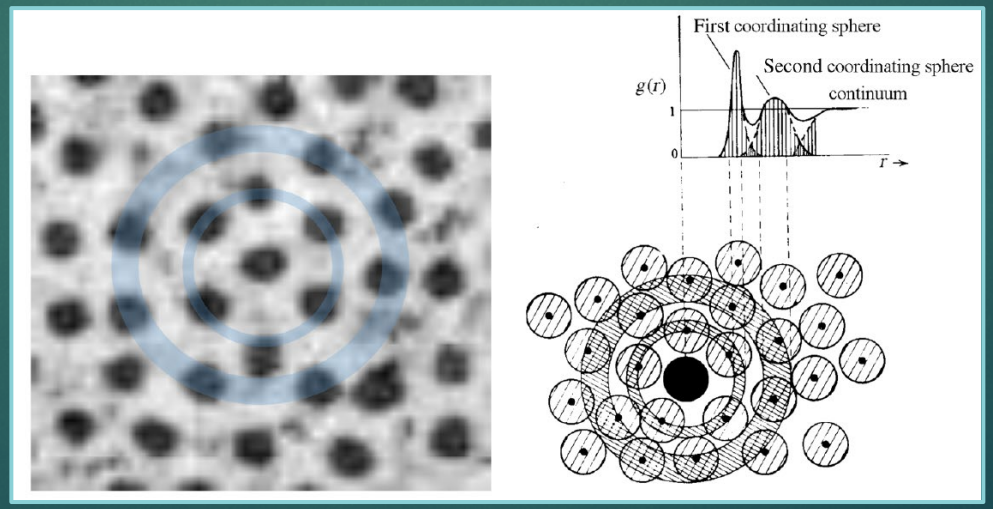

V.V. Tuchin, Polarized light interaction with tissues (tutorial), JBO 21(7), 071114 (2016)

OCT : Examples of clear and turbid (scattering) tissues

OCT images and in-depth signal

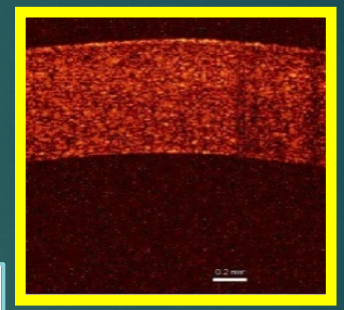

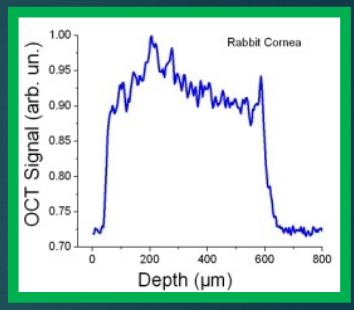

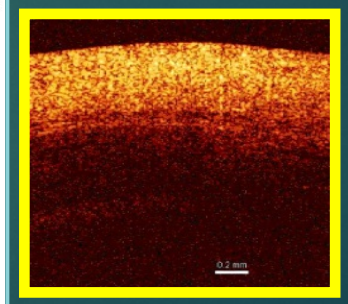

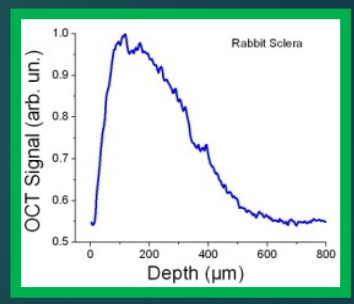

M.G. Ghosn, V. V Tuchin, K. V. Larin, IOVS, 2007

Optical clearing agents (OCAs)

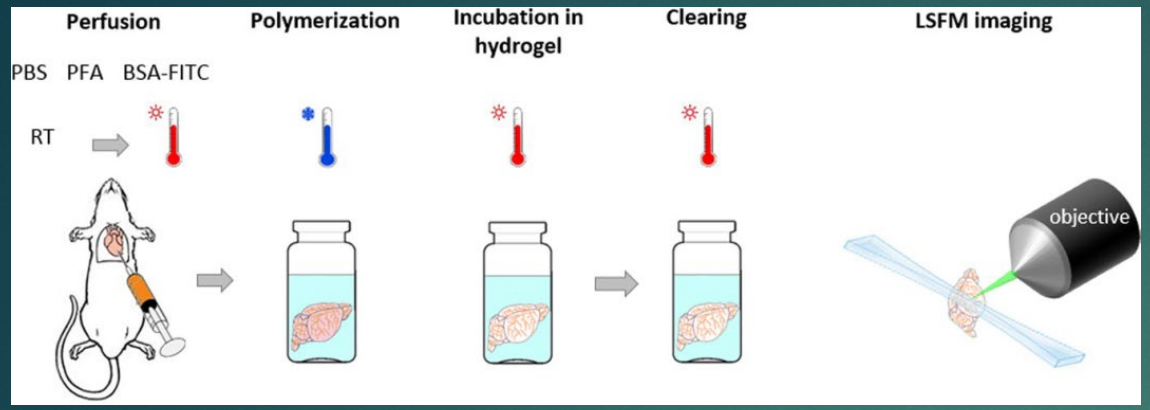

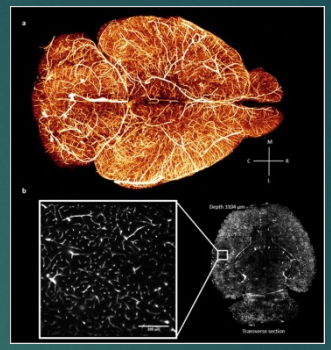

Francesco Pavone et al., Whole-Brain Vasculature Reconstruction at the Single Capillary Level, Scientific Reports, 8:12573 (2018)

Dan Zhu et al. Evaluation of seven optical clearing methods in mouse brain, Neurophoton. 5(3), 035007 (2018)
3-D imaging of solvent-cleared organs (3DISCO), ultimate DISCO (uDISCO), see deep brain (SeeDB), ScaleS, Clear T2, and passive CLARITY technique (PACT)

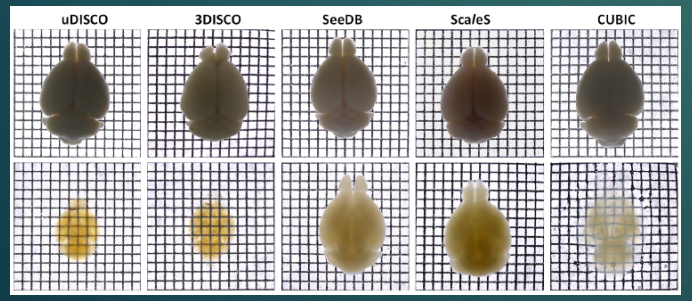

Hiroki R. Ueda et al. Chemical Landscape for Tissue Clearing Based on Hydrophilic Reagents, Cell Reports (2018)
More than 1,600 chemicals were screened by a high-throughput evaluation system for each chemical process.

In vitro measured optical clearing potential (OCP) at OCA application to dermis side of human skin using a Franz diffusion chamber

B. Choi et al. "Determination of chemical agent optical clearing potential using *in vitro* human skin," *Lasers Surg. Med.* 36, 72-75, 2005

Hydroxy-terminated chemical agent	Refractive index	Osmolality (mOsm/kg)	OCP
Glycerol	1.47	14,550	2.9±0.8
50% TMP (trimethylolpropanol)	1.43	6,830	2.2±0.3
100% TMP	1.47	13,660	2.1±0.7
1,3-butanediol	1.44	22,050	2.4±0.7
1,4-butanediol	1.44	26,900	2.8±0.5
Ethylene glycol	1.43	22,640	1.9±0.6
MPDiol glycol (1,3-diol, 2-methyl-propane)	1.44	23,460	2.3±0.2
P-0062[1]	1.48	1,643	2.0±0.5

[1] P-0062 is a polyethylene glycol based prepolymer (Univ. of California, Irvine)

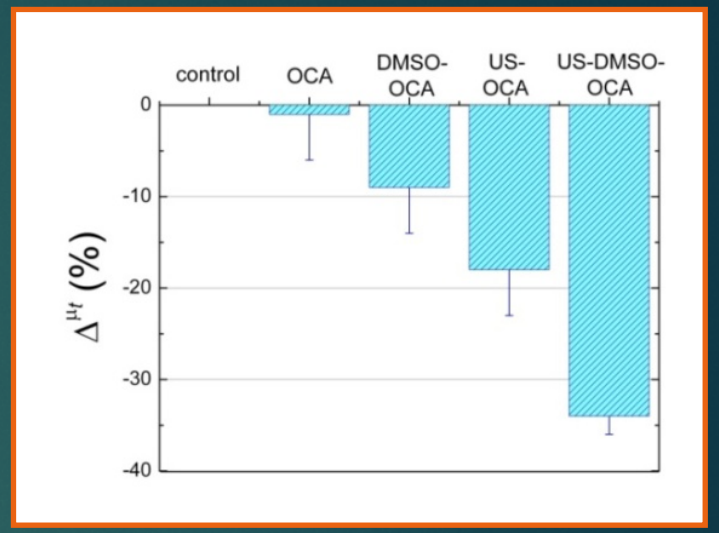

Rat skin *in vivo*

$$OCP \equiv \mu_s'(\text{before})/\mu_s'(\text{in 20 min after application})$$

Saccharides: glucose, sucrose, maltose, fructose
PEGs, Propylene glycol (1,2-propanediol), DMSO, et. al

Iodine based non-ionic X-ray contrast media have lower osmolarity and tend to have less side-effects:
Omnipaque, Ultravist, Visipaque, etc.

Enhancers for *in vivo* delivery of OCAs through biological membranes

E.V. Lengert, E. E. Talnikova, V. V. Tuchin, Yu. I. Svenskaya, Prospective strategies for enhanced intra- and transdermal delivery of antifungal drugs, *Skin Pharmacology and Physiology* **33**, 261–269 (2020)

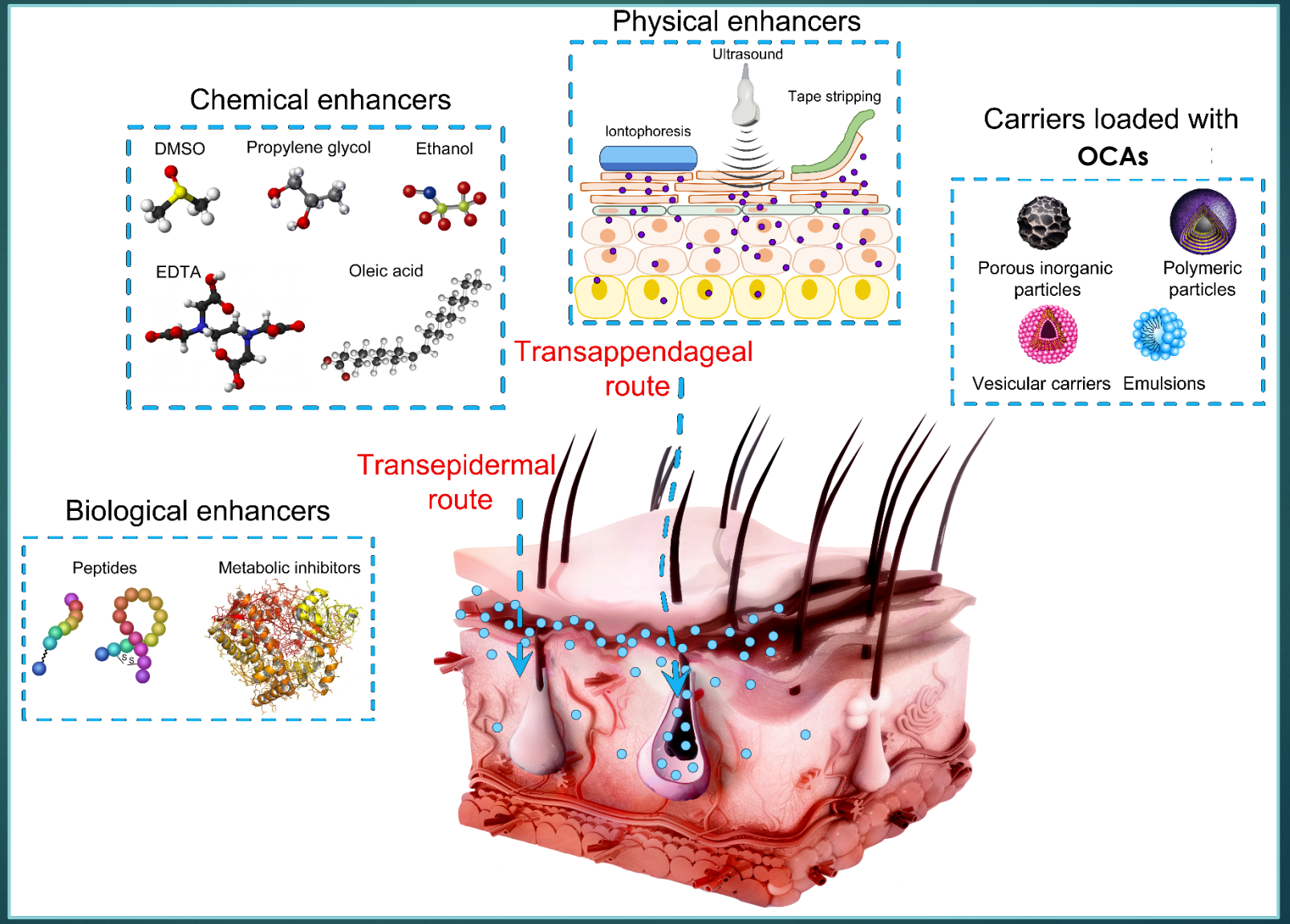

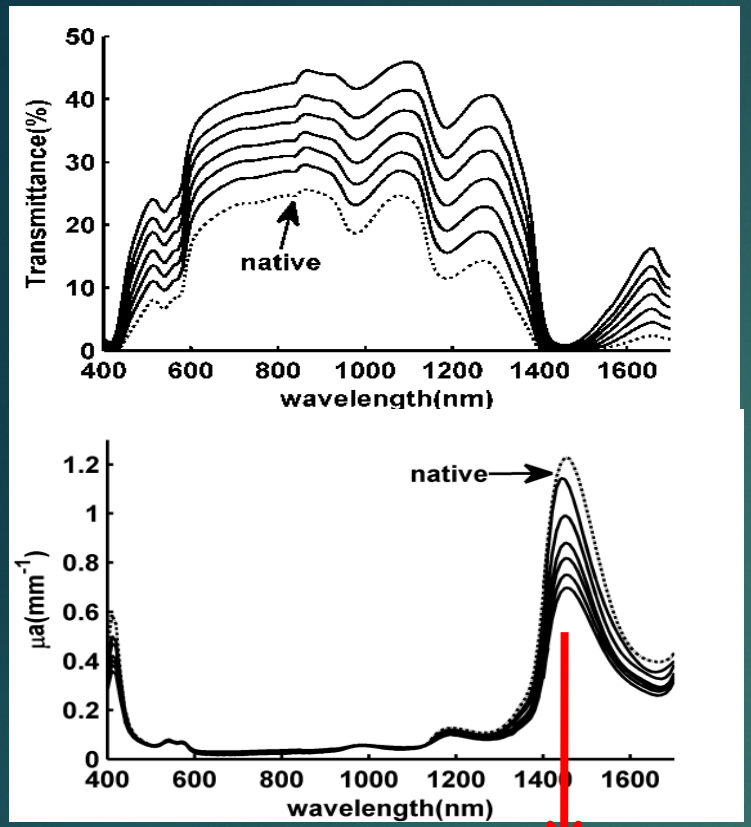

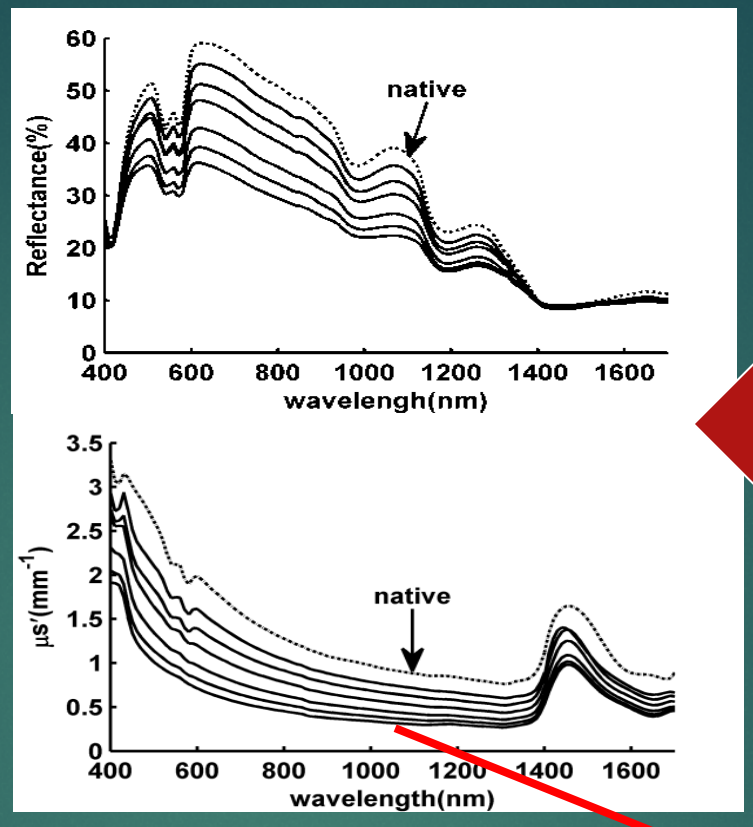

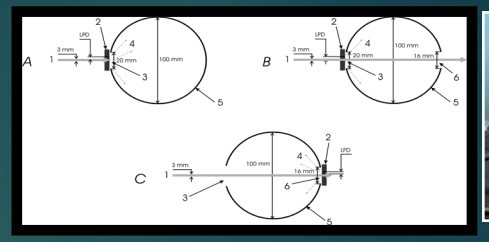

T. Yu, X. Wen, V.V .Tuchin, Q. Luo, D. Zhu, *J. Biomed. Opt.* 16 (2011)

Pig skin sample before and after treatment
by 1,2-propanediol
at time intervals of
0 (native), 10, 20, 30, 40, 50 and 60 min

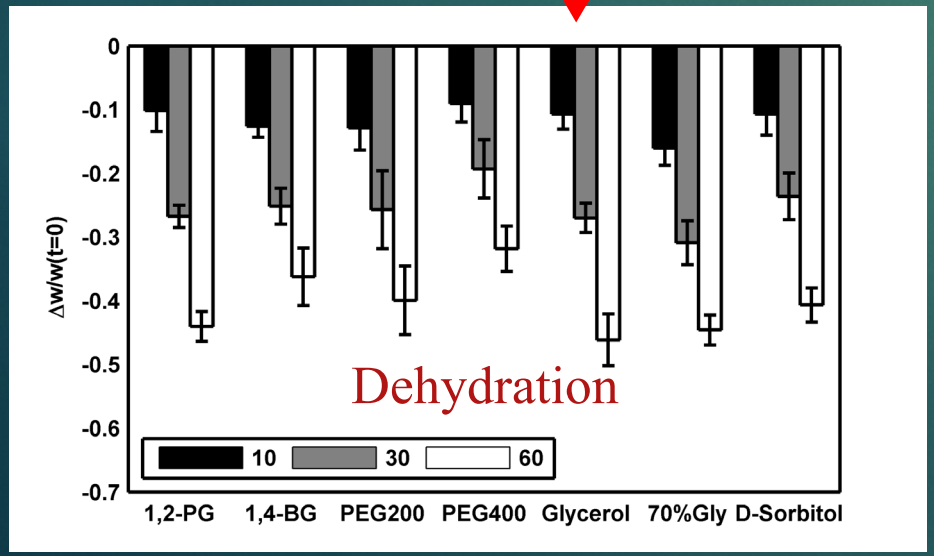

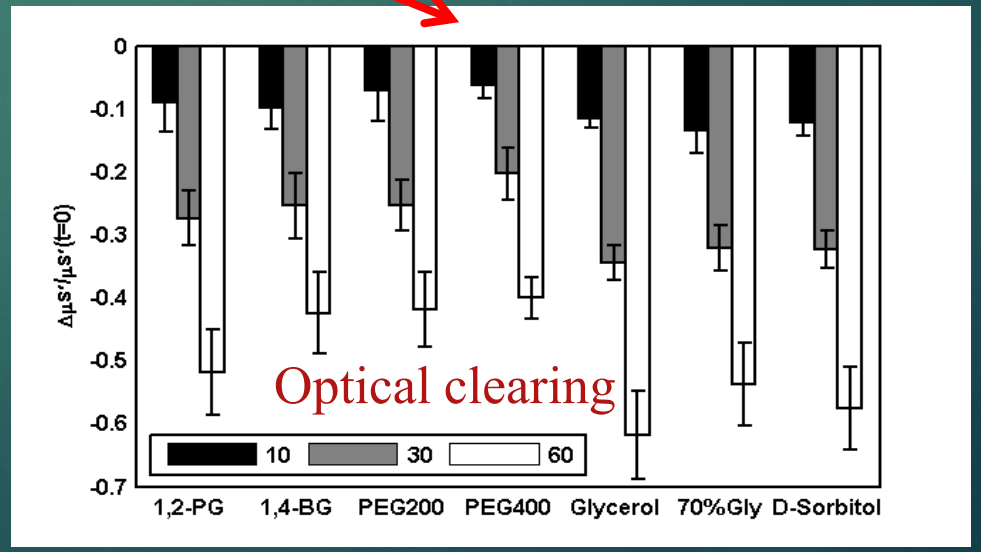

Time dependence for collimated transmittance for the rat muscle treatment with glucose

(L.Oliveira, M.I. Carvalho, E. Nogueira, V. V. Tuchin *JIOHS*, Vol. 6, No. 2, 1350012, 2013; JBO, 2015)

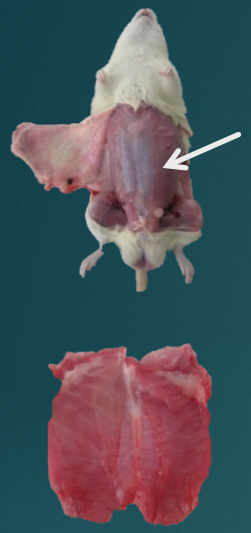

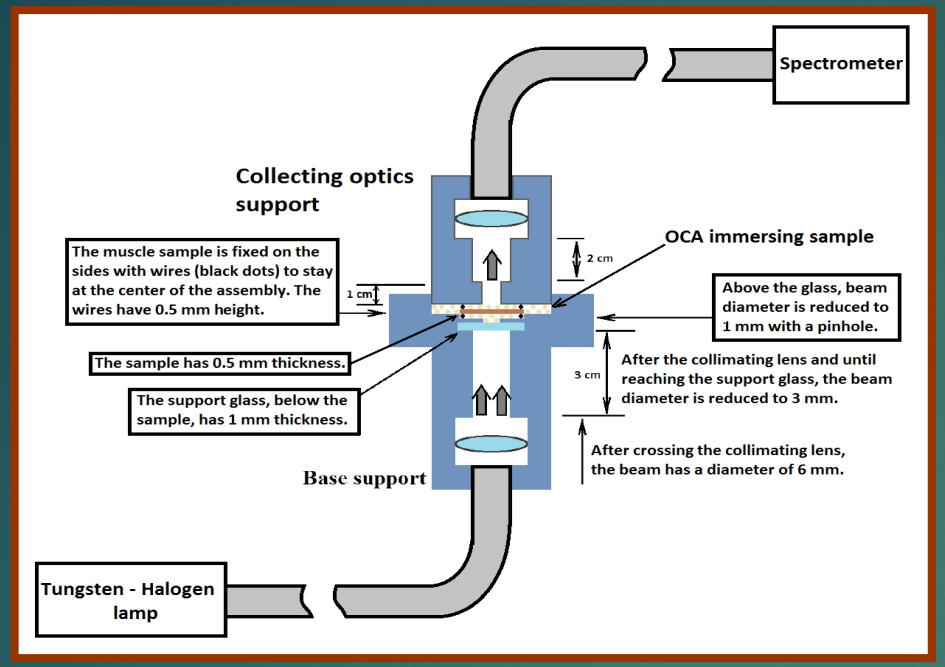

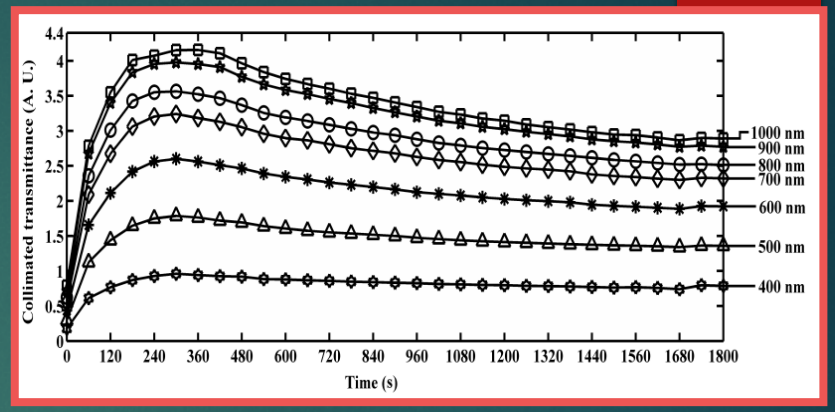

Glucose 20%

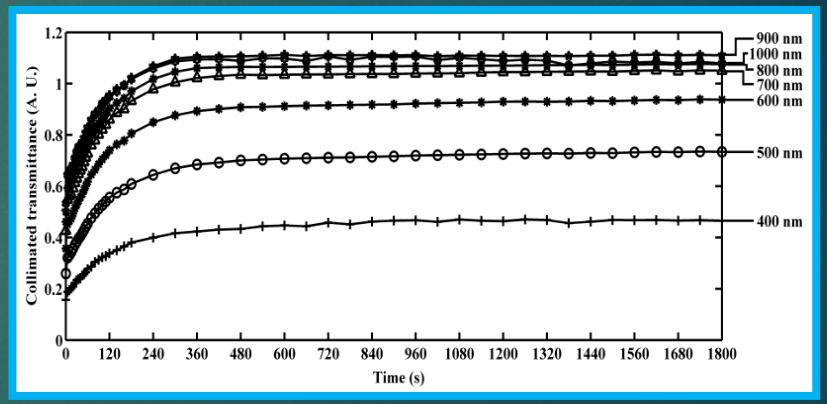

Glucose 50%

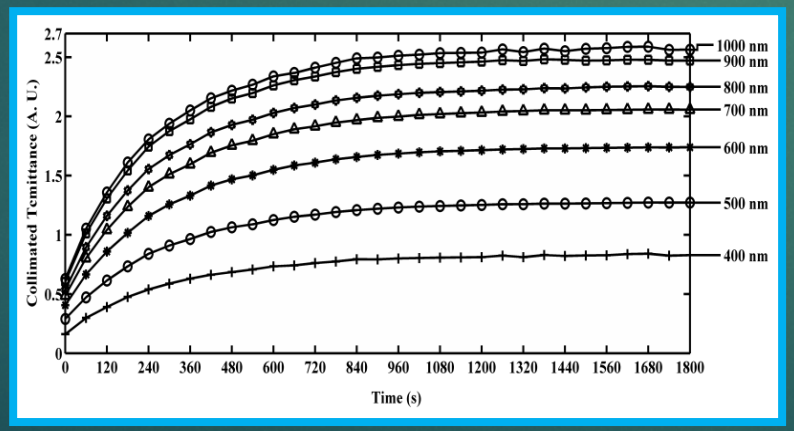

Glucose 40%

$$T_c(\lambda) \propto 1 - \exp\left(-\frac{t}{\tau}\right)$$

Diffusion time of Glucose and Ethylene Glycol in rat muscle

(L.Oliveira, M.I. Carvalho, E. Nogueira, V. V. Tuchin, *Laser Physics*, 2013, JBO, 2015)

$$\tau = \frac{l^2}{\pi^2 D_a}$$

$$D_a = 8.4 \times 10^{-7}\ cm^2 / s$$

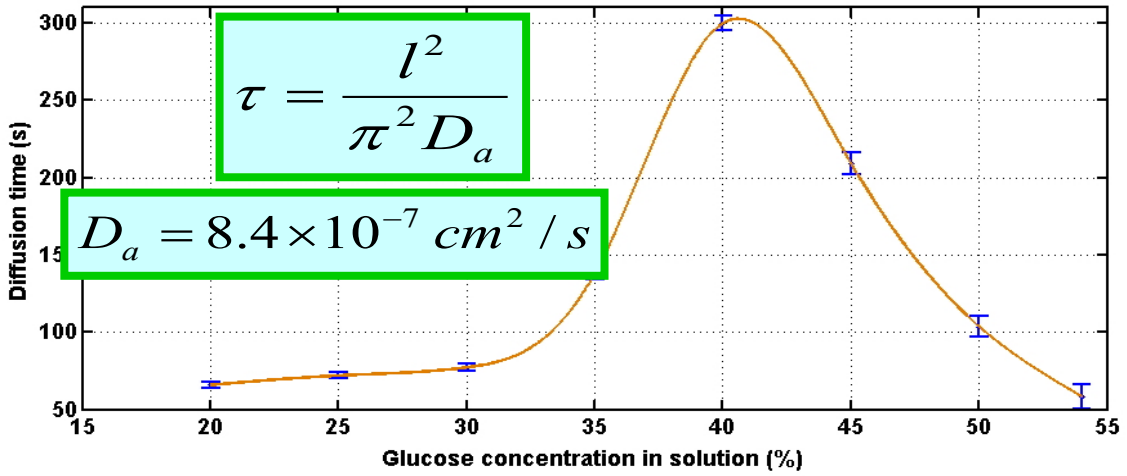

$$D_{EG} = 5.7 \times 10^{-7}\ cm^2 / s$$

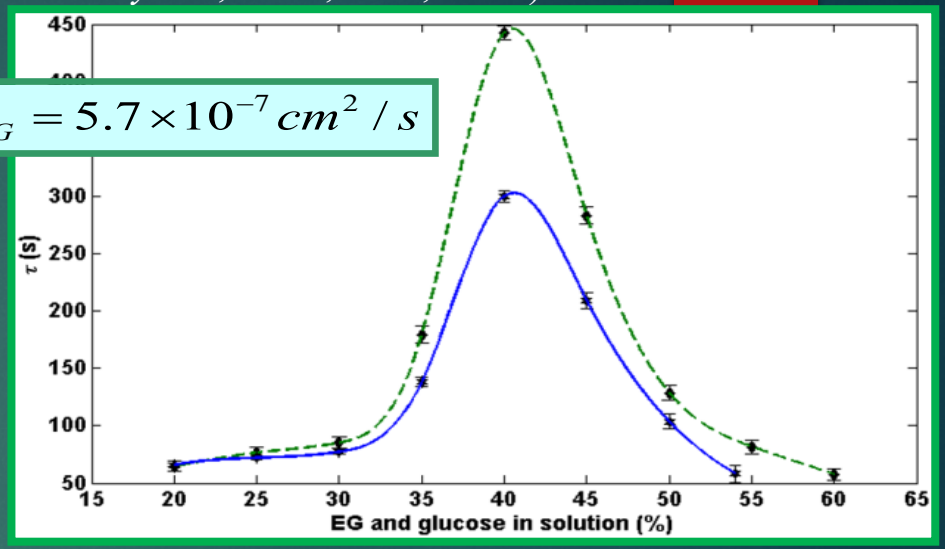

$$f_{water\ \ natural} = f_{bound\ \ water} + f_{free\ \ water} = 0.161 + 0.595 = 0.756$$

$$f_{solid\ part} = 0.244$$

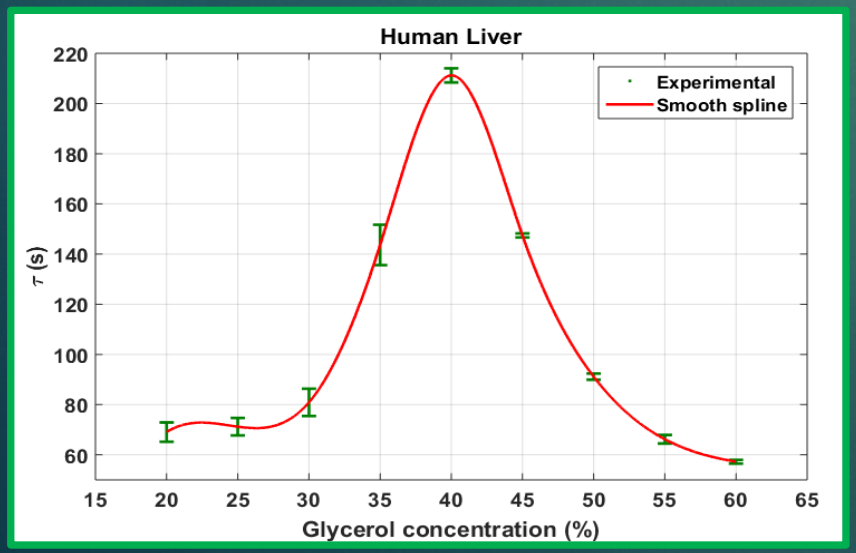

Evaluation of Water Content in **Human Liver**

I. Carneiro , S. Carvalho , R. Henrique , L. Oliveira , V. V. Tuchin, Simple multimodal optical technique for evaluation of free/bound water and dispersion of human liver tissue *J. Biomed. Opt.* 22(12), 125002 (2017)

Glycerol-Water Solution

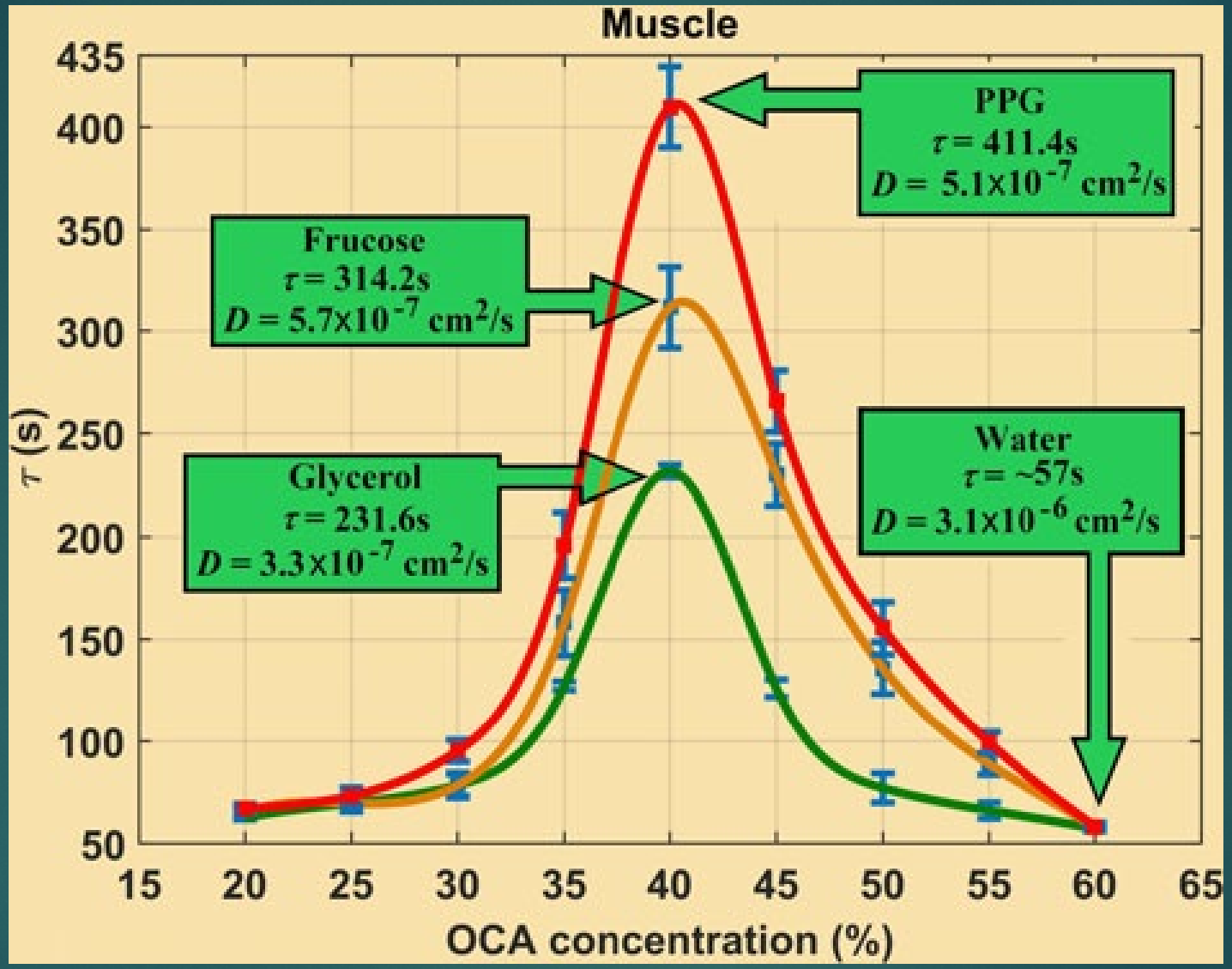

I. Carneiro, S. Carvalho, R. Henrique, L. M. Oliveira, V. V. Tuchin, A robust *ex vivo* method to evaluate the diffusion properties of agents in biological tissues, *J. Biophotonics* **12**(4), e201800333 (2019)

Diffusion time for healthy colon mucosa and tumor

Tissue type	Mucosa									
OCA concentration	10%	15%	20%	25%	30%	35%	40%	45%	50%	54%
Diffusion time , s			65.1	69.4	81.1	138.4	299.2	211.5	104.3	55.7
SD			0.2	3.2	6.1	5.9	4.7	6.1	1.3	5.9
Tissue type	**Tumor**									
Diffusion time , s	62.9	68.6	71.1	73.9	136.1	320.6	234.9	139.0	82.7	58.4
SD	0.5	0.2	0.5	1.5	1.1	10.6	4.1	14.0	2.0	1.7

(L. Oliveira *et al*, Glucose diffusion in colon mucosa – a comparative study between healthy and cancerous tissue, J. Biomed. Opt. 22(9), 091506 (2017)**)**

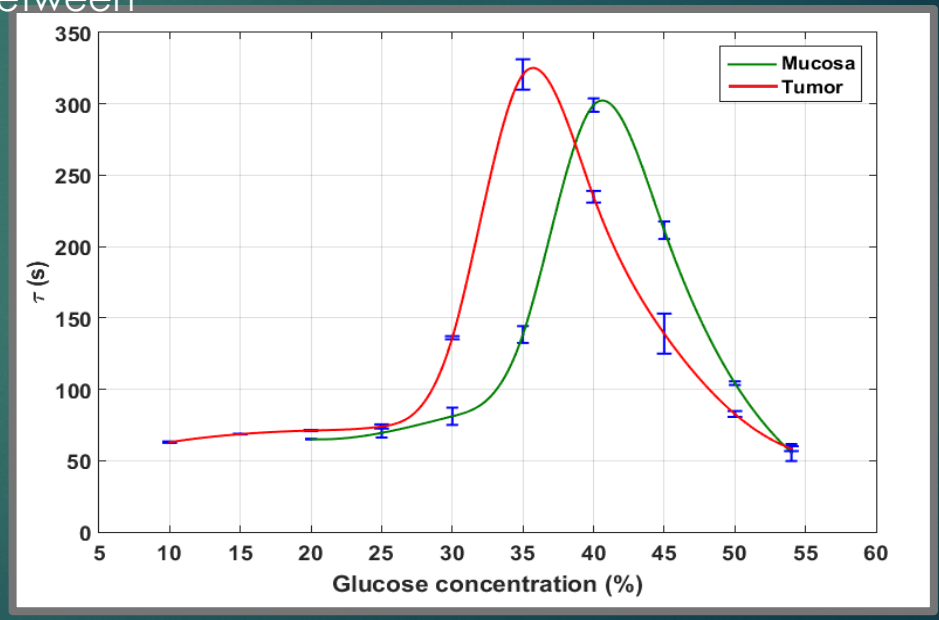

(Software from: P. Peixoto, L. Oliveira, M. I. Carvalho, E. Nogueira, and V.V. Tuchin, Software development for estimation of optical clearing agent's diffusion coefficients in biological tissues, *J. Biomed. Photonics & Eng* **1**(4) 255, 2016**)**

Diffusion time for healthy colon mucosa and tumor

Tissue type	Mucosa									
OCA concentration	10%	15%	20%	25%	30%	35%	40%	45%	50%	54%
Diffusion time , s			65.1	69.4	81.1	138.4	299.2	211.5	104.3	55.7
SD			0.2	3.2	6.1	5.9	4.7	6.1	1.3	5.9
Tissue type	**Tumor**									
Diffusion time , s	62.9	68.6	71.1	73.9	136.1	320.6	234.9	139.0	82.7	58.4
SD	0.5	0.2	0.5	1.5	1.1	10.6	4.1	14.0	2.0	1.7

(L. Oliveira *et al*, Glucose diffusion in colon mucosa – a comparative study between healthy and cancerous tissue, J. Biomed. Opt. 22(9), 091506 (2017)**)**

Tumor has ~5% more free-water content than mucosa

Glucose takes more time to diffuse into tumor than into mucosa

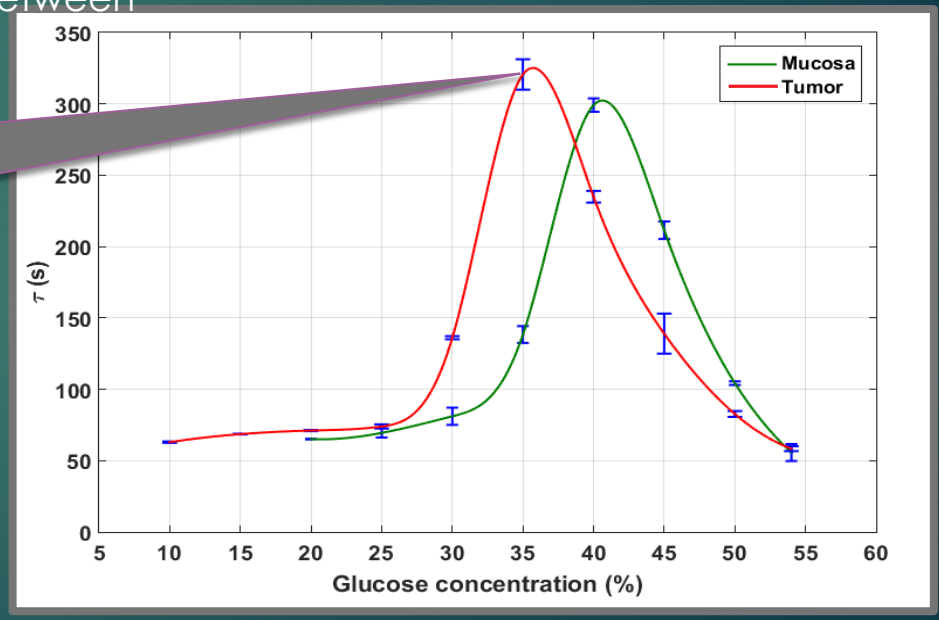

(Software from: P. Peixoto, L. Oliveira, M. I. Carvalho, E. Nogueira, and V.V. Tuchin, Software development for estimation of optical clearing agent's diffusion coefficients in biological tissues, *J. Biomed. Photonics & Eng* **1**(4) 255, 2016**)**

Diffusion time for healthy colon mucosa and tumor

Tissue type	Mucosa									
OCA concentration	10%	15%	20%	25%	30%	35%	40%	45%	50%	54%
Diffusion time , s			65.1	69.4	81.1	138.4	299.2	211.5	104.3	55.7
SD			0.2	3.2	6.1	5.9	4.7	6.1	1.3	5.9
Tissue type	**Tumor**									
Diffusion time , s	62.9	68.6	71.1	73.9	136.1	320.6	234.9	139.0	82.7	58.4
SD	0.5	0.2	0.5	1.5	1.1	10.6	4.1	14.0	2.0	1.7

(L. Oliveira *et al*, Glucose diffusion in colon mucosa – a comparative study between healthy and cancerous tissue, J. Biomed. Opt. 22(9), 091506 (2017)**)**

Tumor has ~5% more free-water content than mucosa

Glucose takes more time to diffuse into tumor than into mucosa

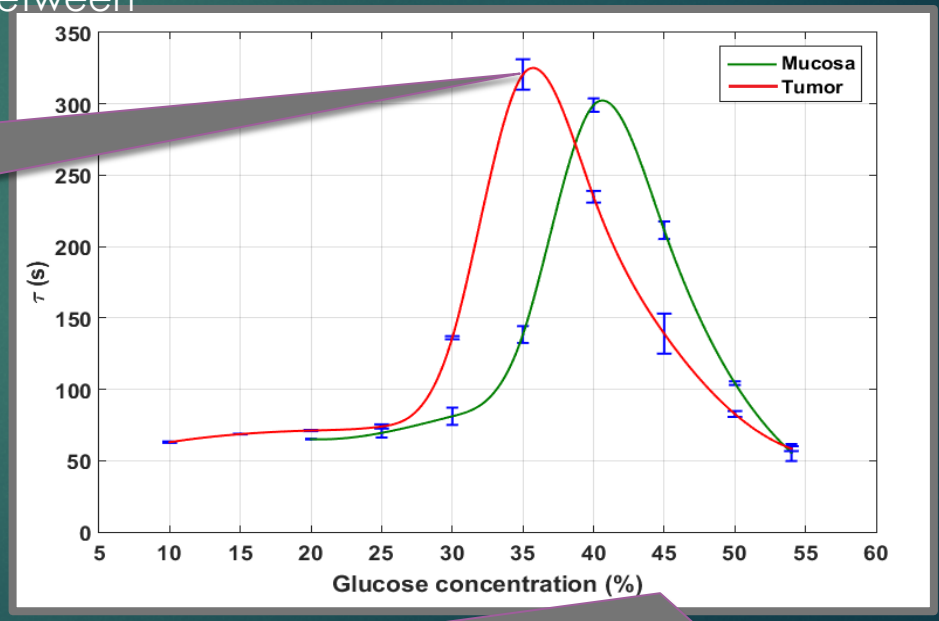

(Software from: P. Peixoto, L. Oliveira, M. I. Carvalho, E. Nogueira, and V.V. Tuchin, Software development for estimation of optical clearing agent's diffusion coefficients in biological tissues, *J. Biomed. Photonics & Eng* **1**(4) 255, 2016**)**

Normal mucosa shows similar results to muscle tissue (Oliveira *et al*, 2013)

Protocol for *diabetes mellitus* model

Diabetes mellitus was induced by injection of a single dose of alloxan (Acros Organic, Belgium) mixed with saline to white Wistar rats as 10 mg of alloxan per 100 g body mass

Control group

Average level of glucose in blood

Time	Before	3 weeks	4 weeks
Free glucose in blood, mg/dL	70±5	290±159	420±86

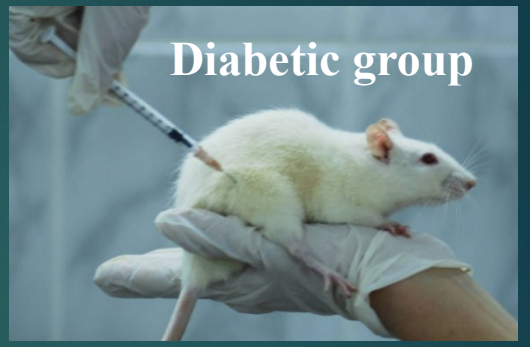

Spectral measurements

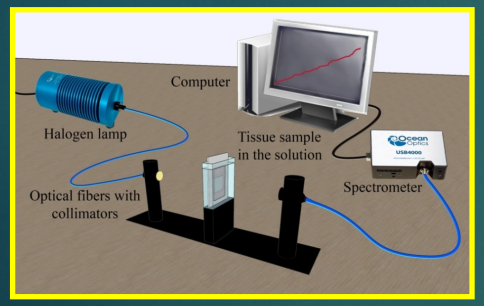

Collimated transmittance

UV-3600 spectrometer (Shimadzu), 350-2500 nm

OCT

Spectral Radar OCT System OCP930SR 022 (Thorlabs Inc., 930 nm)
Spectral band 100 nm
Output power – 2 mW
Scanning depth on air – 1.6 mm
In depth spatial resolution - 6.2 um (air)

GANYMEDE, SD-OCT (930 nm) Spectral band 150 nm
Scanning rate A-scan 30 kHz
Scanning depth on air – 2.7 mm
In depth spatial resolution - 5.8 /4.4 um (air/water)

Ex Vivo Measurements of Collimated Transmittance

Collimated transmittance kinetics of control and diabetic skin samples during treatment by 30%- (a, b), 43%- (c, d), and 56%- (e, f) glucose solutions measured for different wavelengths

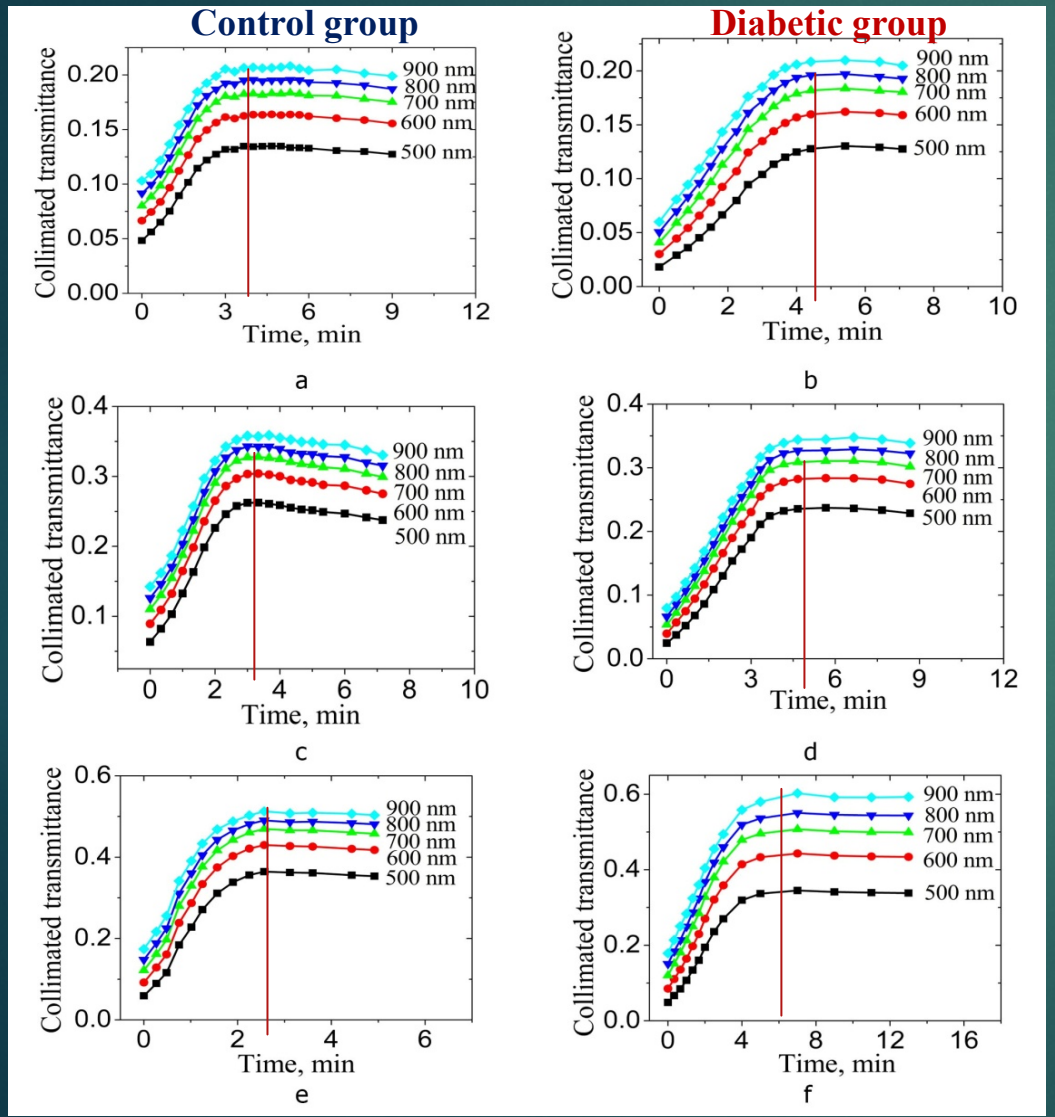

$$T_c(\lambda) \propto 1 - \exp\left(-\frac{t}{\tau}\right)$$

ex vivo

$$\tau = \frac{l^2}{\pi^2 D_a}$$

$$P = \frac{\pi^2 D}{l}$$

in vivo

$$\tau = \frac{4d^2}{\pi^2 D_a}$$

Glucose diffusion coefficients in the skin of mice of control and diabetic groups

Conc.	D (cm^2/sec)
Control group	
30%	$(2.87\pm1.53)\times10^{-6}$
43%	$(2.70\pm2.22)\times10^{-6}$
56%	$(1.40\pm0.96)\times10^{-6}$
Diabetic group	
30%	$(1.06\pm0.55)\times10^{-6}$
43%	$(1.15\pm0.63)\times10^{-6}$
56%	$(1.02\pm0.44)\times10^{-6}$

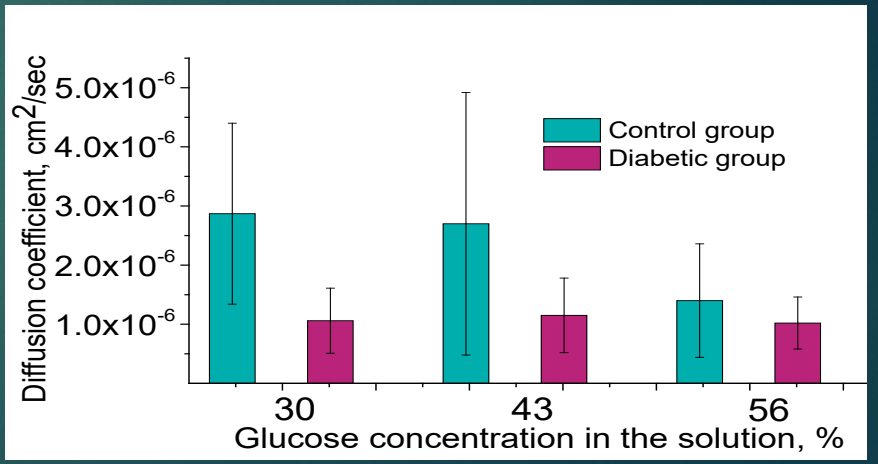

Tuchina D. K., et al. *Ex vivo* optical measurements of glucose diffusion kinetics in native and diabetic mouse skin, *Journal of Biophotonics*, 8(4), 273-356, 2015 (85)

Ex Vivo Measurements of Collimated Transmittance

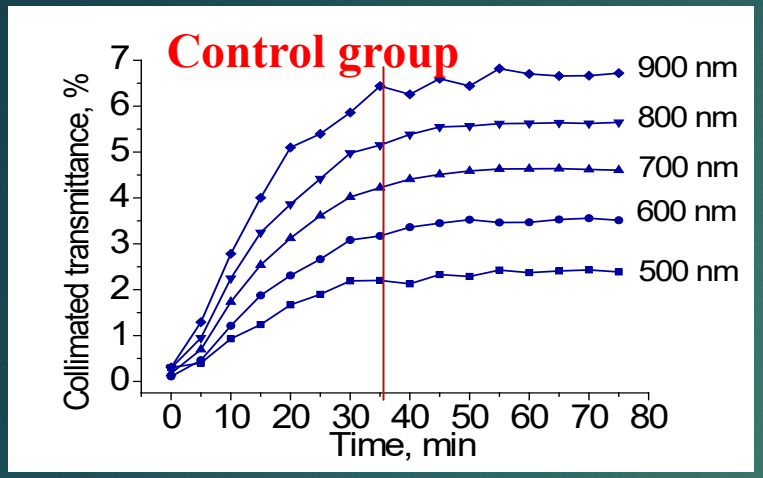

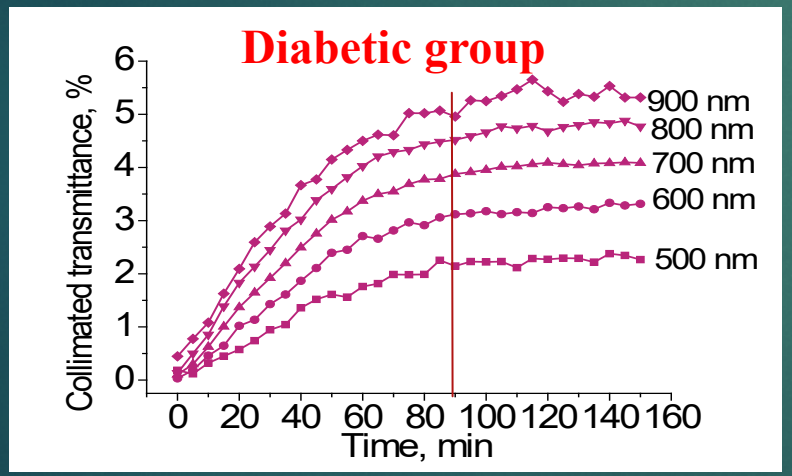

Time dependences of collimated transmittance of the skin samples from control and diabetic groups during the immersion in 60%-glycerol solution

60%-glycerol solution

Glycerol diffusion and permeability coefficient for tissues

Tissue (Group)	*D*, cm²/sec	*P*, cm/sec
Skin (Control/ Diabetic)	$(2.13\pm1.21)\times10^{-6}$/ $(0.761\pm0.28)\times10^{-6}$	$(7.18\pm4.40)\times10^{-5}$/ $(1.30\pm0.67)\times10^{-5}$
Myocardium (Control/ Diabetic)	$(8.65\pm4.59)\times10^{-7}$/ $(5.32\pm1.99)\times10^{-7}$	$(9.20\pm4.42)\times10^{-5}$/ $(7.52\pm2.24)\times10^{-5}$

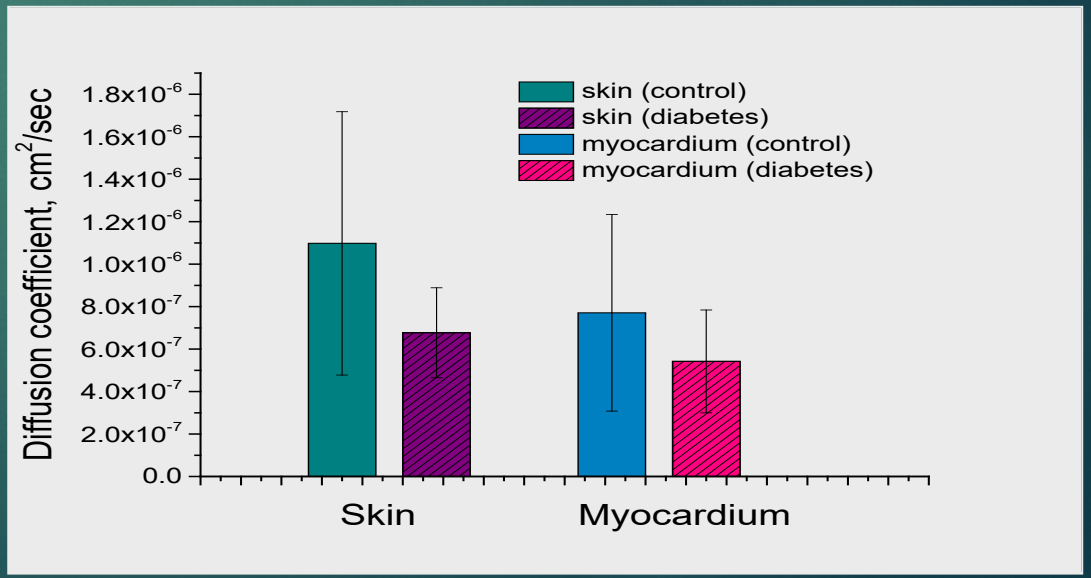

Glycerol as a biomarker of diabetes impact on tissues (D. K. Tuchina, et al. (2018))

Control group

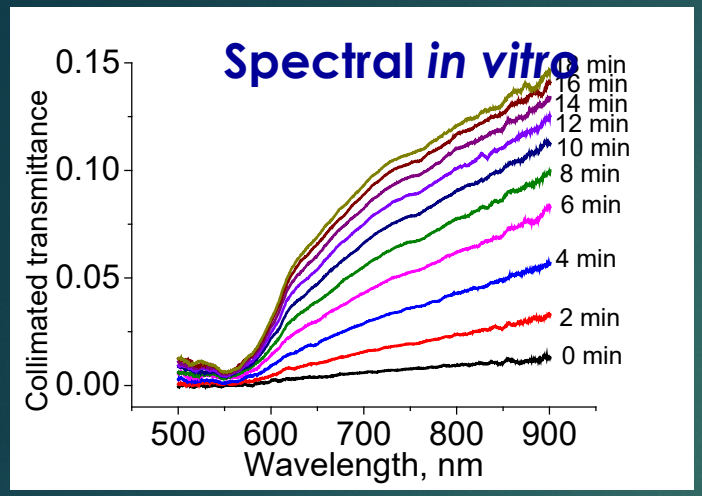

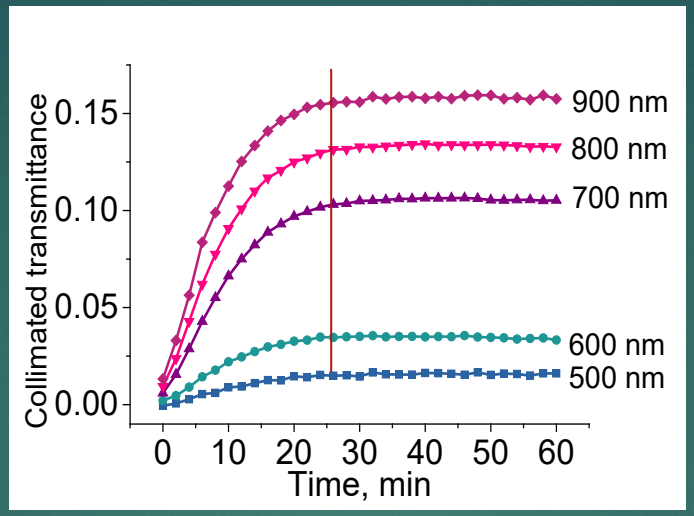

Diabetic group

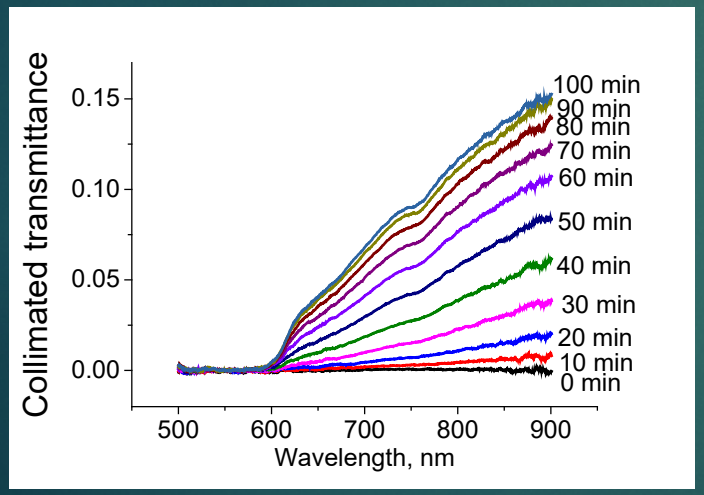

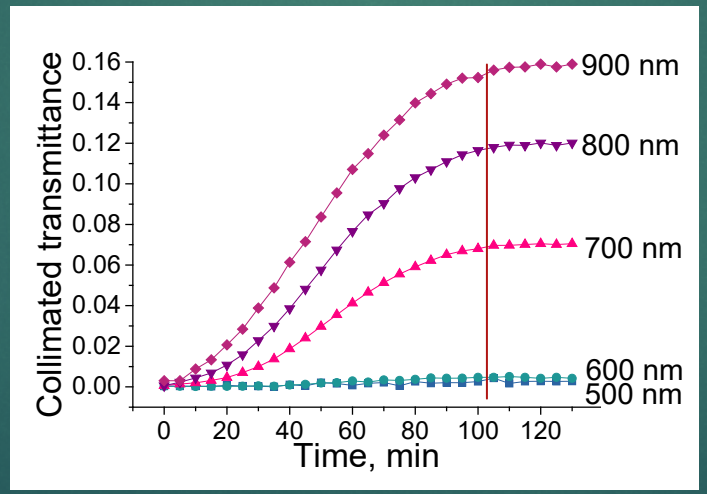

OCT *in vivo*

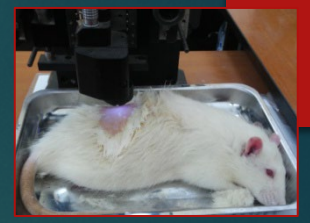

Control group

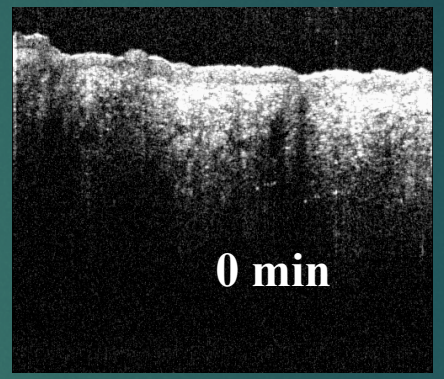

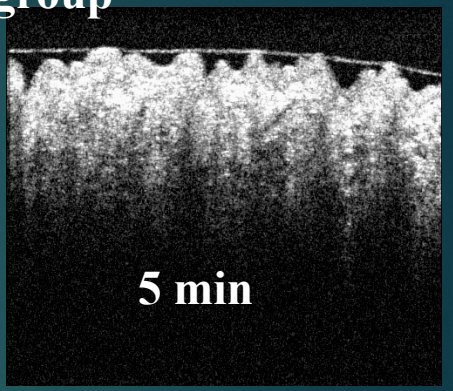

Diabetic group

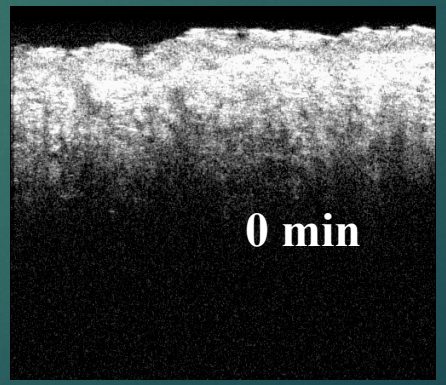

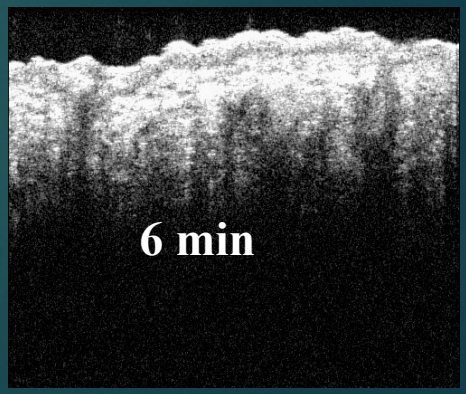

Parameter	Control group	Diabetic group
Skin	$(1.68\pm0.88)\times10^{-5}$	$(1.00\pm0.57)\times10^{-5}$
Myocardium	$(11.8\pm6.1)\times10^{-5}$	$(1.04\pm0.65)\times10^{-5}$

	Control group	Diabetic group
Optical clearing degree (A×100%)	46±19	37±16
Characteristic time of optical clearing, min (τ)	2.7±0.4	8.9±7.7

Creation of UV window

I. Carneiro, S. Carvalho, R. Henrique, L. M. Oliveira, V. V. Tuchin, Moving tissue spectral window to the deep-ultraviolet via optical clearing, *J. Biophotonics*. **12** (12), e201900181 (2019).

The sample was immersed in the **glycerol** solution and measurements (200-1000 nm) were aquired during 30 min treatment with a 5 s - time resolution

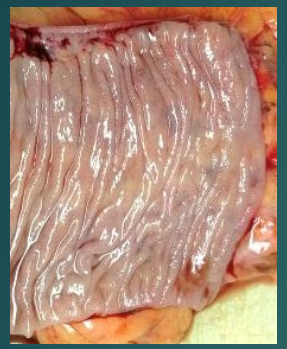

Surgical colorectal specimen

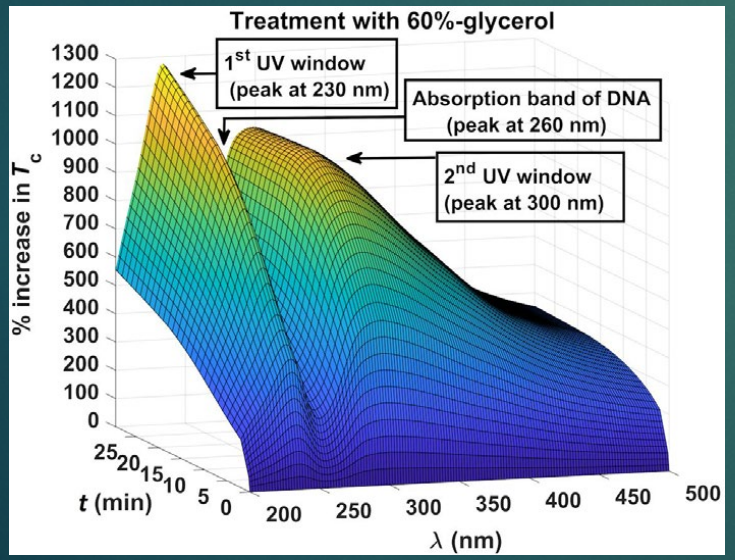

$$\%\ \boldsymbol{increase\ in}\ T_c = \frac{T_c(\lambda,t) - T_c(\lambda,t=0)}{T_c(\lambda,t=0)} \times 100\%$$

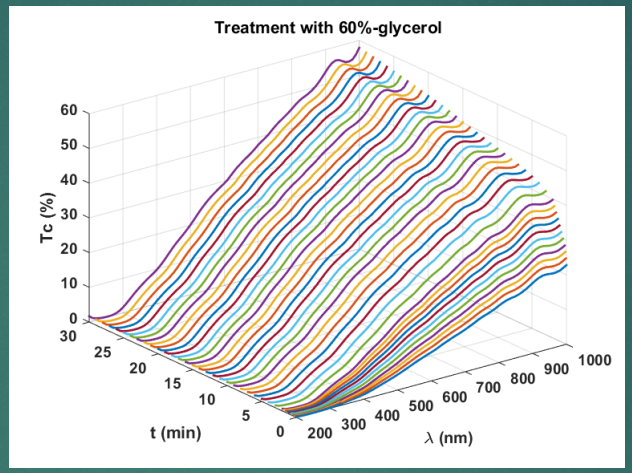

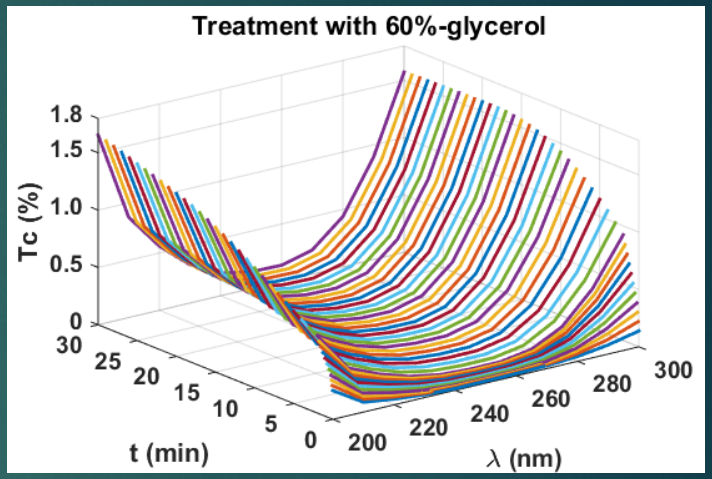

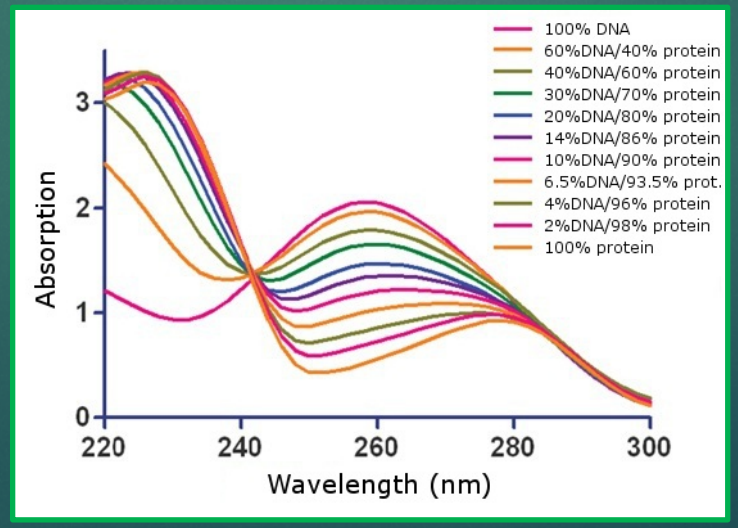

Similar behavior is observed on both sides of the DNA/Protein absorption band

The OC effect in UV improves with the increase of glycerol concentration in the solution

The effectiveness of human gum optical clearing

A. A. Selifonov , V. V. Tuchin, Kinetics of optical properties on selected laser lines of human periodontal gingiva when exposed to glycerol-propylene glycol mixture , FLAMN, St. Petersburg, July 2019.

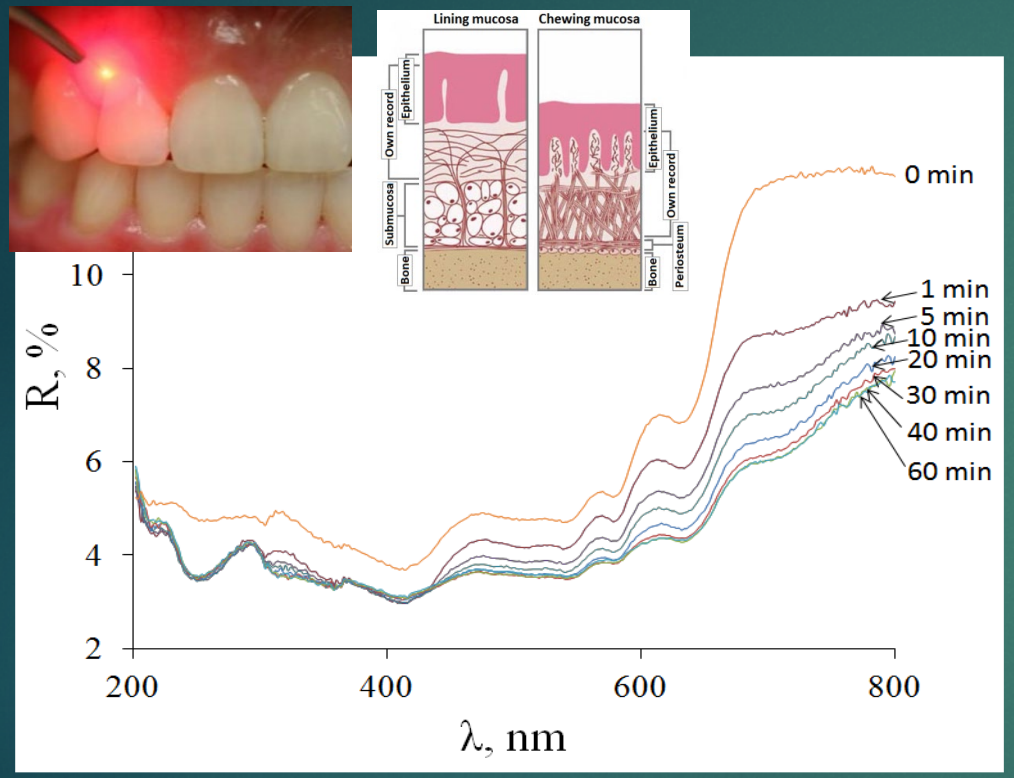

OCA: 99.7% glycerol

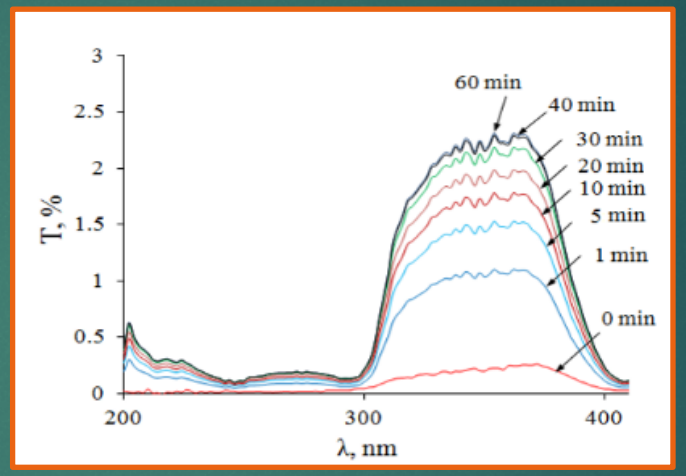

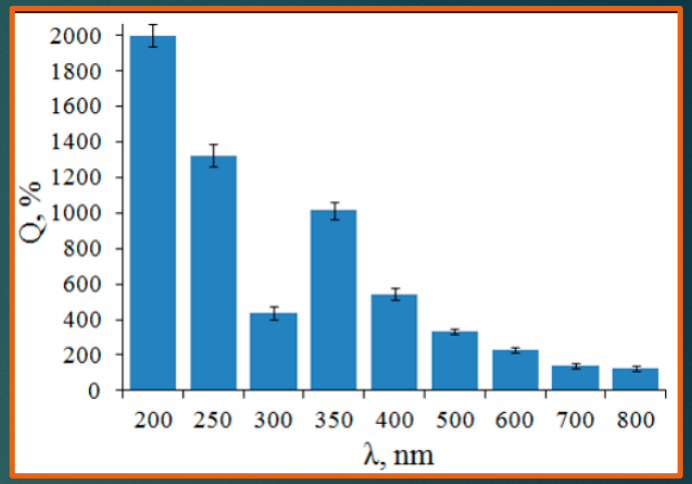

The effectiveness of human gum OC in propylene glycol / glycerol / water mixture

E-cigarette vapor liquid

The effective diffusion coefficient of mixtures in human gum mucous tissue measured *in vitro* :

D **(30/70/0) = (2.3±0.4) ·10^{-6} cm^2/s**

D **(50/50/0) = (2.6±0.6) ·10^{-6} cm^2/s**

D **(55/35/10) = (3.2±0.8) ·10^{-6} cm^2/s**

Fingerprint Raman spectra of porcine ear skin at OC

A. Yu. Sdobnov et. al. J. Physics D: Appl. Phys. 50, 285401(2017)

Confocal Raman Microscope (CRM) for *in vivo/ex vivo* skin measurements
River Diagnostics, Model 3510 SCA, Rotterdam, The Netherlands: 785 nm, oil objective ×50, laser power 20 mW, exposure 5 s, resolutions ≤ 5 μm and 2 cm^{-1}

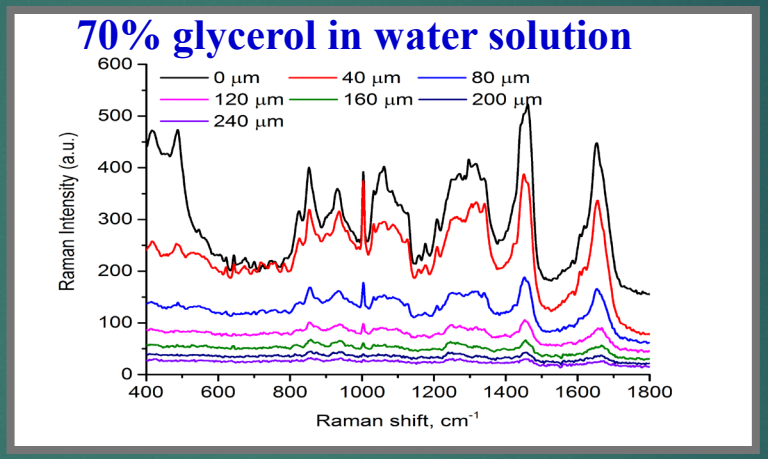

Glycerol

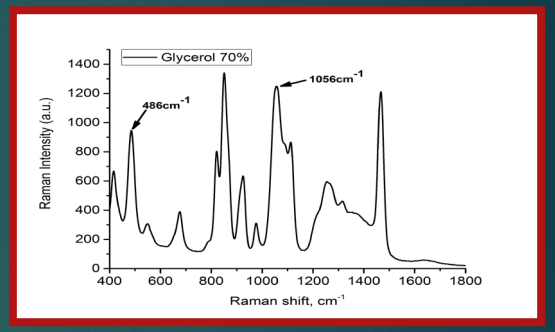

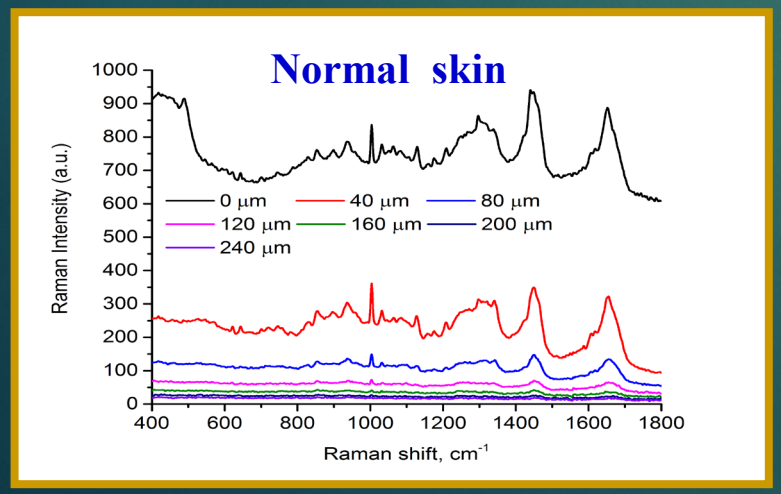

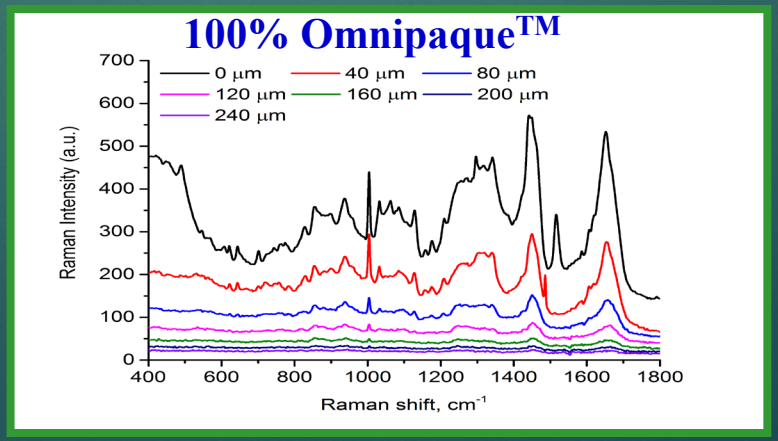

Omnipaque™

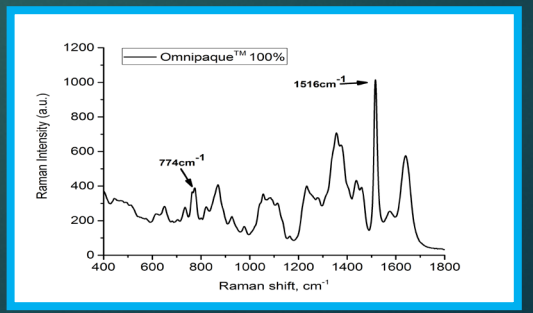

A. Sdobnov et al., Hydrogen bound water profiles in the skin influenced by optical clearing molecular agents- quantitative analysis using confocal Raman microscopy, *J. Biophotonics* 12 (5), e201800283 (2019)

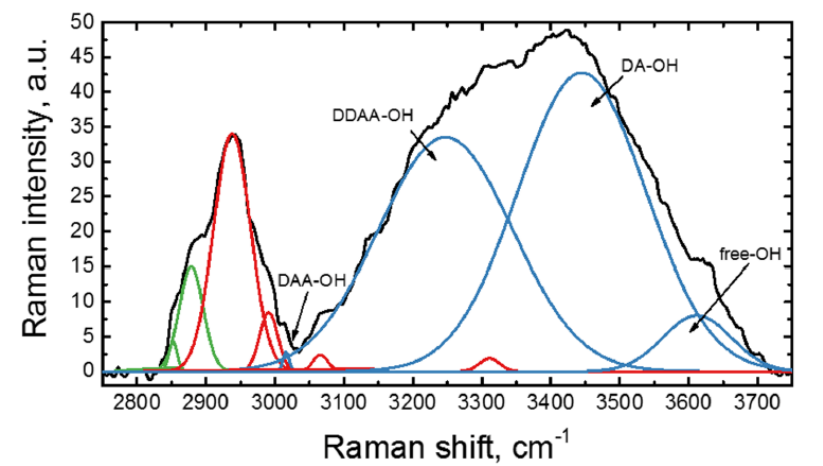

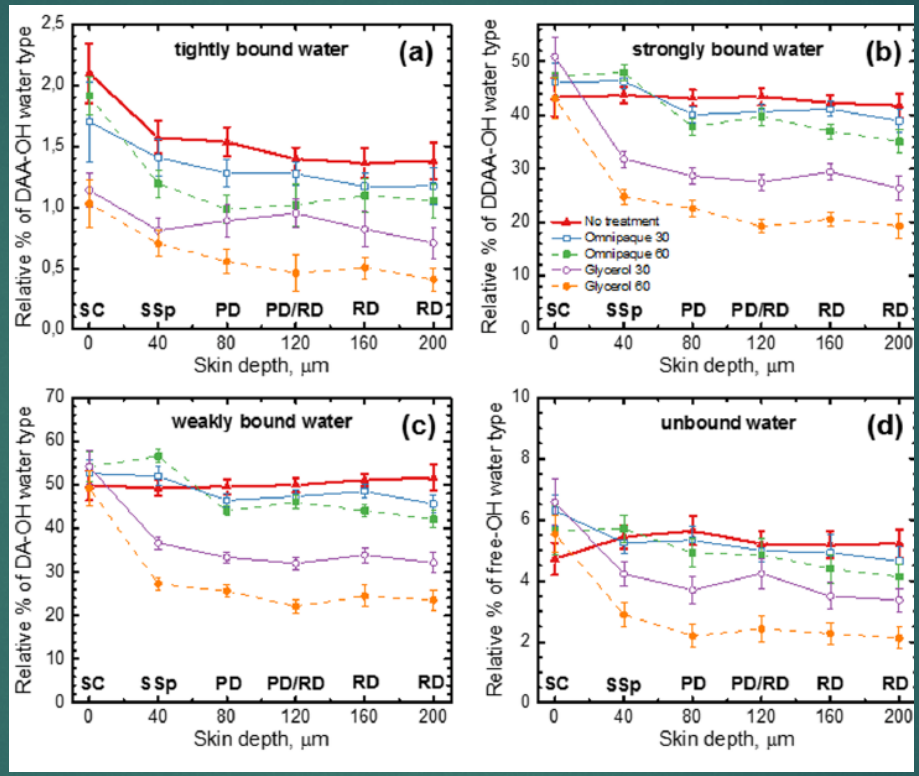

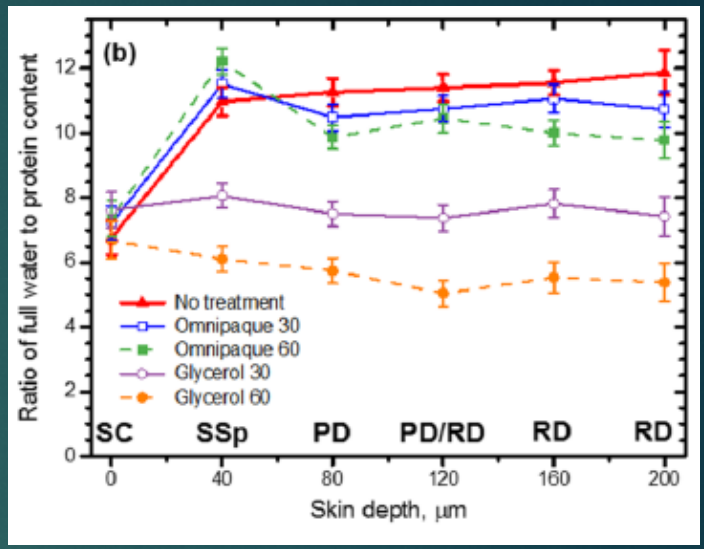

Total water content (the ratio of full water to content of proteins).

The depth distribution of the relative percentage of DAA–OH (a), DDAA–OH (b), DA–OH (c) and free–OH (d) water types in the untreated skin (thick red line) and in the skin treated with Omnipaque for 30 min / 60 min and in the skin treated with glycerol for 30 min / 60 min)

SC – stratum corneum; SSp – stratum spinosum; PD – papillary dermis; RD – reticular dermis.

Kinetics of OC of human skin studied *in vivo* using a fiber Raman probe

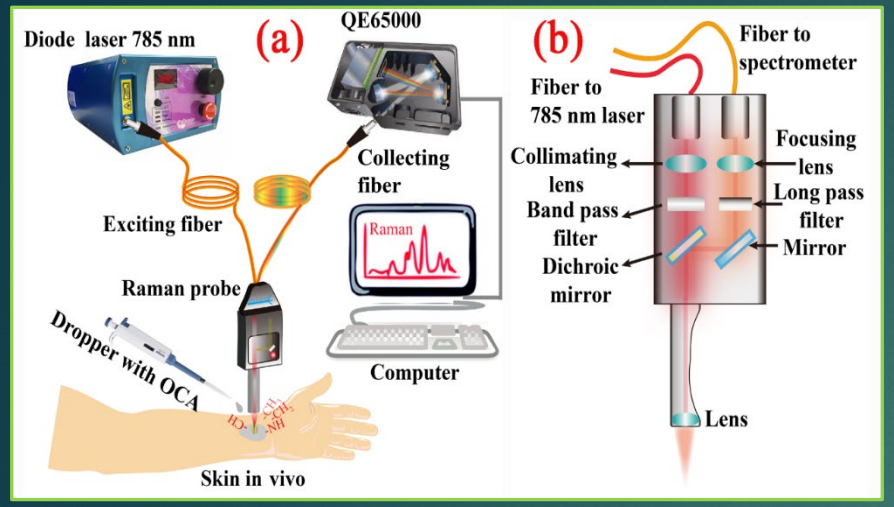

Diagram of the Raman experimental device (a) and detail of Raman probe (b)

Q. Lin et al., *Laser Phys. Lett.* (2020)

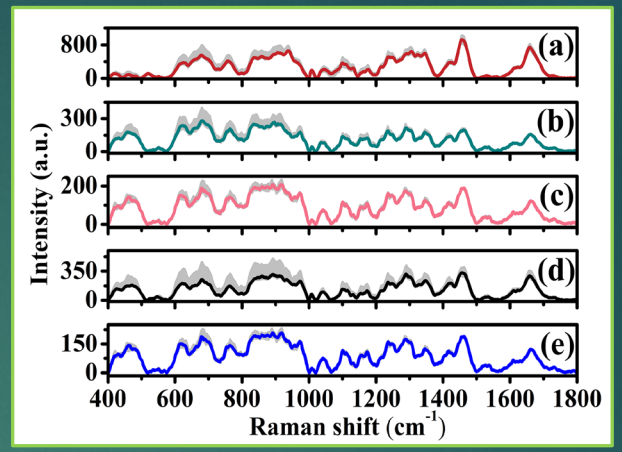

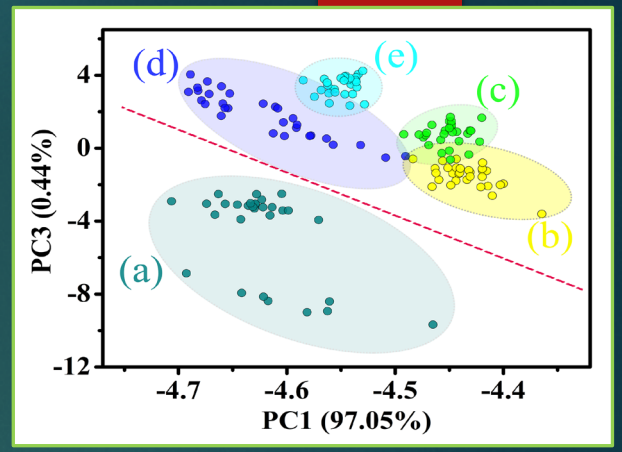

In vivo Raman spectra and PC scores scatter plots for the Raman spectra acquired from different body sites: : fingernail (a), finger (b), arm (c), palm (d), and wrist (e)

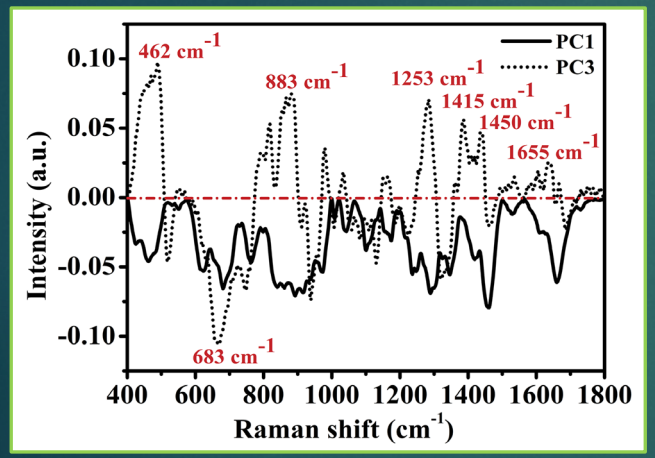

PC loading plots of the 1st (solid-line) and 3rd PCs (dotted-line) for the Raman spectra of different body sites

Raman spectra contribute differently to the classification

The PC variations of the different skin sites were largely dominated by bands at:

- **462 cm^{-1} (δ(CCC), proteins)**
- 683 cm^{-1} (ν(CS), amino acid)
- 883 cm^{-1} (ρ(CH$_2$)/ν(CC)/ν(CN), collagen)
- 1253 cm^{-1} (δ(CH$_2$)/ν(CN), nucleus)
- **1415 cm^{-1} (δ(CH$_3$), lipids)**
- 1450 cm^{-1} (δ(CH$_2$)/δ(CH$_3$); keratin, collagen)
- 1655 cm^{-1} (ν(C=O), keratin)

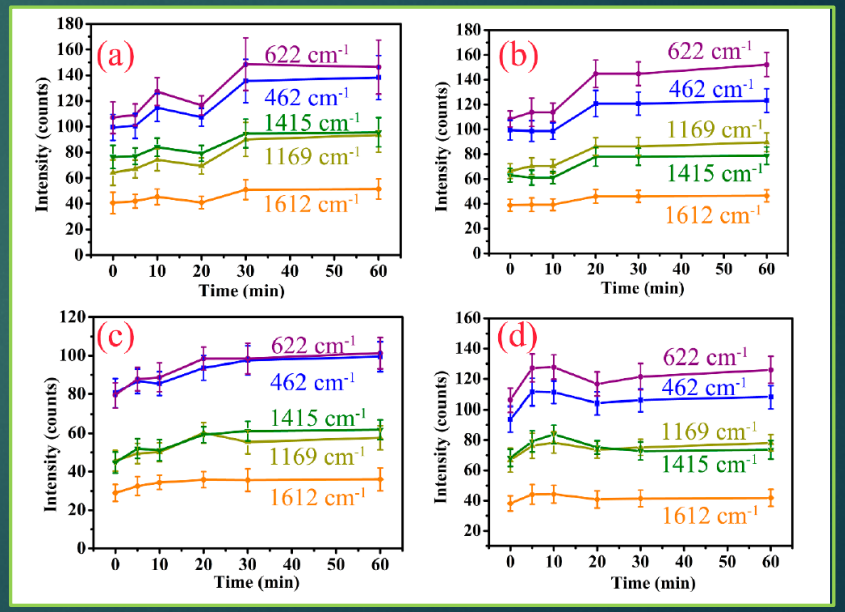

The time dependencies of wrist skin Raman peaks after application of glycerol with different concentration: 30% (a), 50% (b), 70% (c), and 99.9% (d).

Nonlinear Microscopy

A. Sdobnov, M. E. Darvin, J. Lademann, V. Tuchin, Enhanced Two-photon Microscopy of Skin by Immersion Optical Clearing, *J. Biophotonics* (2017)

TPEAF and SHG images of skin layers obtained *ex vivo* on porcine ear skin samples for Omnipaque™ and glycerol solutions

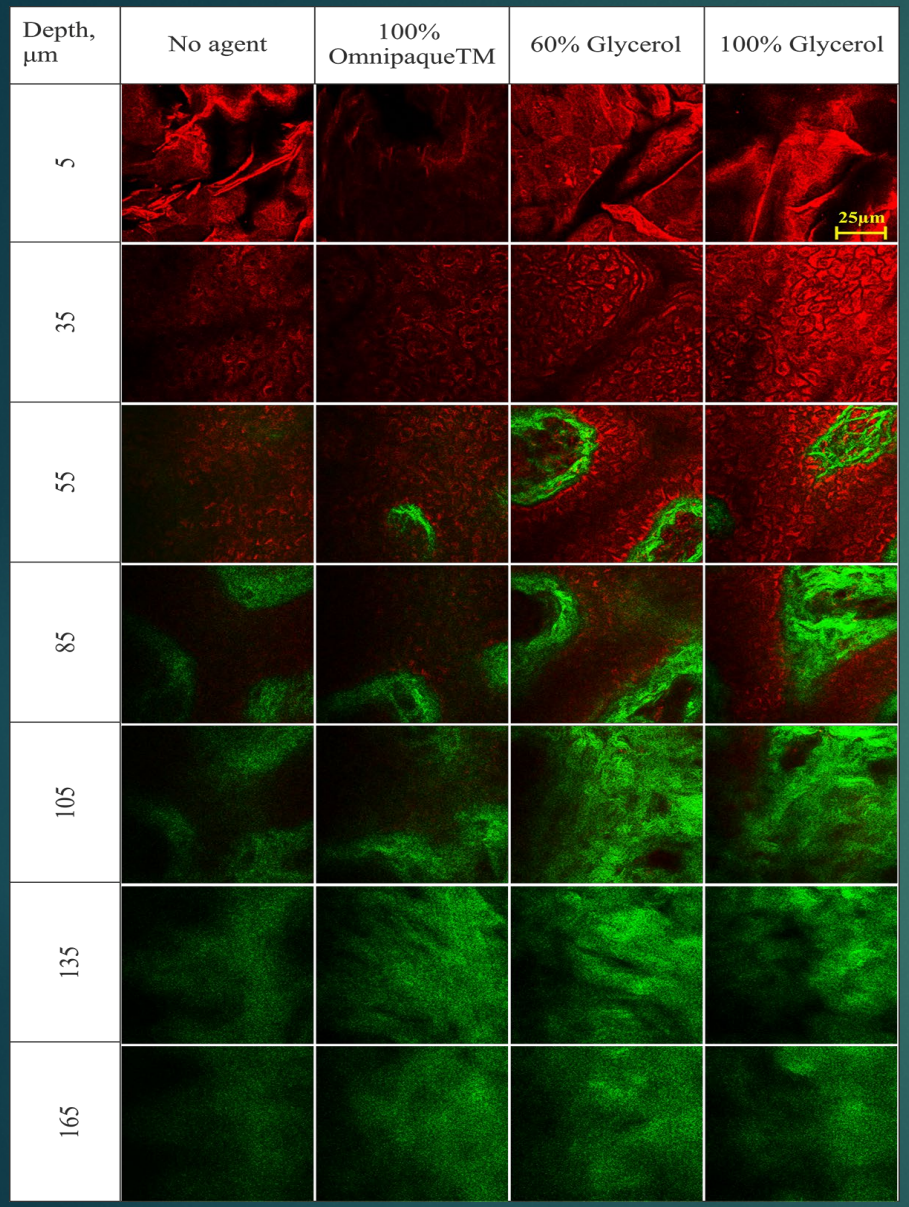

Red – **TPEAF** signal
Green - **SHG** signal

OCA	Glycerol			Omnipaque	
Concentration,%	40	60	100	60	100
Refractive index, n	1.384	1.413	1.474	1.392	1.432
Osmolarity, Osm/L	5.5	8.2	10.9	0.33	0.465
Viscosity, cp	3.7	10.8	1410	3.1	11.8

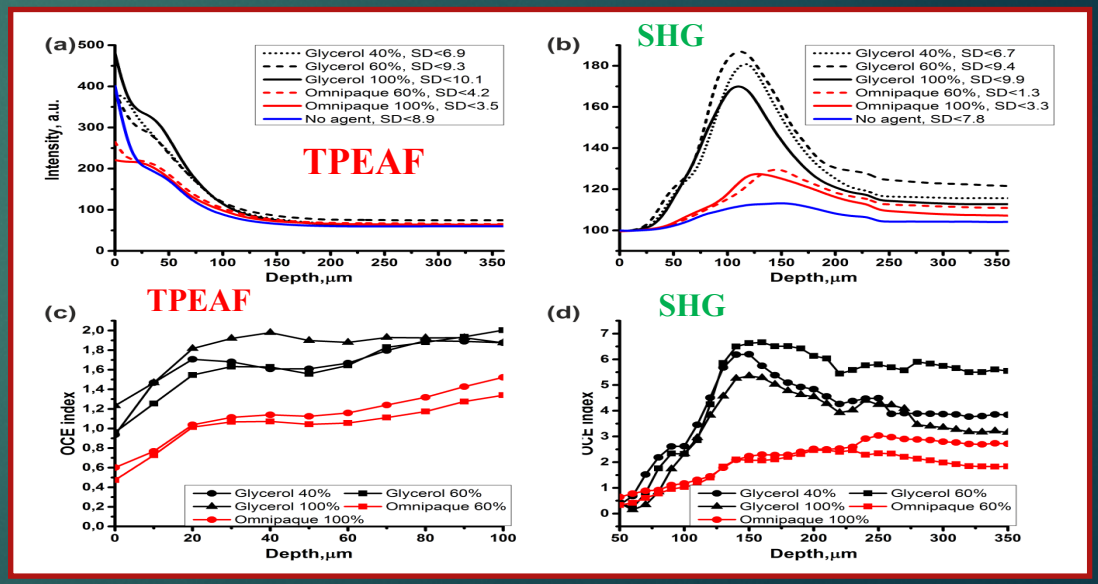

Averaged depth-dependent intensity profiles and **OCE** indices for TPEAF (a, c) and SHG (b, d) signals

OCT/Cartilage/Omnipaque as an OCA

A. Bykov et.al. , Imaging of subchondral bone by optical coherence tomography upon optical clearing of articular cartilage, J. Biophotonics, 2015; DOI: 10.1002/jbio.201500130)

Cleared cartilage

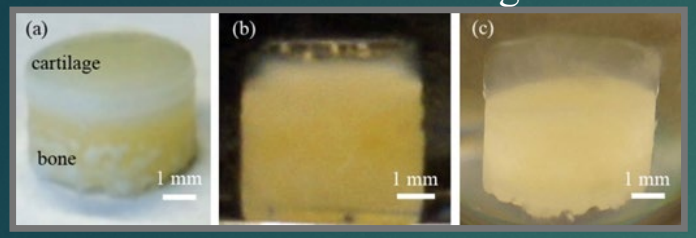

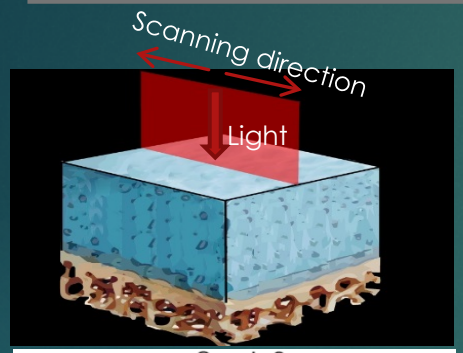

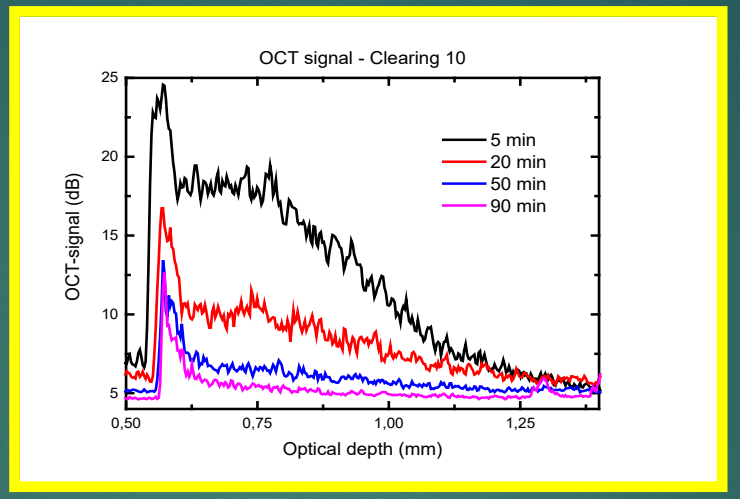

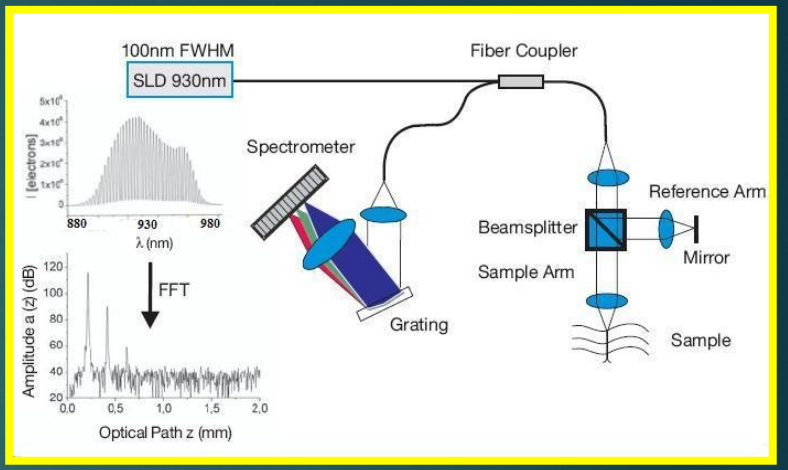

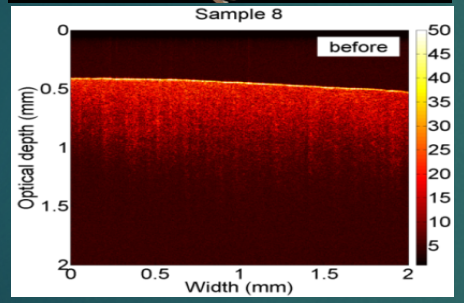

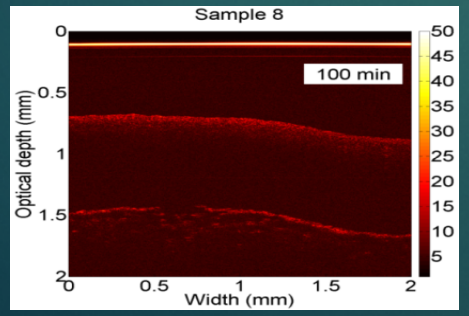

15 min of clearing by Omnipaque

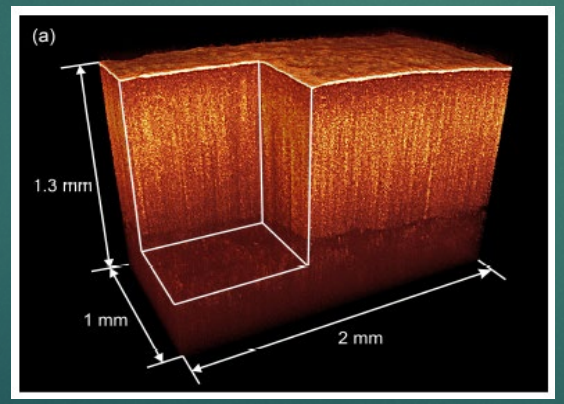

3D OCT image

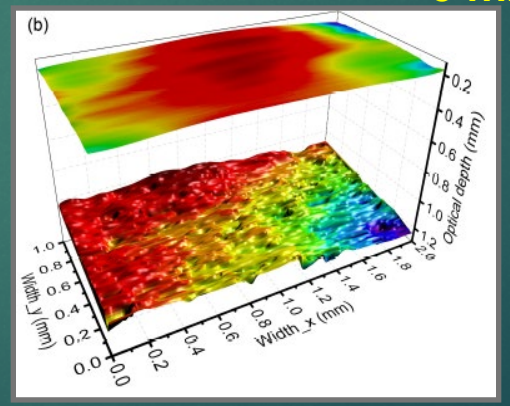

Roughness of the cartilage-bone interface Sa = 10 μm

5 min of clearing by Propylene Glycol

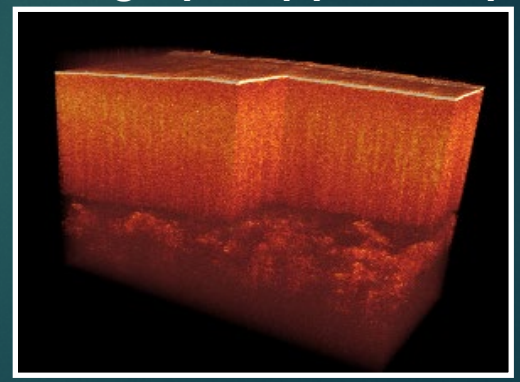

3D OCT image

Photoacoustic microscopy and flow cytometry

Y.A. Menyaev, D.A. Nedosekin, M. Sarimollaoglu, M.A. Juratli, E.I. Galanzha, V.V. Tuchin, and V.P. Zharov, Skin optical clearing for in vivo photoacoustic flow cytometry, Biomed. Opt. Express 4 (**12**), 3030-3041 **(2013)**

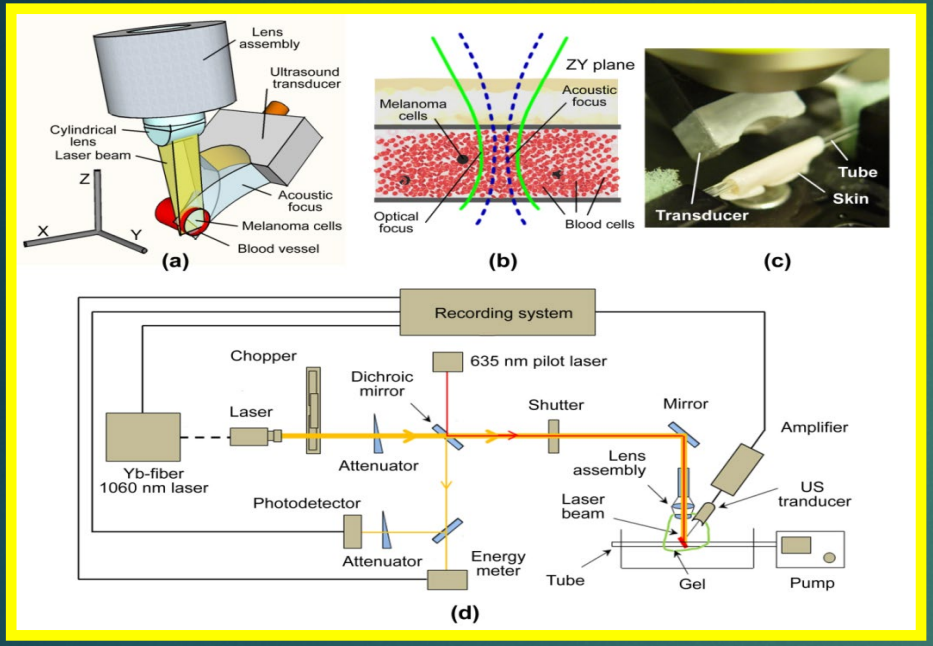

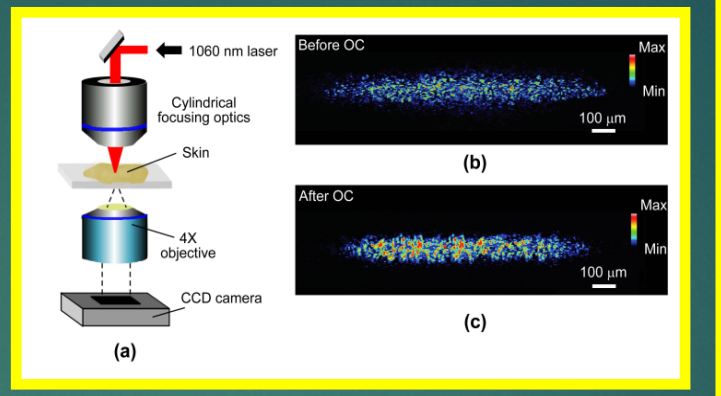

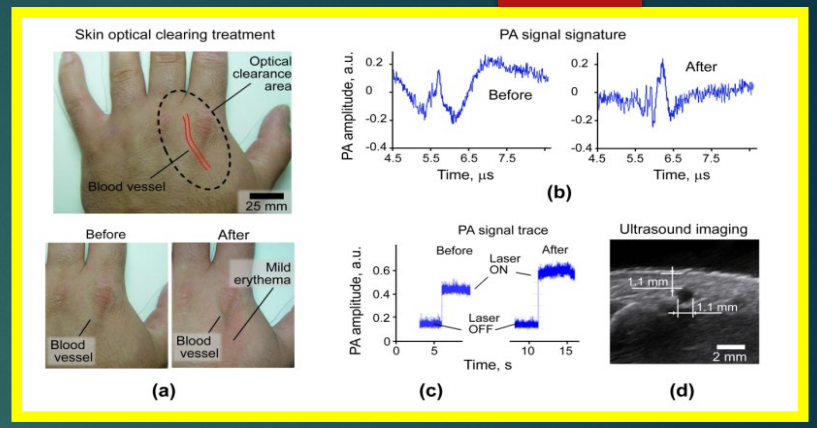

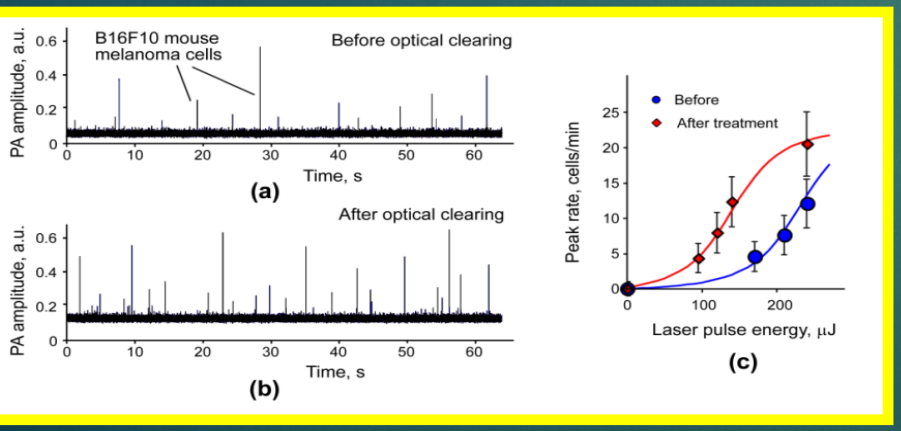

Kinnunen M., et al, Optical Clearing at Cellular Level. *J. Biomed. Opt*. 19, 71409 (2014)

Dan Zhu and Xunbin Wei et al. Signal and depth enhancement for *in vivo* flow cytometer measurement of ear skin by optical clearing agents, *Biomed. Opt. Express* 4 (11), 2518-2526 (2013)

OC for photoacoustic lympho- and angiography

Marina V. Novoselova et al., Optical clearing for photoacoustic lympho- and angiography beyond conventional depth limit in vivo, *Photoacoustics* 20 100186 (2020)

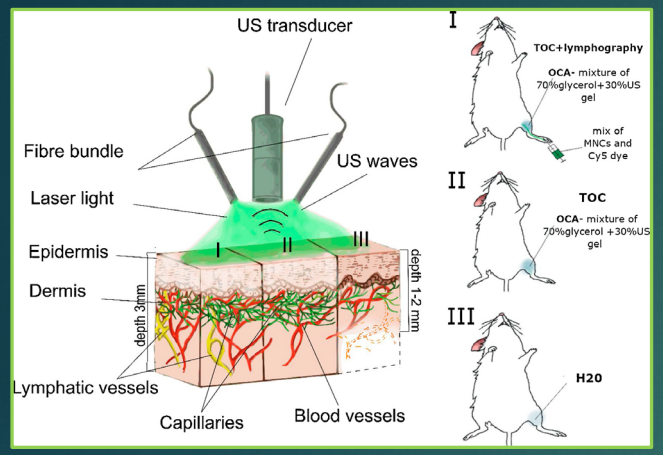

Schematic of RSOM system and experimental protocol

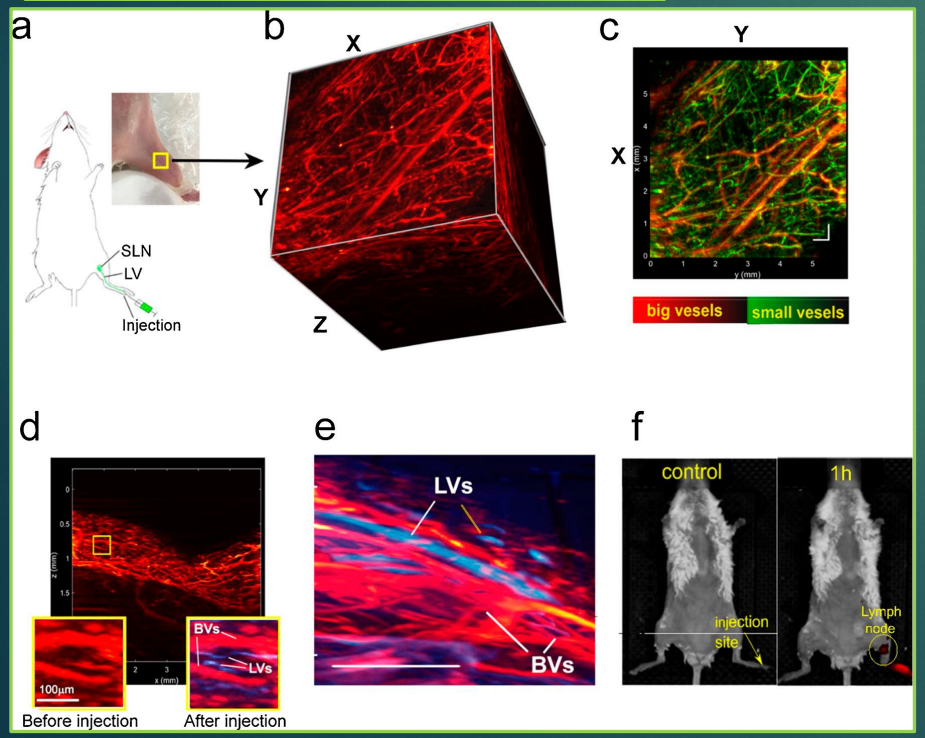

3D PA lymphography + angiography of mouse limb *in vivo*

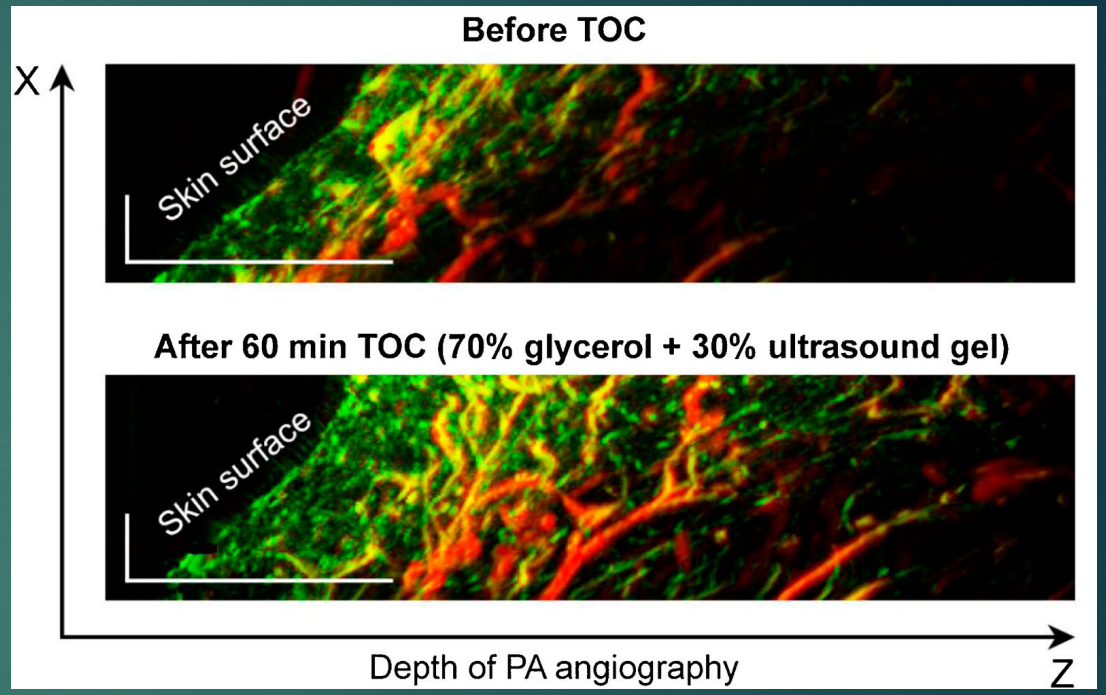

In vivo effects of RSOM & TOC at the topical application of the OCA on the skin surface of mouse limb during RSOM imaging: PA images (XZ scans) of the same area before and after 70 % glycerol + 30 % US gel TOC. Scale bar=0.5 mm.

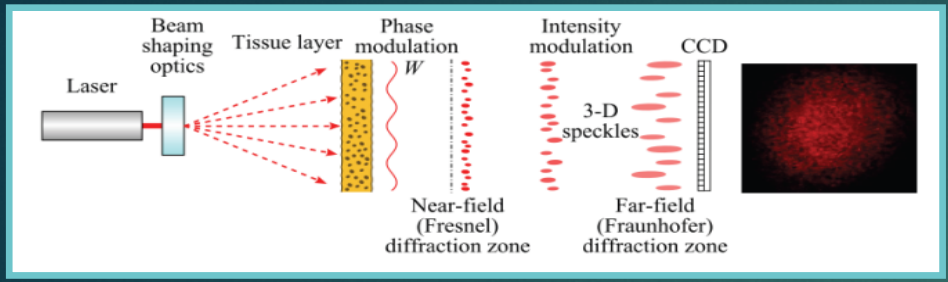

Laser speckle contrast imaging microscopy

K = σ/<I> ~ 1/ <V>,

σ is the standard deviation of the intensity fluctuations

<I> is the mean intensity, and <V> is the mean velocity

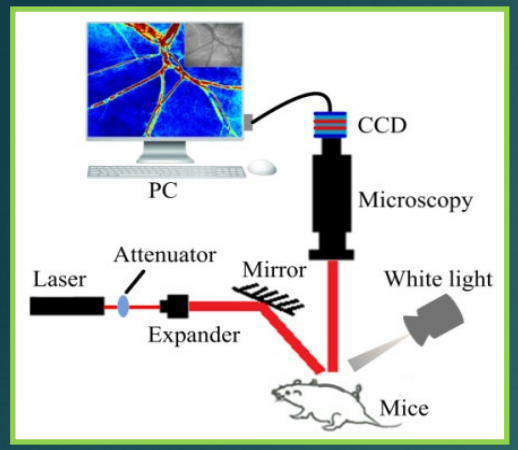

Blood vessel visibility at topical treatment of rat skin *in vivo* by a mixture of PEG-400 and thiazone
Zhu D., et al. *J. Biomed. Opt.* 15(2), 026008 (2010)

Imaging of brain blood vessels

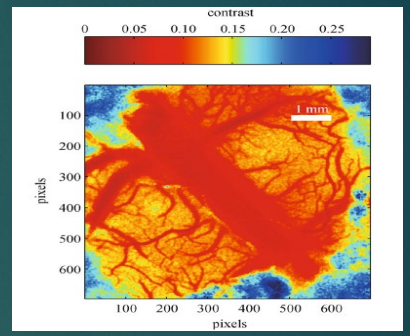

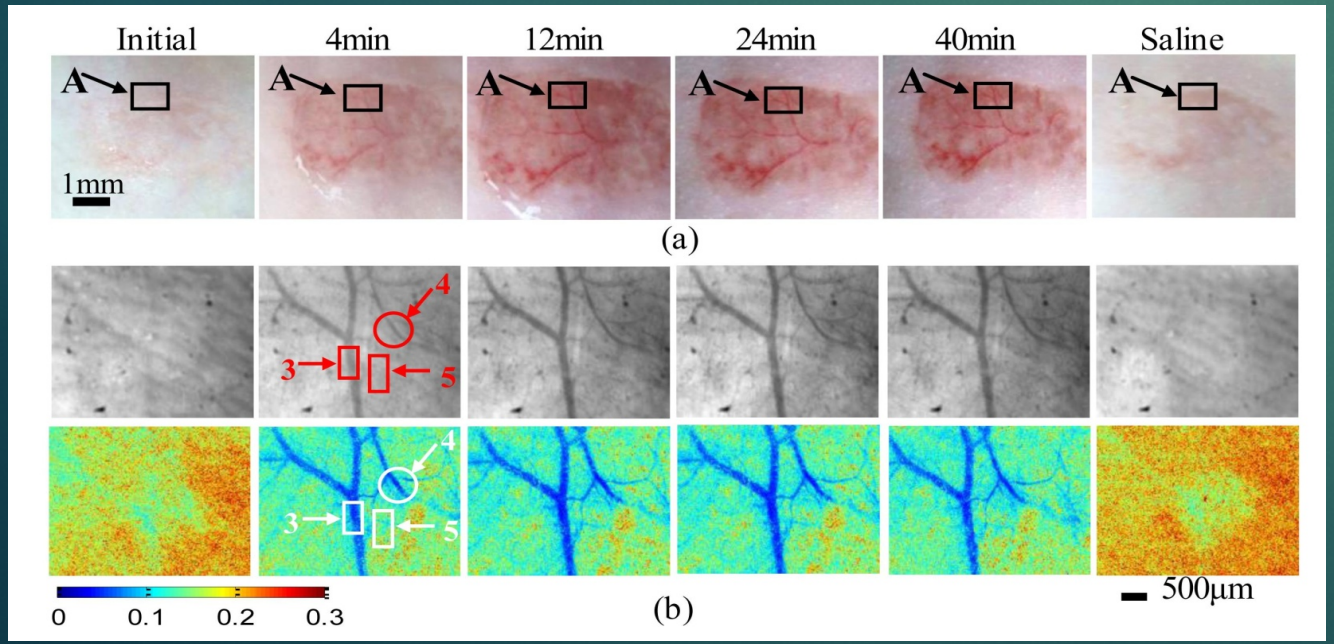

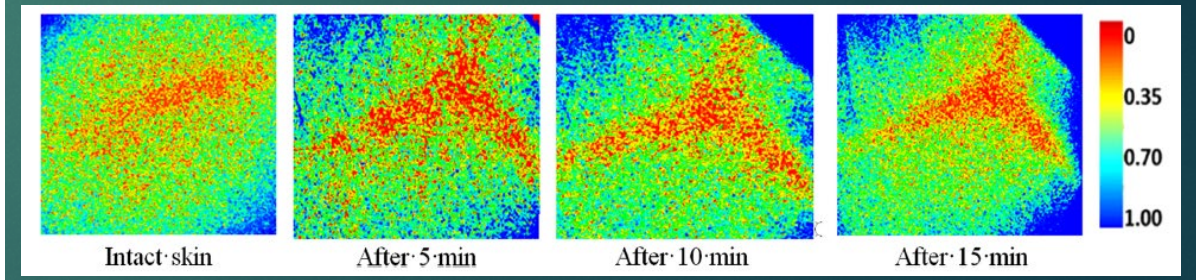

LSCI of cerebral vessels at application of 60% glycerol solution to skin surface of the newborn mouse in the fontanelle area

Tissue optical clearing using MRT or CT contrast agents

D.K. Tuchina, I.G. Meerovich, O.A. Sindeeva, V. V. Zherdeva, A. P. Savitsky, A. A. Bogdanov Jr, V. V. Tuchin, Magnetic resonance contrast agents in optical clearing: Prospects for multimodal tissue imaging. *J. Biophotonics* **13**(11) 2020; e201960249. https://doi.org/10. 1002/jbio.201960249

Imaging through albino mouse skin *ex vivo*

MR CA	0 min	30min	60 min
Gadovist®			
Magnevist®			
Dotarem®			
CT CA Visipaque®			
Saline			

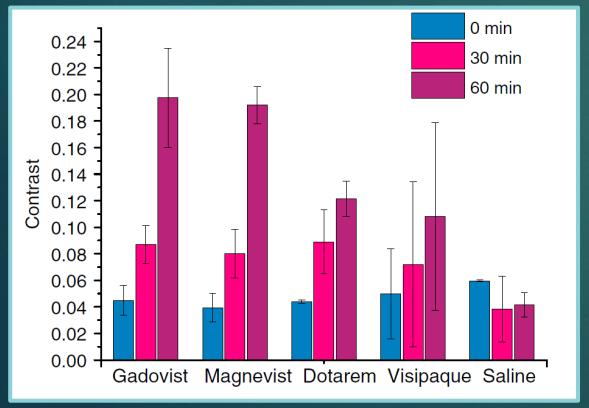

Administration of MRI agents

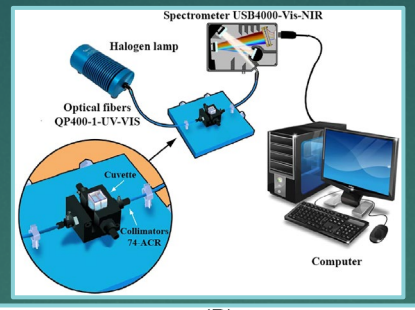

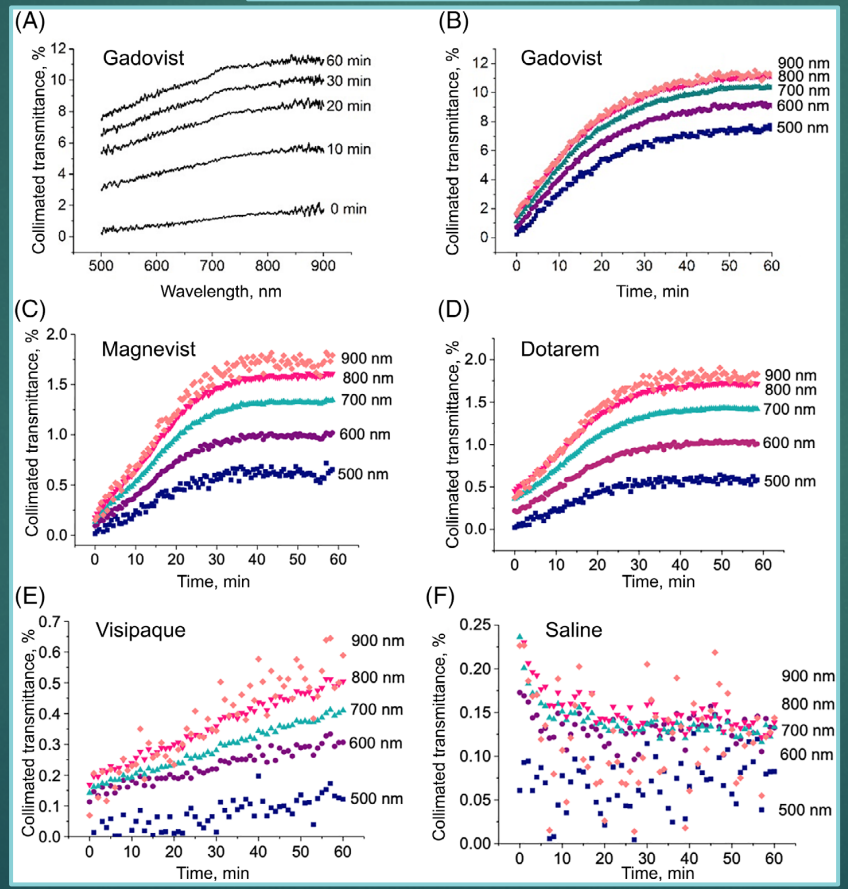

Collimated transmittance

- MRI contrasts can be successfully used as optical clearing agents for enhancing optical imaging
- This application clears the path for a fundamentally new approach in multimodal imaging, since synchronization in time and space occurs for enhancement of optical, CT and MRI image contrasts

OCT measurements of albino mouse skin *ex vivo*

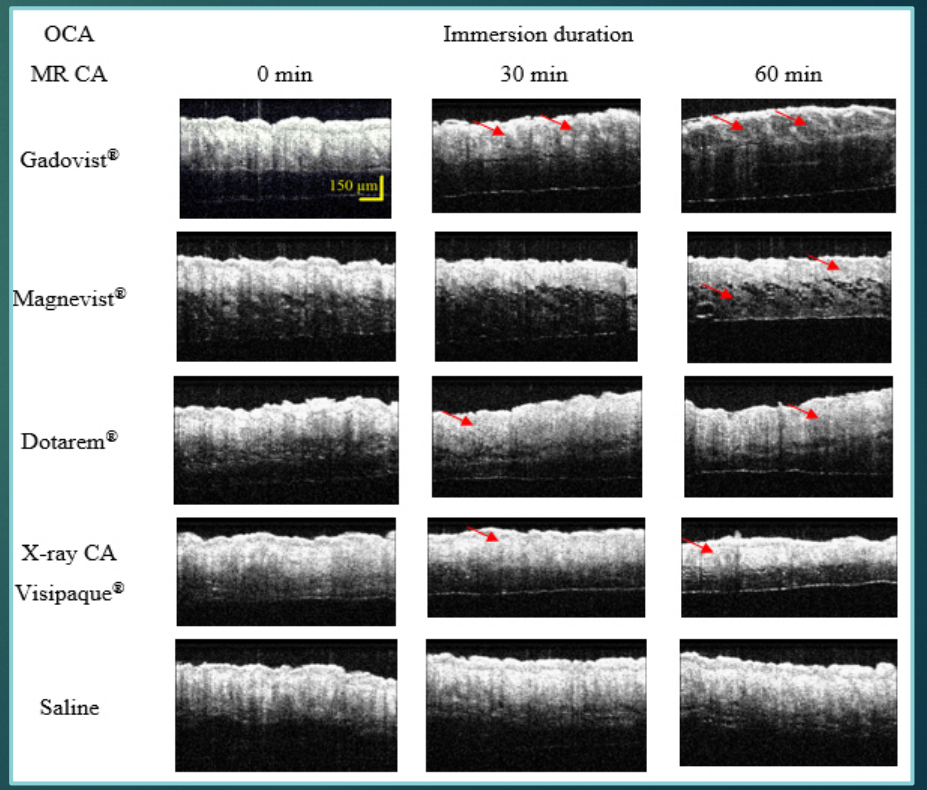

Multi-wavelength measurements RI of MRI agents

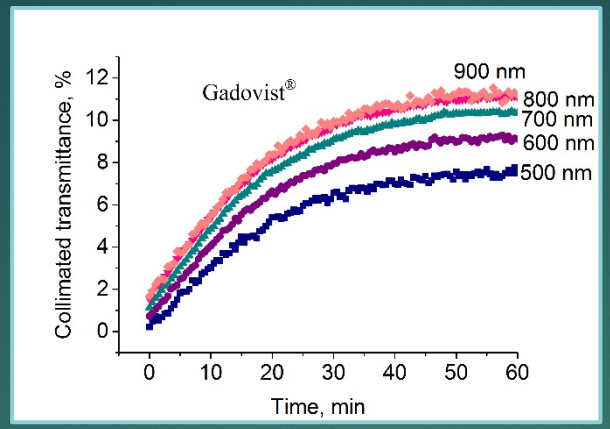

$$T_c(\lambda) \propto 1 - \exp\left(-\frac{t}{\tau}\right)$$

$$\tau = \frac{L^2}{\pi^2 D_a}$$

$$\frac{l_d}{L} = \sqrt{\frac{D_a^{free}}{D_a^{tissue}}}$$

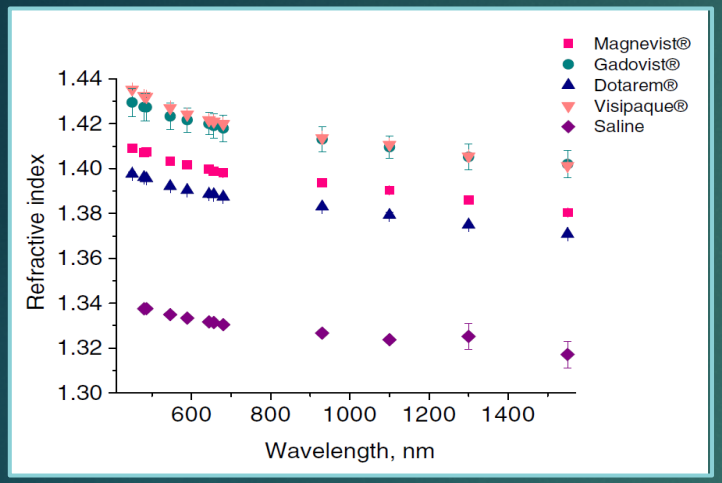

	OCE = T_c^{OC}/T_c^0			
Wavelength, nm	**Gadovist**	**Magnevist**	**Dotarem**	**Visipaque**
500	32.9 ± 5.5	29.7 ± 4.0	11.3 ± 7.7	7.5 ± 1.2
600	16.0 ± 2.8	16.0 ± 5.7	5.0 ± 1.0	5.0 ± 1.1
700	9.2 ± 0.3	10.5 ± 0.7	3.9 ± 0.1	2.8 ± 0.3
800	7.2 ± 0.2	9.5 ± 0.7	4.4 ± 0.6	2.7 ± 0.2
900	6.5 ± 0.7	9.5 ± 2.1	4.4 ± 0.6	3.8 ± 0.8

MRI agent diffusion coefficients measured in mouse skin *ex vivo*

Agent	**MR**			**X-ray**
Trademark	**Gadovist**	**Magnevist**	**Dotarem**	**Visipaque**
D_a^{tissue}, cm^2/s	$(4.29 \pm 0.39) \times 10^{-7}$	$(5.00 \pm 0.72) \times 10^{-7}$	$(3.72 \pm 0.67) \times 10^{-7}$	$(1.64 \pm 0.18) \times 10^{-7}$
D_a^{free}, cm^2/s	3.9×10^{-6}	—	4.5×10^{-6}	—
Tortuosity, l_d/L	3.0	—	3.5	—

❑ Gadovist – is the most effective OCA

FLIM measurements + OC

Fluorescence intensity images of mouse cancer cells *in vivo*

D.K. Tuchina, I.G. Meerovich, O.A. Sindeeva, V. V. Zherdeva, A. P. Savitsky, A. A. Bogdanov Jr, V. V. Tuchin, Magnetic resonance contrast agents in optical clearing: Prospects for multimodal tissue imaging. *J. Biophotonics* **13**(11) 2020; e201960249. https://doi.org/10. 1002/jbio.201960249

20 days after tumor cell enucleation (HEp2-TagRFP line) in BALBc/nude mice

OCA: 70% glycerol, 5% DMSO, 25% water

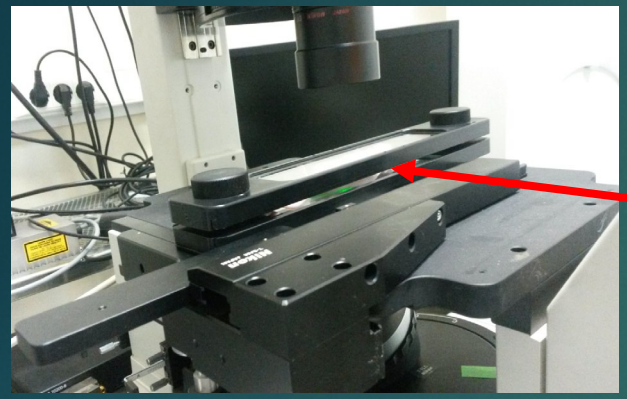

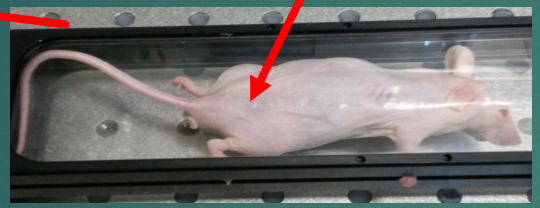

Cassette with animal

Profiles for fluorescence signal

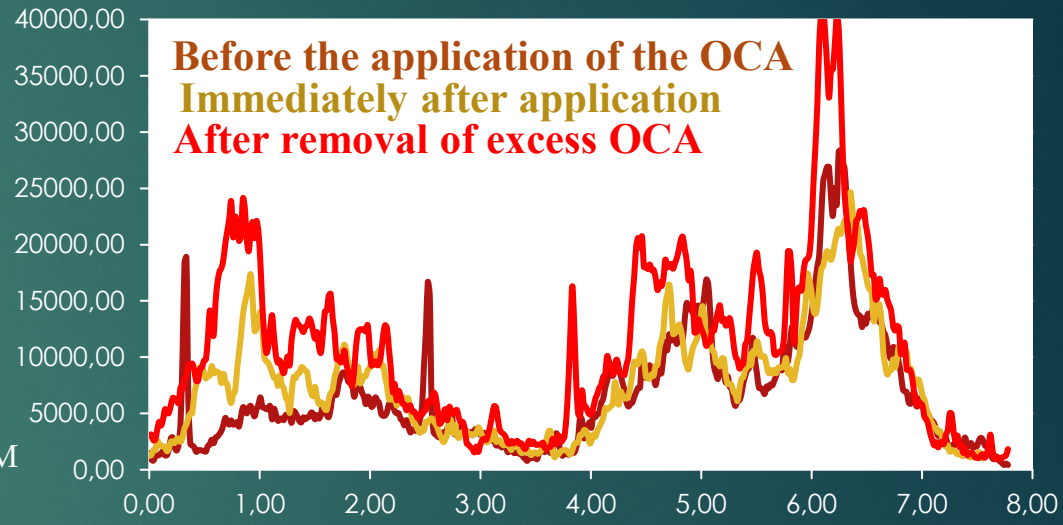

Instrumentation and Protocol

- DCS-120 confocal scanning system (Becker & Hickl GmbH)
- WhiteLase SC480-10 supercontinuum laser with acousto-optic tunable filter AOTF-V1-D-FDS-SM (FIANIUM)
- HPM-100-40 hybrid detector (Becker & Hickl GmbH)
- Fluorescence excitation wavelength was 540 nm
- Fluorescence emission from a tumor was collected through the skin in the epi-illumination configuration
- Long- and bandpass filters were used (HQ550LP and 580BP)
- SPCImage 3.2 data analysis software (Becker & Hickl GmbH).
- NIH ImageJ 1.48v software
- Animals were anesthetized by Zoletil-Rometar mixture and were put in a cassette on a mobile stage
- Optical clearing was performed for 15 min using a 70% glycerol, 5% DMSO, 25% water solution
- Image collection time for anesthetized mouse varied from 3.5 to 8 min depending of fluorophore expression level

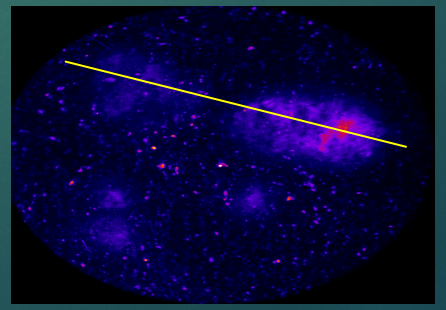

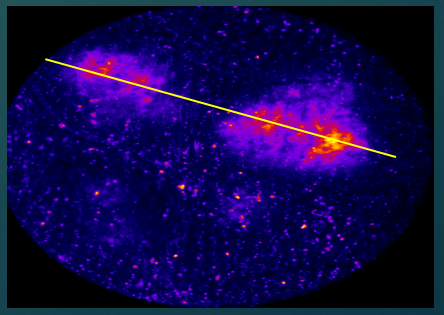

Fluorescence intensity images of mouse cancer cells *in vivo*

D.K. Tuchina, I.G. Meerovich, O.A. Sindeeva, V. V. Zherdeva, A. P. Savitsky, A. A. Bogdanov Jr, V. V. Tuchin, Magnetic resonance contrast agents in optical clearing: Prospects for multimodal tissue imaging. *J. Biophotonics* **13**(11) 2020; e201960249. https://doi.org/10. 1002/jbio.201960249

20 days after tumor cell enucleation (HEp2-TagRFP line) in BALBc / nude mice

OCA: Gadovist®

Protocol	Time, min																				
	1-10	11-15	16-17	18	19	20-34	35	36-37	38-39	40	41-66	67	68-69	70	71-96	97	98-99	100	101-111	112	113-114	115
	Before OC					OC		**After OC**				In 30 min				**In 60 min**				In 75 min		
Anesthesia and placing the animal in a cassette																						
Measurement setup																						
Measurements																						
Data storage																						
Cassette opening																						
OCA application																						
Cassette closing																						
Measurement setup																						
Measurements																						
Data storage																						

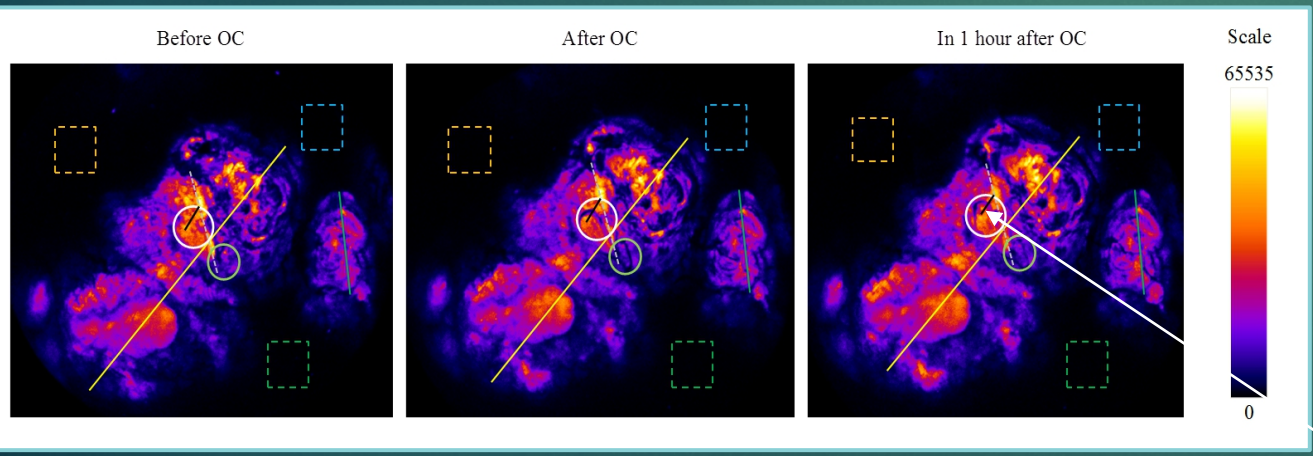

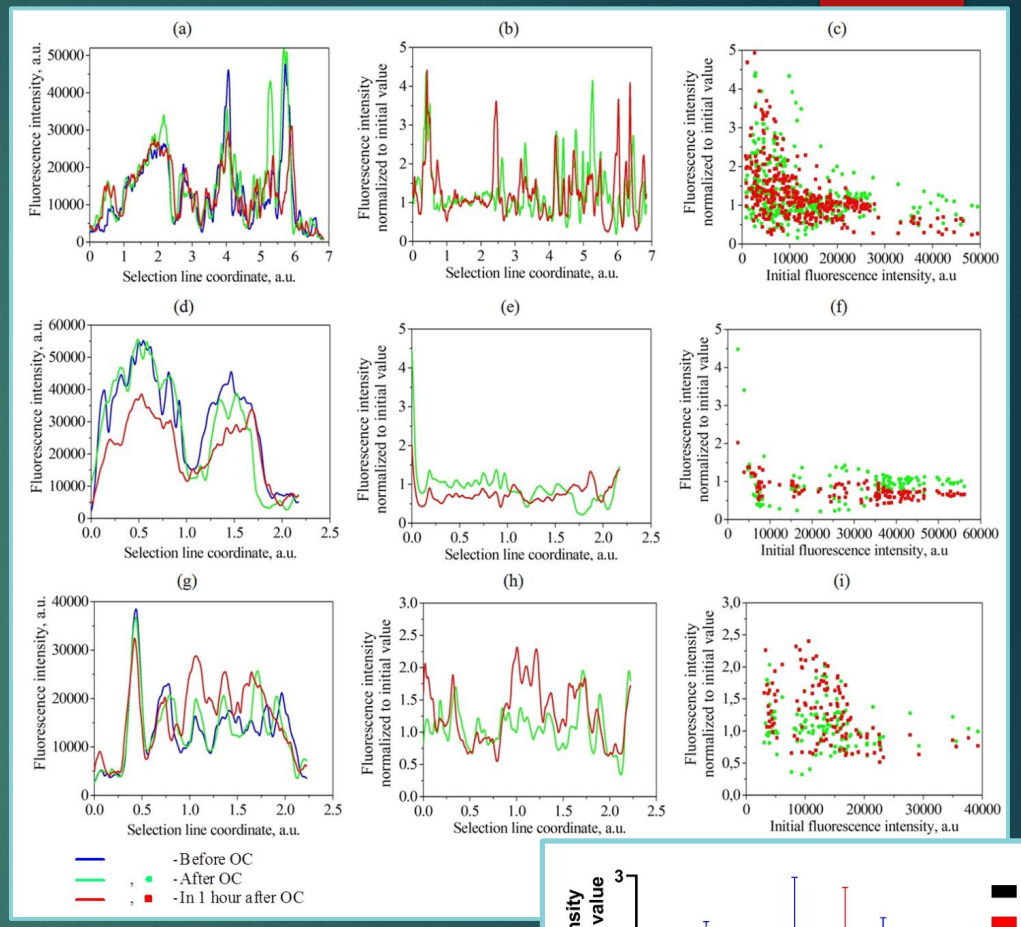

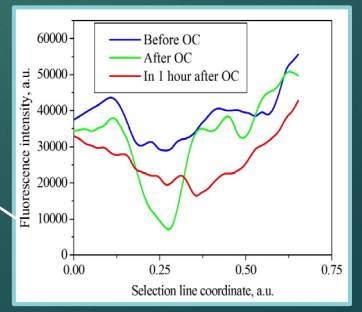

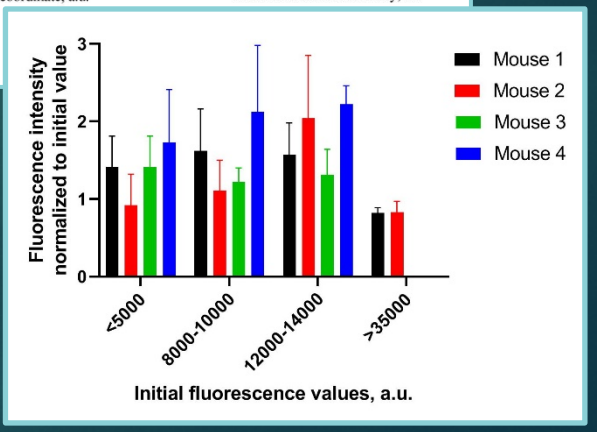

Upconversion nanoparticles (UCNP) for deep-tissue imaging

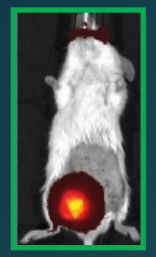

A.P. Popov, E.V. Khaydukov, A.V. Bykov, V.A. Semchishen, V.V. Tuchin, Enhancement of upconversion deep-tissue imaging using optical clearing, Proc. of SPIE-OSA **9540,** 95400B-5, 2015

[NaYF4 matrix is doped with ions of ytterbium, erbium and thulium)]

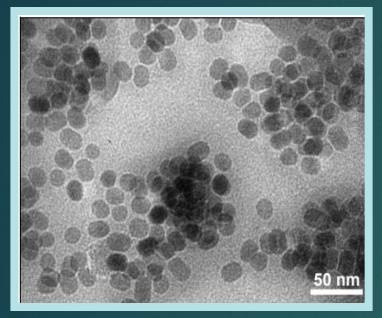

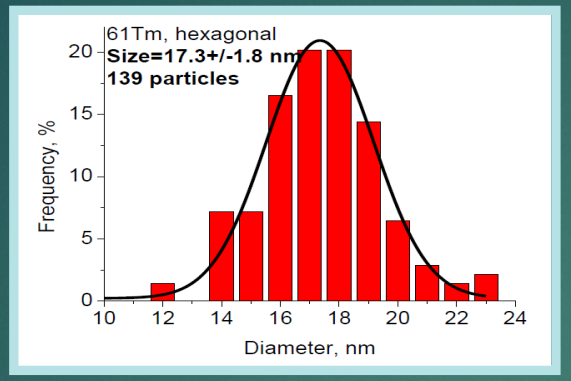

Size distribution

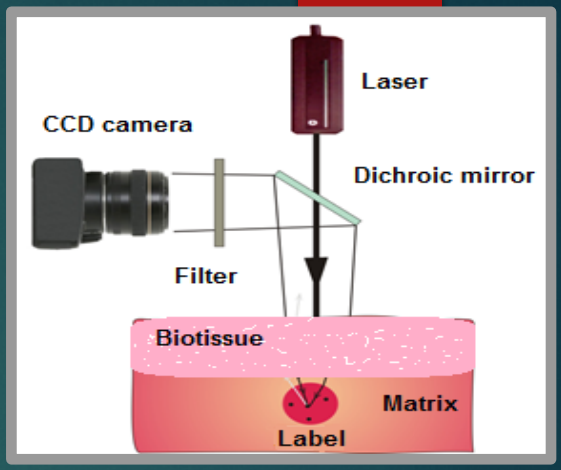

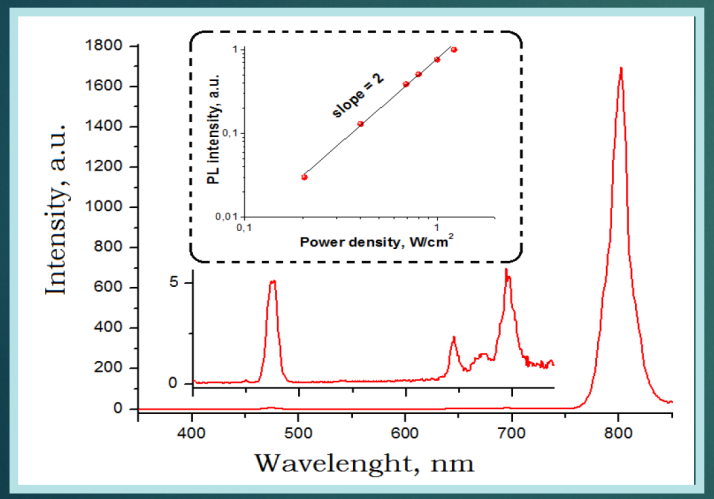

Spectra of luminescent radiation at pumping on **975 nm**

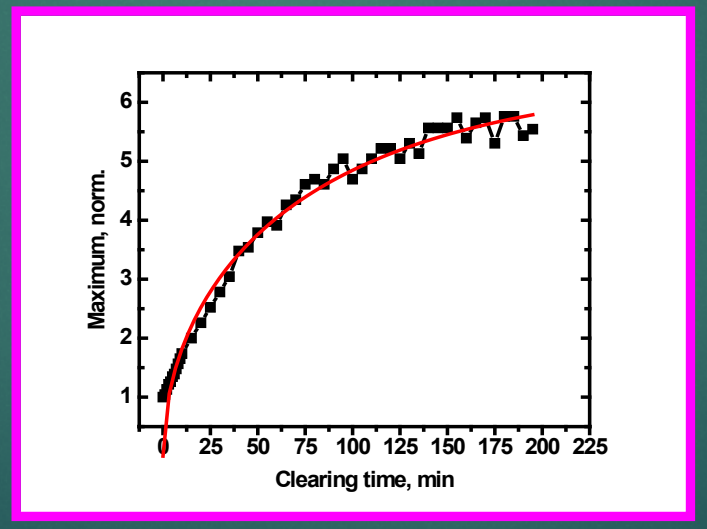

Upconversion luminescence of a star-shaped label at **800 nm,** glycerol clearing of 6-mm-thick porcine muscle tissue

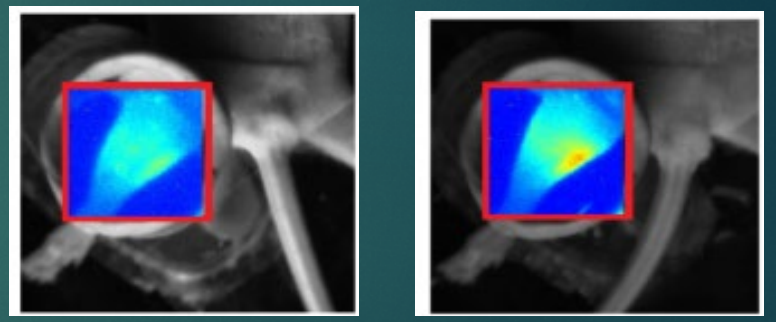

Before and after **255 min** of **glycerol** clearing mouse leg ***in vivo***

Silicone-glycerol mixture tissue phantoms

M.S. Wróbel et al., Nanoparticle-free tissue-mimicking phantoms with intrinsic scattering *Biomed. Opt. Express* **7**(6), 2088-2094 (2016)

Phantom

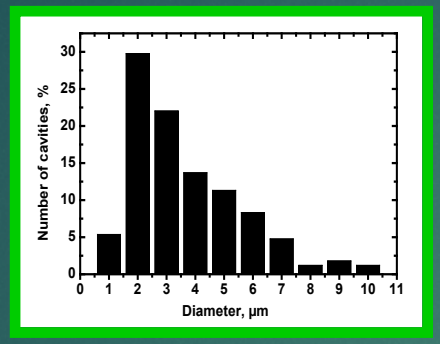

Size distribution of microcavities

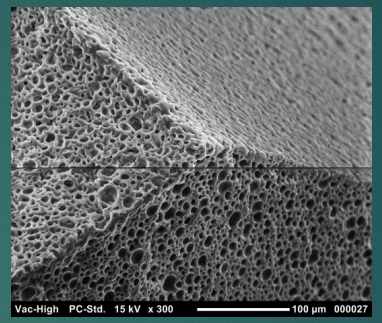

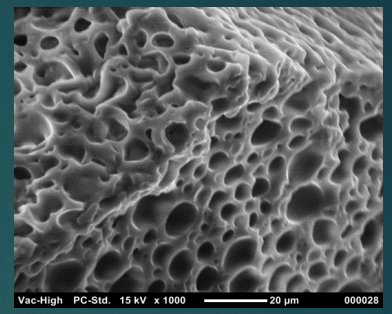

Electronic micrographs of phantom

P. Listewnik, M. Ronowska, M. Wasowicz, V.V. Tuchin, M. Szczerska, Porous phantoms mimicking tissues—investigation of optical parameters stability over time. Materials **2021**, 14, 423-1-11

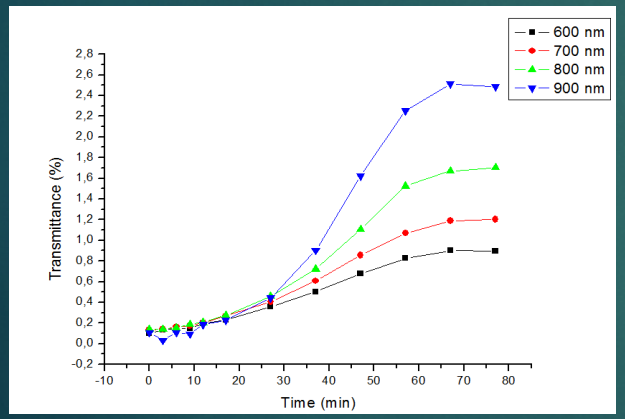

Transmittance kinetics (glucose solution, 40%)

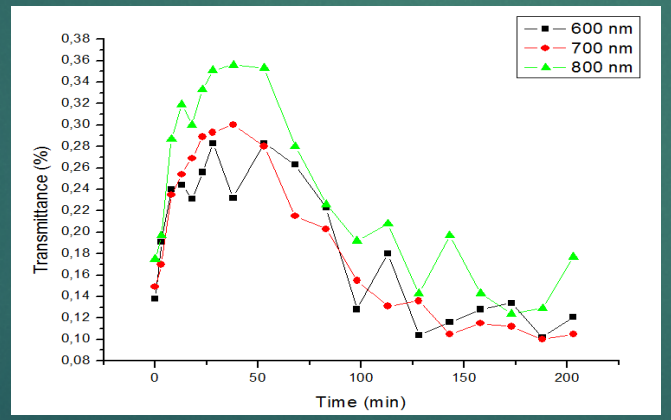

Transmittance kinetics (water)

Quirk et al. OPTICS LETTERS **39**(10):2888-2891, 2014

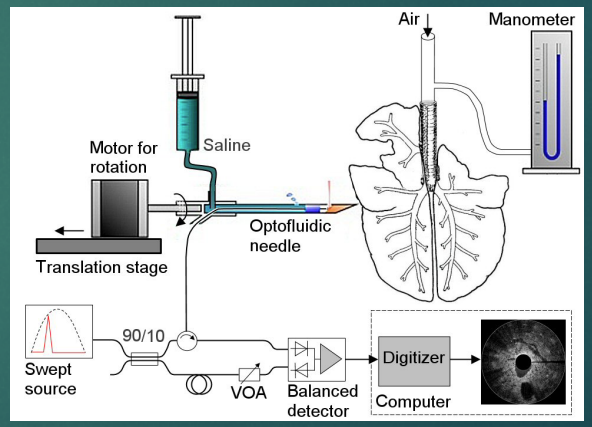

Schematic of the OCT optofluidic needle probe

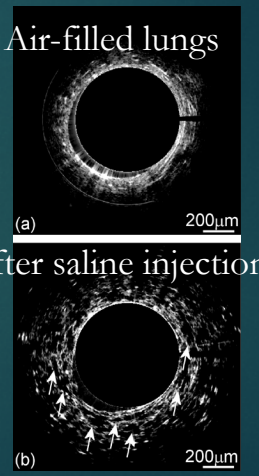

Arrows indicate representative alveoli

Additional benefit: sound and light propagate in phantom with properties close to the actual tissue

OCAs for THz waves

Guzel R. Musina et al., The efficiency of hyperosmotic agents for immersion optical clearing of ex vivo rat brain tissues in the terahertz range, *J. Biophotonics* (2020)

THz pulsed spectrometer

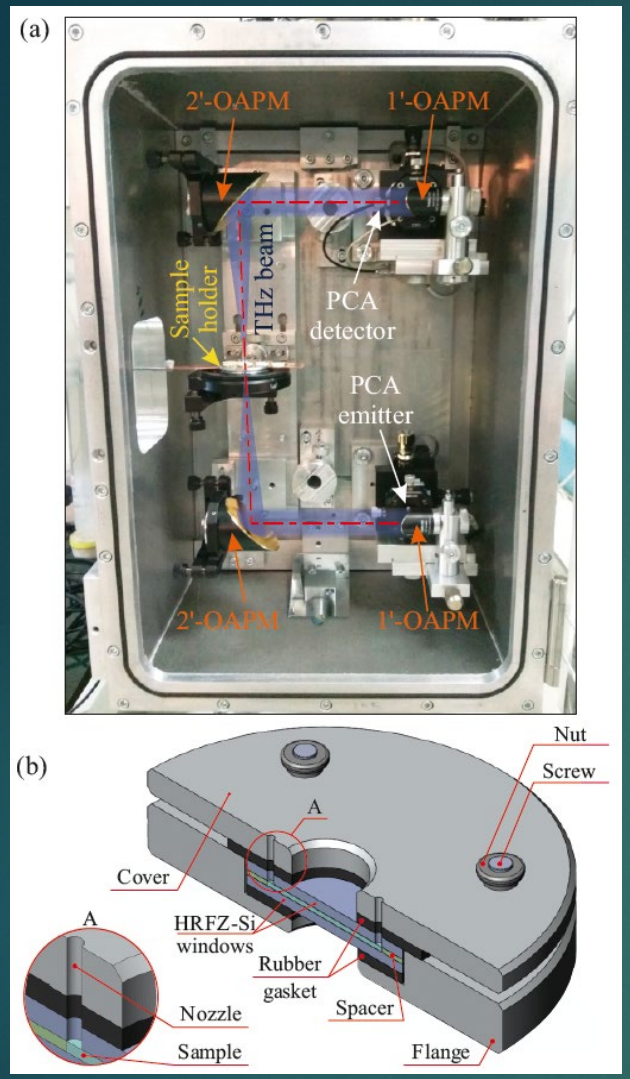

(a) A general view with a vacuum sample chamber, the THz beam is shown in blue, PCA – photoconductive antenna, OAPM – off-axis parabolic mirror

(b) cuvette for the transmission-mode spectroscopy of liquids, A shows the filling location at the enlarged scale

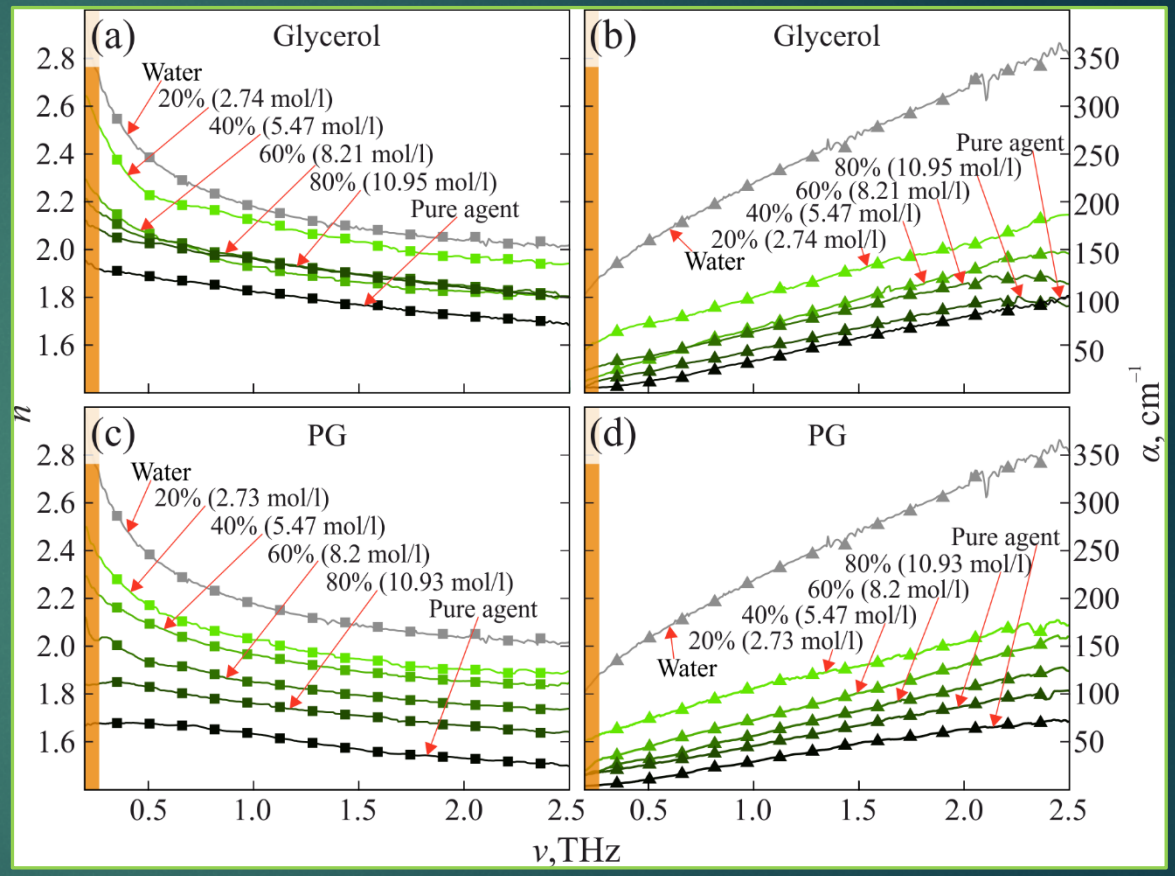

THz optical properties of Glycerol and PG, and their aqueous solutions: (a),(b) refractive index *n* and amplitude absorption coefficient α of Glycerol and its aqueous solutions; (c),(d) equal data set for PG

Summary

Polarization

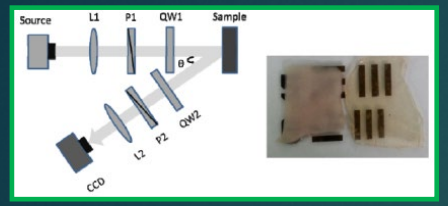

Adaptive OCT

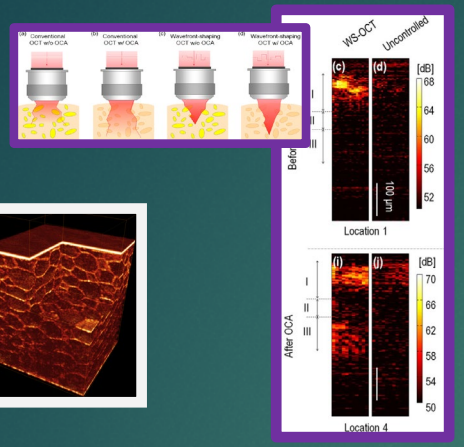

Skull, tooth, bone, cartilage

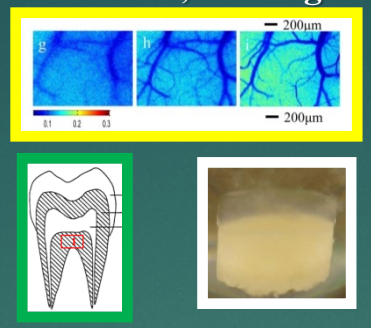

Rheumatoid arthritis

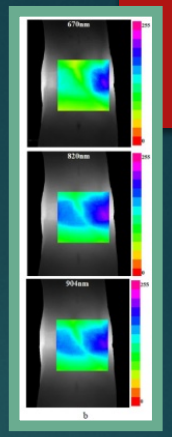

Glucose sensing

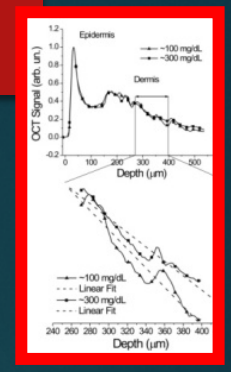

OCT

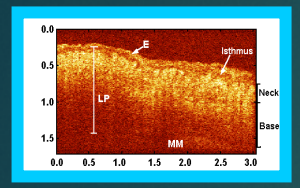

Blood vessel imaging

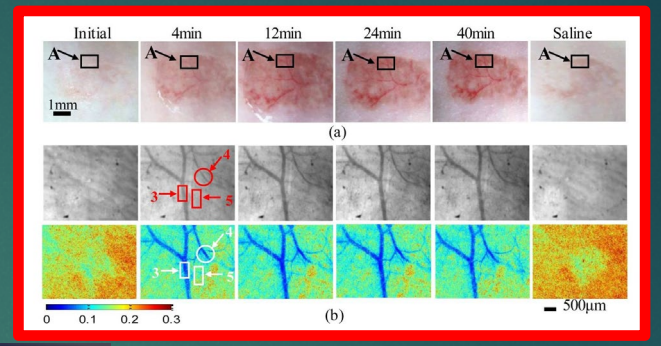

Confocal microscopy

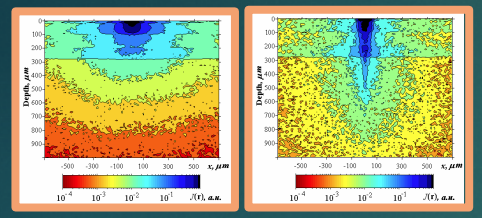

Speckles

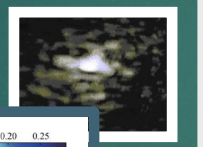

Optical Clearing of Tissues and Blood

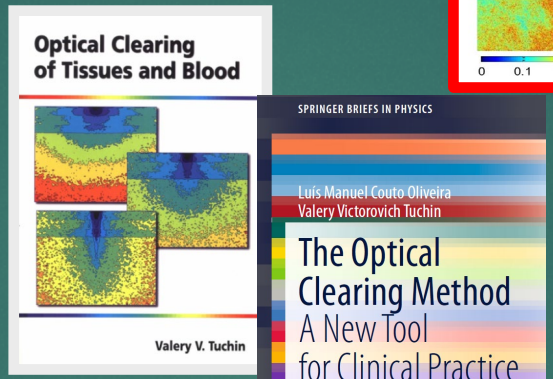

Glycated tissue differentiation

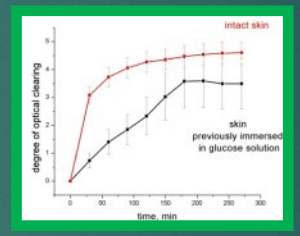

Cell nanophotonics

Upconversion nanoparticles

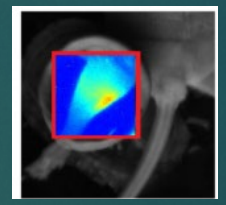

Gold nanoparticles

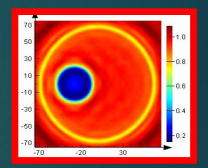

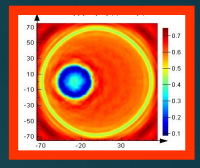

Raman spectroscopy

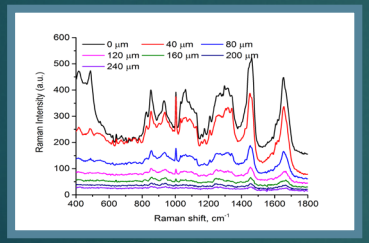

THz clearing

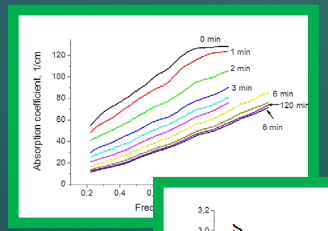

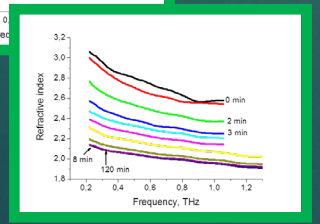

Two-photon and SHG microscopy

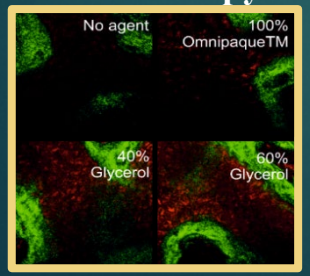

Cell imaging in lymph nodes

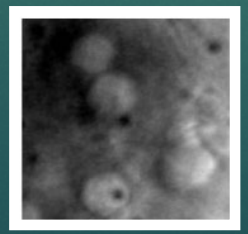

Cancerous tissue differentiation

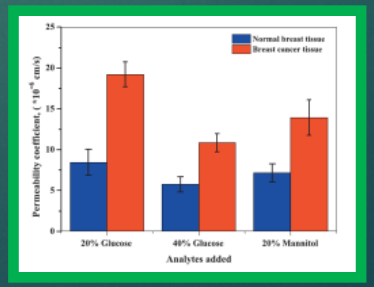

Precise laser surgery

Scarred vocal fold

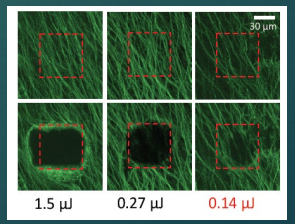

Laser tattoo removal

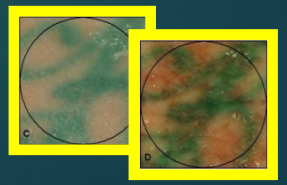

PA microscopy & flow cytometry

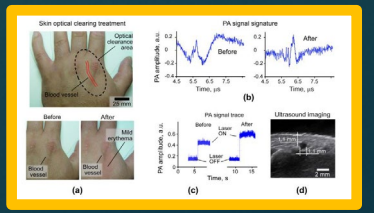

OC multimodality concept

Technique

- Integrating sphere spectroscopy
- Diffuse reflectance & fluoresc. spectrosc./imaging (DRFSI)
- Optical Coherence Tomography (OCT)
- Confocal Microscopy (CM)
- Raman spectrosc./imaging
- Photoacoustics (PA)
- Multiphoton microscopy (MPM)
- THz Spectrosc./Imaging
- X-ray computer tomography (CT)
- MRI

Experimental validation

- Multilayered, multimodal optical tissue phantoms
- *Ex vivo* & *in vivo studies*
- Healthy & pathological tissues
- Animal & human tissues

Optical Clearing

- Multicomponent biocompatible optical clearing agents (OCAs) for effective tissue optical clearing (OC) and enhancement of tissue image contrast
- Multimodal OCAs for OC and contrasting of CT and MRI

Data processing

- Inverse problem solution: tissue absorption, scattering & fluorescence properties
- Mathematical models
- Image processing (DRFSI OCT, CM, PA, Raman, MPM, THz)
- Multidimensional data classification including feature extraction/selection

❖ Improve and provide

- ➢ quantitative estimation of the concentration of chromophores and fluorophores of tissue at various depths
- ➢ multi-category classification of tissue properties based on the extraction of meaningful multimodal spectroscopic biomarkers
- ➢ clinically compatible spectroscopy-based methods of tissue pathology diagnosis
- ➢ practical recommendations for increasing *in vivo* efficacy of diagnostics in UV/visible/NIR (200-2000 nm), THz combined with x-ray CT and MRI

Conclusion

- Optical clearing agents are beneficial for enhanced multimodal spectroscopy/imaging: combination of optical techniques (Raman, OCT, FLIM, MPM, SHG, PA, Diffuse, THz) with X-ray CT and MRI

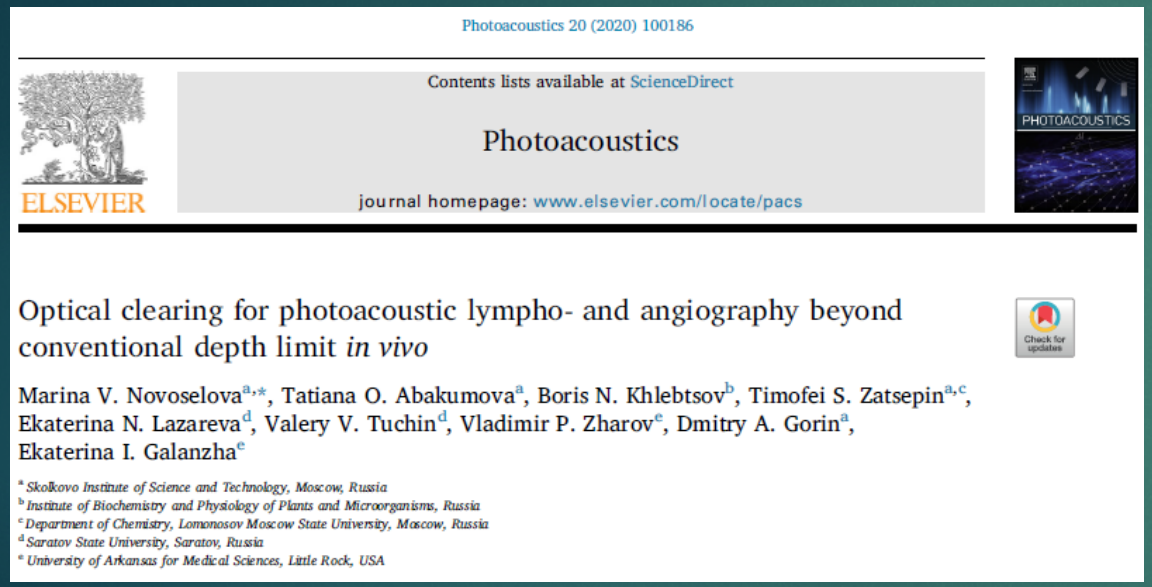
Photoacoustics 20 (2020) 100186

Contents lists available at ScienceDirect

Photoacoustics

journal homepage: www.elsevier.com/locate/pacs

Optical clearing for photoacoustic lympho- and angiography beyond conventional depth limit *in vivo*

Marina V. Novoselova[a,*], Tatiana O. Abakumova[a], Boris N. Khlebtsov[b], Timofei S. Zatsepin[a,c], Ekaterina N. Lazareva[d], Valery V. Tuchin[d], Vladimir P. Zharov[e], Dmitry A. Gorin[a], Ekaterina I. Galanzha[e]

[a] Skolkovo Institute of Science and Technology, Moscow, Russia
[b] Institute of Biochemistry and Physiology of Plants and Microorganisms, Russia
[c] Department of Chemistry, Lomonosov Moscow State University, Moscow, Russia
[d] Saratov State University, Saratov, Russia
[e] University of Arkansas for Medical Sciences, Little Rock, USA

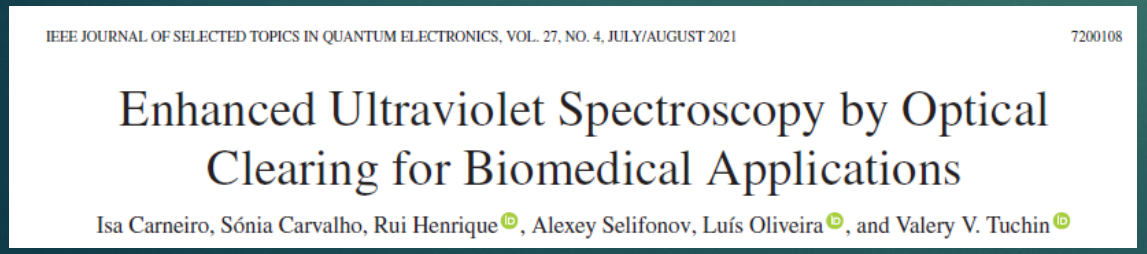
IEEE JOURNAL OF SELECTED TOPICS IN QUANTUM ELECTRONICS, VOL. 27, NO. 4, JULY/AUGUST 2021 7200108

Enhanced Ultraviolet Spectroscopy by Optical Clearing for Biomedical Applications

Isa Carneiro, Sónia Carvalho, Rui Henrique, Alexey Selifonov, Luís Oliveira, and Valery V. Tuchin

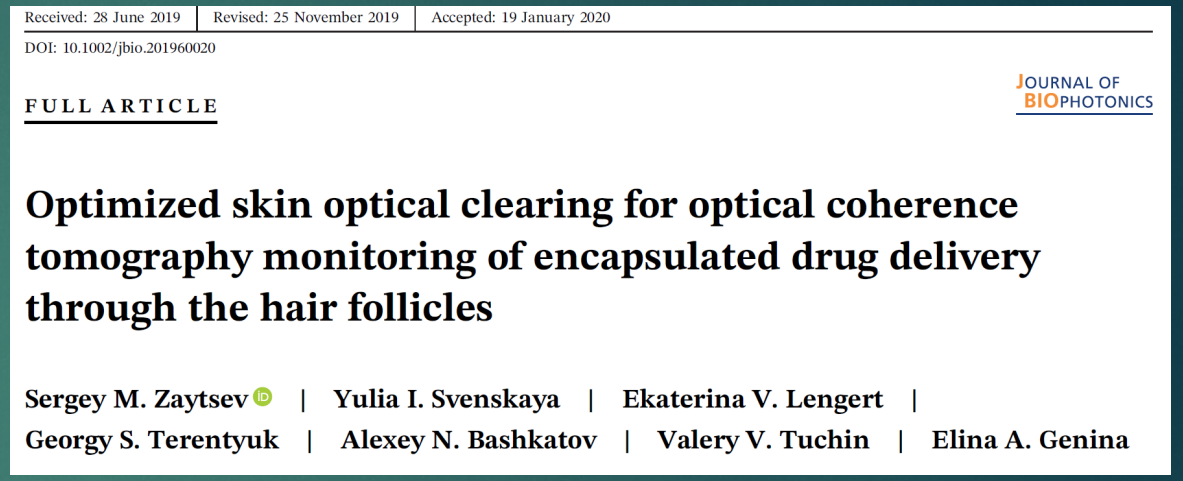
Received: 28 June 2019 | Revised: 25 November 2019 | Accepted: 19 January 2020

DOI: 10.1002/jbio.201960020

FULL ARTICLE

JOURNAL OF BIOPHOTONICS

Optimized skin optical clearing for optical coherence tomography monitoring of encapsulated drug delivery through the hair follicles

Sergey M. Zaytsev | Yulia I. Svenskaya | Ekaterina V. Lengert | Georgy S. Terentyuk | Alexey N. Bashkatov | Valery V. Tuchin | Elina A. Genina

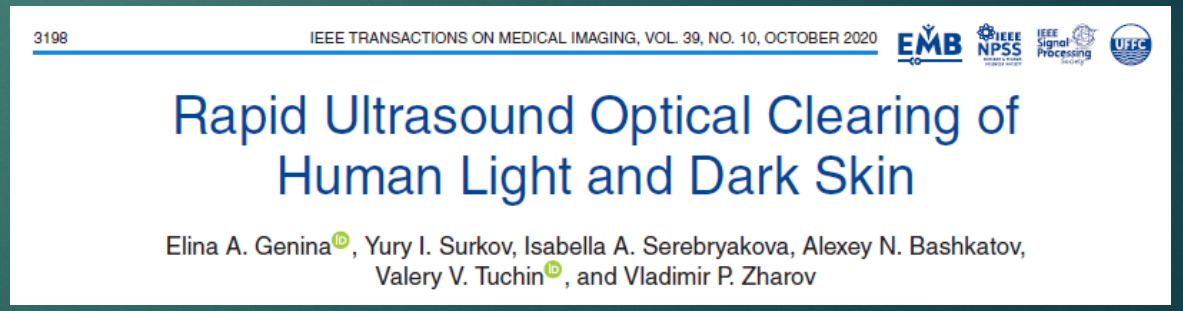
3198 IEEE TRANSACTIONS ON MEDICAL IMAGING, VOL. 39, NO. 10, OCTOBER 2020

Rapid Ultrasound Optical Clearing of Human Light and Dark Skin

Elina A. Genina, Yury I. Surkov, Isabella A. Serebryakova, Alexey N. Bashkatov, Valery V. Tuchin, and Vladimir P. Zharov

G. R. Musina, I. N. Dolganova, N. V. Chernomyrdin, A. A. Gavdush, V. E. Ulitko, O. P. Cherkasova, D. K. Tuchina, P. V. Nikitin, A. I. Alekseeva, N. V. Bal, G. A. Komandin, V. N. Kurlov, V. V. Tuchin, K. I. Zaytsev, Optimal hyperosmotic agents for tissue immersion optical clearing in terahertz biophotonics, *J. Biophotonics*. 2020; https://doi.org/10.1002/jbio.202000297

To read

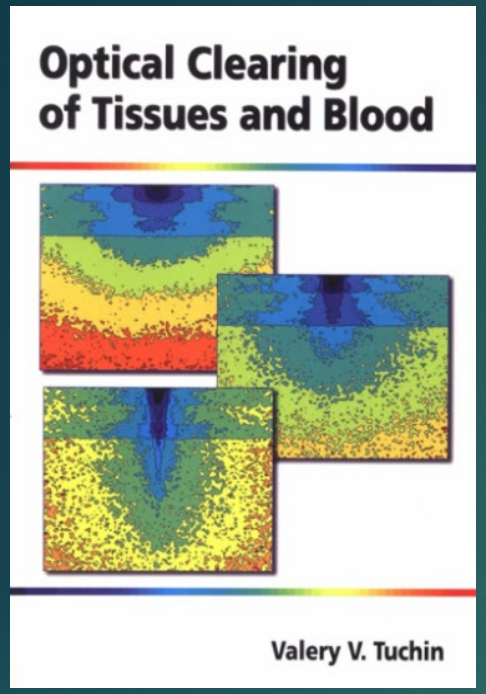

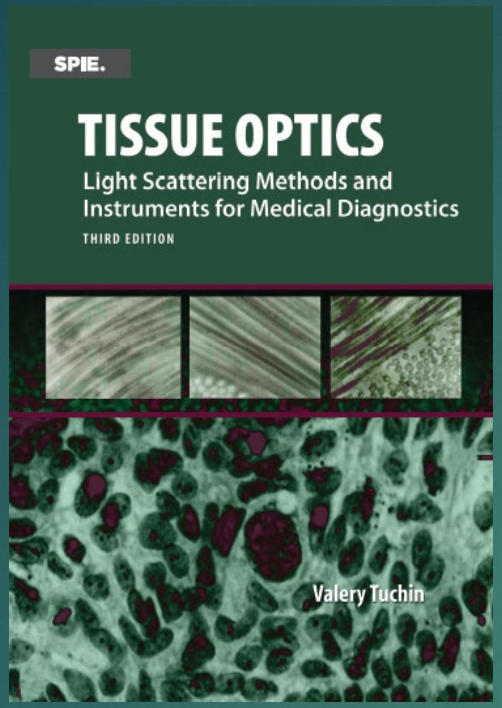

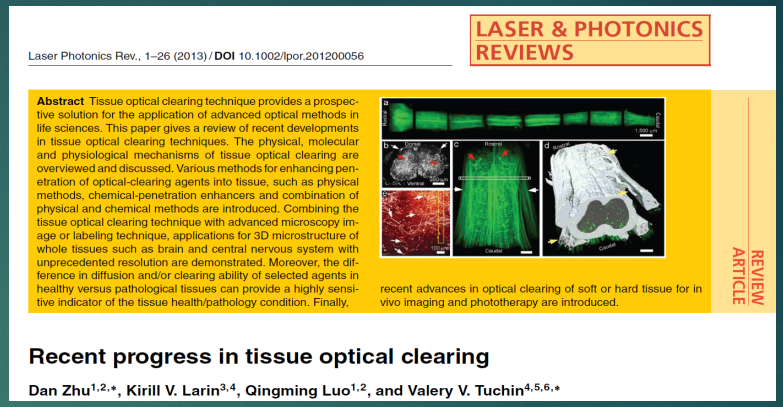

New books:

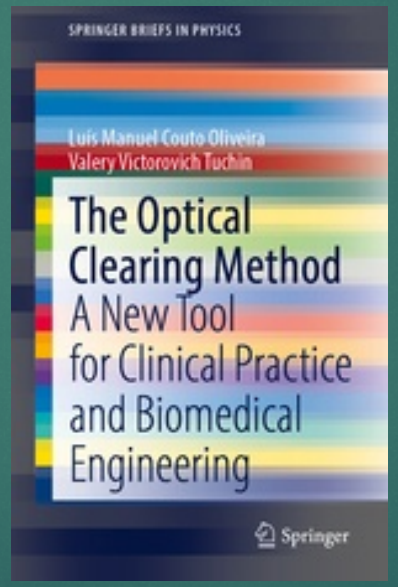

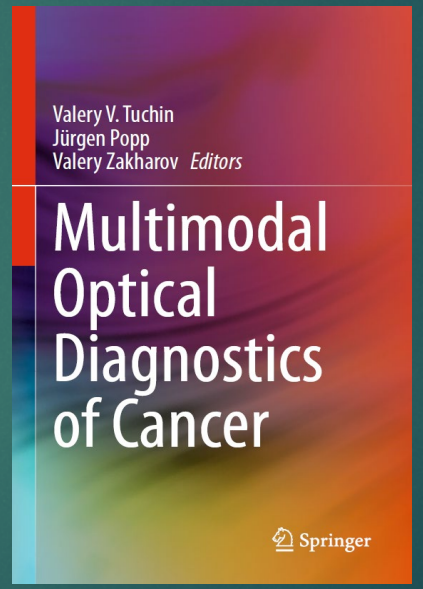

Chapter 2
Optical Clearing of Biological Tissues: Prospects of Application for Multimodal Malignancy Diagnostics

Elina A. Genina, Luís M. C. Oliveira, Alexey N. Bashkatov, and Valery V. Tuchin

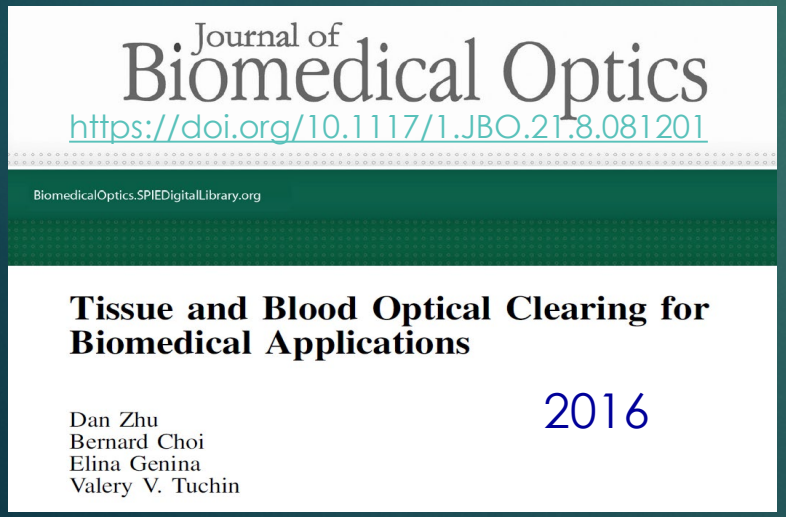

CRC PRESS
Taylor & Francis Group

D. Zhu, E. Genina, and V. Tuchin (Eds.), *Tissue optical clearing: new prospects in optical imaging*, CRC Press (2021)

37 Chapters

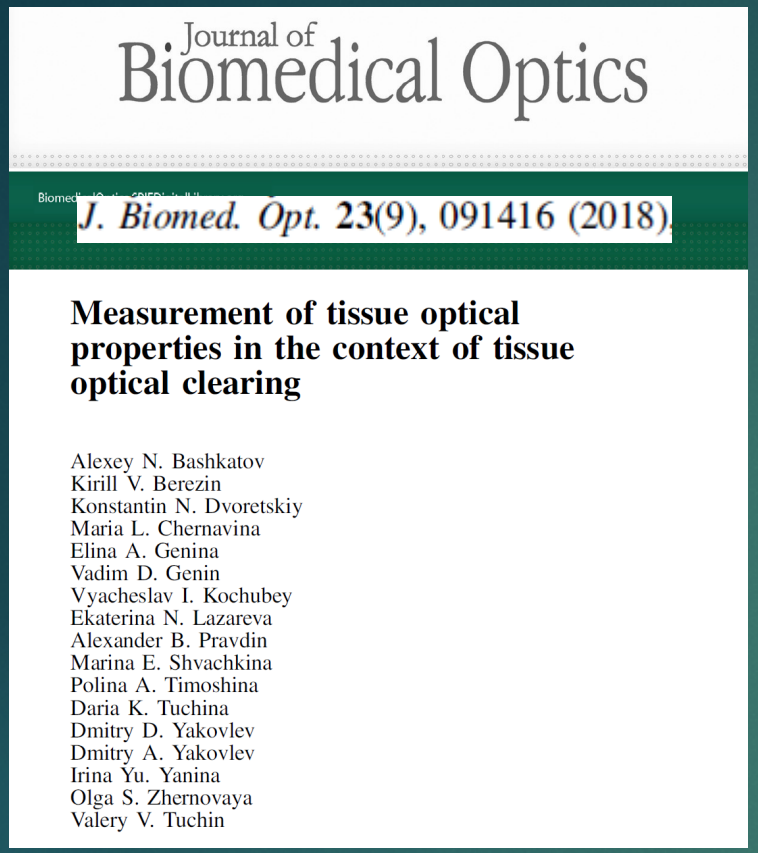

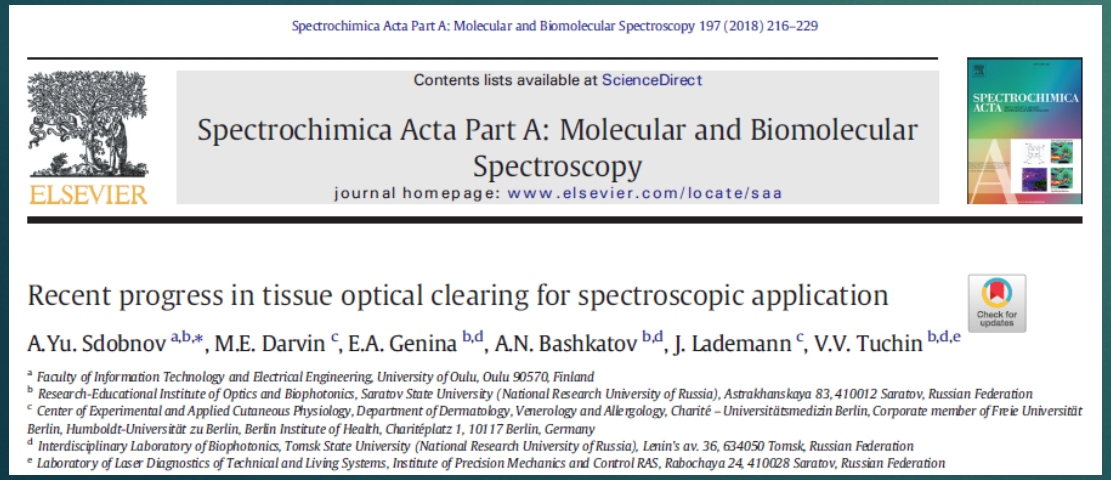

Terahertz biophotonics as a tool for studies of dielectric and spectral properties of biological tissues and liquids related to water content

O.A. Smolyanskaya, N.V. Chernomyrdin, A.A. Konovko, K.I. Zaytsev, I.A. Ozheredov, O.P. Cherkasova, M.M. Nazarov, J.-P. Guillet, S.A. Kozlov, Yu.V. Kistenev, J.-L. Coutaz, P. Mounaix V.L. Vaks, J.-H. Son, H. Cheon, V. Wallace, Yu. Feldman, I. Popov, A.N. Yaroslavsky, A.P. Shkurinov, and V.V. Tuchin

ITMO University
Bauman Moscow State Technical University
Sechenov First Moscow State Medical University
Prokhorov General Physics Institute of RAS
Lomonosov Moscow State University
Institute of Laser Physics of SB RAS
Tomsk State University
National Research Center "Kurchatov Institute
IMS Laboratory, UMR CNRS 5218, University of Bordeaux
IMEP-LAHC, UMR 5130 CNRS, University Savoie Mont Blanc, Le Bourget du Lac
Institute for Physics of Microstructures of RAS
University of Seoul
The University of Western Australia
The Hebrew University of Jerusalem
University of Massachusetts, Lowell
Saratov State University
Institute of Precision Mechanics and Control of RAS

Acknowledgements

SSU

Profs. and Drs. Alexey Bashkatov, Elina Genina, Irina Yanina, Yury P. Sinichkin, Olga Zhernovaya, Polina Timoshina, Daria Tuchina, Alexander Pravdin

PhD students

Vadim Genin, Anton Sdobnov, Marina Shvachkina, Ekaterina Lazareva, Alexey Selifonov, and many others

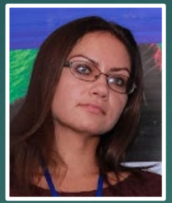

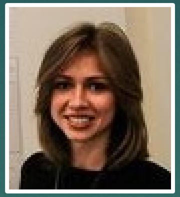

National and international collaborators

Emil Sobol, Yulia Alexandrovskaya et al. Inst. Photon Technologies RAS
Alexander Shkurinov, Maxim Nazarov, MSU
Kirill Zaytsev, Irina Dolganova et al. GPI RAS, Bauman MSTU
Yury Kistenev, National Research Tomsk State University
Olga Smolyanskaya, ITMO University
Dan Zhu, Qingming Luo et al. HUST University, China
Hui Ma, et al. Tsinghua University, Shenzhen, China
Kirill V. Larin et al. Univ. of Houston, USA
Irina Larina, Baylor College of Medicine, USA
Vladimir Zharov, Ekaterina Galanzha, Arkansas Medical Science University, USA
Alexey Popov, Alexander Bykov, Igor Meglinski et al. Univ. of Oulu, Finland
Luis Oliveira et al. ISEP-IPP, Porto, Portugal
YongKeun Park, KAIST, Korea
Maxim Darvin, Juergen Lademann, Olaf Minet, Urszula Zabarylo, Charité, Berlin
Martin J. Leahy, NUI Galway, Ireland
Malgorzata Jedrzejewska-Szczerska et al., Gdańsk University of Technology, Poland
Artashes V. Karmenyan, National Yang-Ming Univ., Taiwan
Viacheslav Artyushenko, Olga Bibikova, artphotonics gmbH, Germany
Qingyu Lin, Sichuan University, China
Alexander P. Savitsky, Irina G. Meerovich, Victoria V. Zherdeva, FRC of Biotechnology, RAS
Alexei A. Bogdanov Jr, UMass, USA

- **RF Presidential grants NSh- 7898.2016.2, SP-3507.2018.4**
- **RF Megagrants 14.Z50.31.0004, 14.Z50.31.0044,14.W03.31.0023, 075-15-2019-1885**
- **RFBR grants: 17-02-00358, 17-02-00358, 17-32-50190 , 17-00-00186**
- **17-00-00275 (K), 18-52-16025, 18-32-00587, and 18-32-00202**
- **RF MES grants 3.1586.2017/4.6 and 17.1223.2017/AP**
- **Russian Science Foundation grants 14-15-00128 ,18-12-00328**